A SIMPLIFIED MODEL OF INTERANNUAL WATER TEMPERATURE VARIATIONS IN HECATE STRAIT AND QUEEN CHARLOTTE SOUND

by

Helai Ma

B.Sc., Ocean University of Qingdao, 1982
M.Sc., Ocean University of Qingdao, 1985

A THESIS SUBMITTED IN PARTIAL FULFILLMENT OF

THE REQUIREMENTS FOR THE DEGREE OF

MASTER OF SCIENCE

in

THE FACULTY OF GRADUATE STUDIES

(Department of Oceanography)

We accept this thesis as conforming
to the required standard

.....

THE UNIVERSITY OF BRITISH COLUMBIA

August 1992

In presenting this thesis in partial fulfilment of the requirements for an advanced degree at the University of British Columbia, I agree that the Library shall make it freely available for reference and study. I further agree that permission for extensive copying of this thesis for scholarly purposes may be granted by the head of my department or by his or her representatives. It is understood that copying or publication of this thesis for financial gain shall not be allowed without my written permission.

Department of OCEANOGRAPHY

The University of British Columbia
Vancouver, Canada

Date Oct. 1, 1992

ABSTRACT

The thermal conditions in the Hecate Strait-Queen Charlotte Sound region are studied. A coupled upwelling/mixing model was developed to simulate the interannual variability of temperature in the region; the switch between the upwelling and mixing models is controlled by the monthly Bakun Index. A theoretically derived velocity field is applied in the upwelling model in summer and a simplified upper mixed layer model is used to simulate winter conditions. The temperature variation is integrated by a finite difference scheme. The region is simplified as a two-layer wedge-shaped volume to represent the Moresby Trough that forms the main passage of cold water intrusion into Hecate Strait. The model was run for 37 years and hindcasted the interannual variations of temperature in the Hecate Strait-Queen Charlotte Sound region from 1953 through 1989. A comparison was made between the model results and observed data. The general features of the temperature variations are well reproduced by the model results.

TABLE OF CONTENTS

LIST OF TABLES

List of Figures

PAGE

1. Introduction

The oceanography of the coastal waters on the British Columbia continental shelf is influenced by deep-ocean processes as well as by the local effects of winds, tides, runoff, heat flux at the sea surface and coastal morphology. Physical oceanographic conditions on the continental shelves influence other important oceanic processes; for instance, most of the biological primary productivity of the world takes place in the relatively fertile surface waters over the shelves. The biological phenomena occurring on continental shelves are highly dependent on fluid mechanical processes.

Observations of currents on continental shelves have shown that the nature of the flow in different regions, such as off the northeast and off the northwest coast of the United States, can be quite different. Major variations in flow patterns appear to be due in part to differences in the shelf width, to the nature of the local and nearby coastal winds, and to the strength and character of offshore currents.

It appears that a primary driving mechanism for the velocity field on many continental shelves is the along-shore component of wind stress. The wind stress typically produces energetic fluctuations of the shelf velocity field on the two-to ten-day time scales that characterize the variability of atmospheric storms and synoptic scale wind events. In addition, on longer time scales, the seasonal variability of the wind field may induce a corresponding seasonal variability in the shelf current (Allen, 1980).

Studies of the oceanography of the Queen Charlotte Sound-Hecate Strait region have revealed the general features of the currents (Crawford, et.al. 1985,1988), the surface temperature and salinity distributions, as well as the seasonal variability of temperature, salinity and dissolved oxygen content of the deep water masses (Dodimead, 1980).

The physical processes and driving mechanisms in the Queen Charlotte Sound-Hecate Strait region, to the extent that they are understood at the present, appear to be due mainly to the nature of local and nearby coastal winds and the specific topographic condition of the strait. In particular, an important process is the northwest-wind-induced upwelling which gives rise to an outward drift of surface water from the Strait and the Sound and an intrusion of cold water at the bottom.

As part of the OPEN program, which reflects the joint efforts of physical and biological oceanographers, fisheries scientists and geneticists to enhance research in fisheries oceanography, an effort was made to model the processes which control bottom water conditions in the Queen Charlotte Sound—Hecate Strait region. In this thesis, a simple two-layer upwelling model is developed to study the summer water conditions and their interannual variations. The model is driven by inputting surface wind (in the form of a Bakun Index). The temperature field and its variation with time and space are deduced from the velocity field. The relationship between the temperature and wind stress and that between temperature distribution and topography are also investigated. To close the annual cycle of variation, a cooling/mixing model was developed to model the winter conditions. Time scales considered range from a few days to a few months. The model is tested against the annual cycle of the temperature variation in the Queen Charlotte Sound- Hecate Strait region revealed by the historical data. Then a coupled model is used to hindcast the thermal conditions in the region over the past four decades.

In Chapter 2, a brief review is given of the bathymetry of Queen Charlotte Sound—Hecate Strait region, the oceanographic conditions in the region and the specific phenomena of interest.

Chapter 3 describes the development of a 2-layer numerical upwelling model of summer conditions and a mixing/cooling model for simulating winter

conditions. The basic physical assumptions and the related processes, such as radiation, mixing and entrainment are discussed. The velocity field is derived analytically for the upwelling model and the temperature field is solved numerically in both models.

Chapter 4 shows the results from the composite model of upwelling and mixing. A long time series of temperature distribution is obtained from the hindcast of the model.

In Chapter 5 a comparison is made between the modeled results and historical data. Statistics are given from the comparison.

Finally, a conclusion is given in Chapter 6 discussing the validity and future use of the model.

2. Oceanographic Conditions in Queen Charlotte Sound-Hecate Strait Region

2.1 Bathymetry

Hecate Strait is a relatively wide area between the British Columbia coast and the Queen Charlotte Islands (Fig. 1). The length of the strait is about 220 km. It is 130 km wide in the south with a water depth of about 300 m and 60 km wide in the north with water depths of 20-80 m. The axis of the Strait is a narrow long submarine valley along the southeast-to-northwest direction. The northwest side of the Strait is a broad platform of glacial sands and gravels less than 100 m deep, adjacent to the flat coastal plain or strand flat of east Graham Island. Hecate Strait connects with Dixon Entrance at its northern end and joins Queen Charlotte Sound in the south.

Queen Charlotte Sound is a broad area between Vancouver Island and the Queen Charlotte Islands with the mainland of British Columbia on the east (Fig. 1). It has a considerably more complex topography than Hecate Strait. Three broad troughs (Moresby Trough, Mitchells Trough and Goose Island Trough) in the Sound area, separated by two wide shallow banks, form the major topographic features and have important influence on the oceanography of the area. The northern trough (Moresby Trough) is the most irregular one and trends 270 km northward to form the deep channel of Hecate Strait. To the west, the Sound connects with the Northeast Pacific; it is therefore one of the main passages for oceanic water flowing into Hecate Strait.

2.2 General features of the waters in the region

Long-term records of daily observations show that the sea surface temperature variations at the northern coastal lightstations in Queen Charlotte

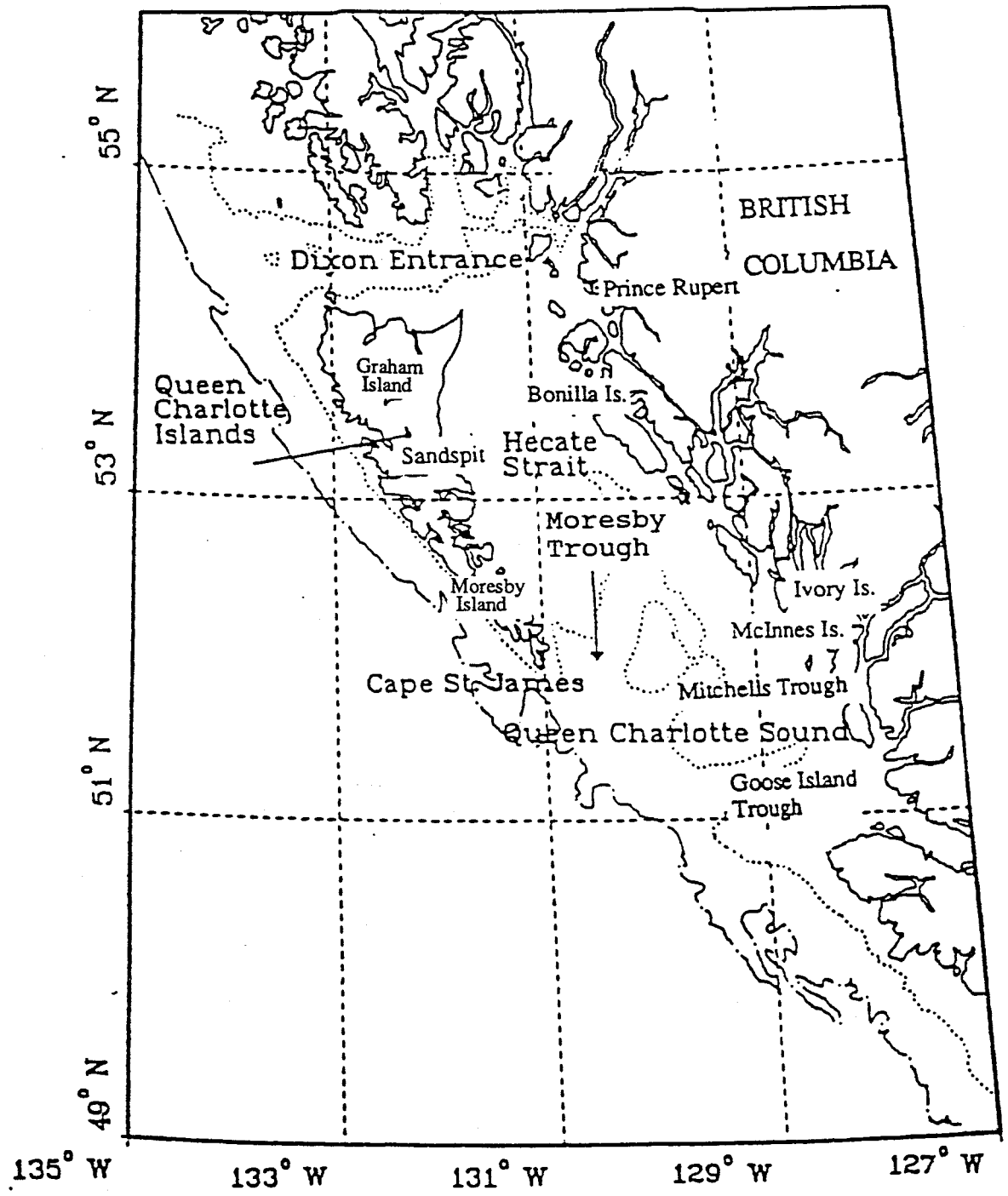

Figure 1 Map of Queen Charlotte Sound-Hecate Strait region. The dotted line is the 200 m depth contour and the chain-dotted line is the 2000 m contour.

Sound and Hecate Strait region are clearly dominated by the annual heating cycle with maximum water temperature typically in the 10-13 °C range in August and minimum temperature in the 4-8 °C ranges in February to March (Fig. 2).

The horizontal distributions of monthly mean temperatures at 50 m and 200 m depths in September 1983 and January 1984 are shown in Fig. 3a, 3b. They represent the temperature patterns in summer and winter respectively. In summer, the isotherms at 50 m approximately parallel the coast. The lower layer shows evidence for a strong eddy and associated frontal system off the southern coast of Moresby Island, although the information is incomplete and does not describe well conditions over most of Hecate Strait. In winter, the temperature at 50 m depth decreases gradually from 8.8 °C in the south (Q.C.S) to 6.8 °C in the north (northern H.S.). At 200 m depth, the temperature is nearly uniform and there is a marked northward warm water intrusion from the Queen Charlotte Sound (Thomson, 1989) , but again, data coverage in Hecate Strait is poor.

The vertical distribution of temperature at selected locations in Queen Charlotte Sound (station C, Fig. 4) and Hecate Strait (station E , Fig. 4) are shown in Fig. 5 (a and b) in summer and late winter respectively (Dodimead 1980). In summer, the distinctive features of the temperature structure are the thin mixed or near-mixed surface layer and the marked thermocline. In the absence of surface mixing, the thermocline will extend to near the surface. The thermocline extends from near-surface to about 75-100 m depth in Queen Charlotte Sound at station C (Fig. 5a) and to about 100-125 m in Hecate Strait at station E. The strength of the thermocline is dependent upon the degree of surface heating and mixing and is about 6 to 8 °C.

During late winter (January-March), the cooling, mixing and conductive processes started in October continue. The main features are the near-isothermal conditions to depths of 150-200 m and the relatively large temperature inversions common at depth, particularly at station C and E.

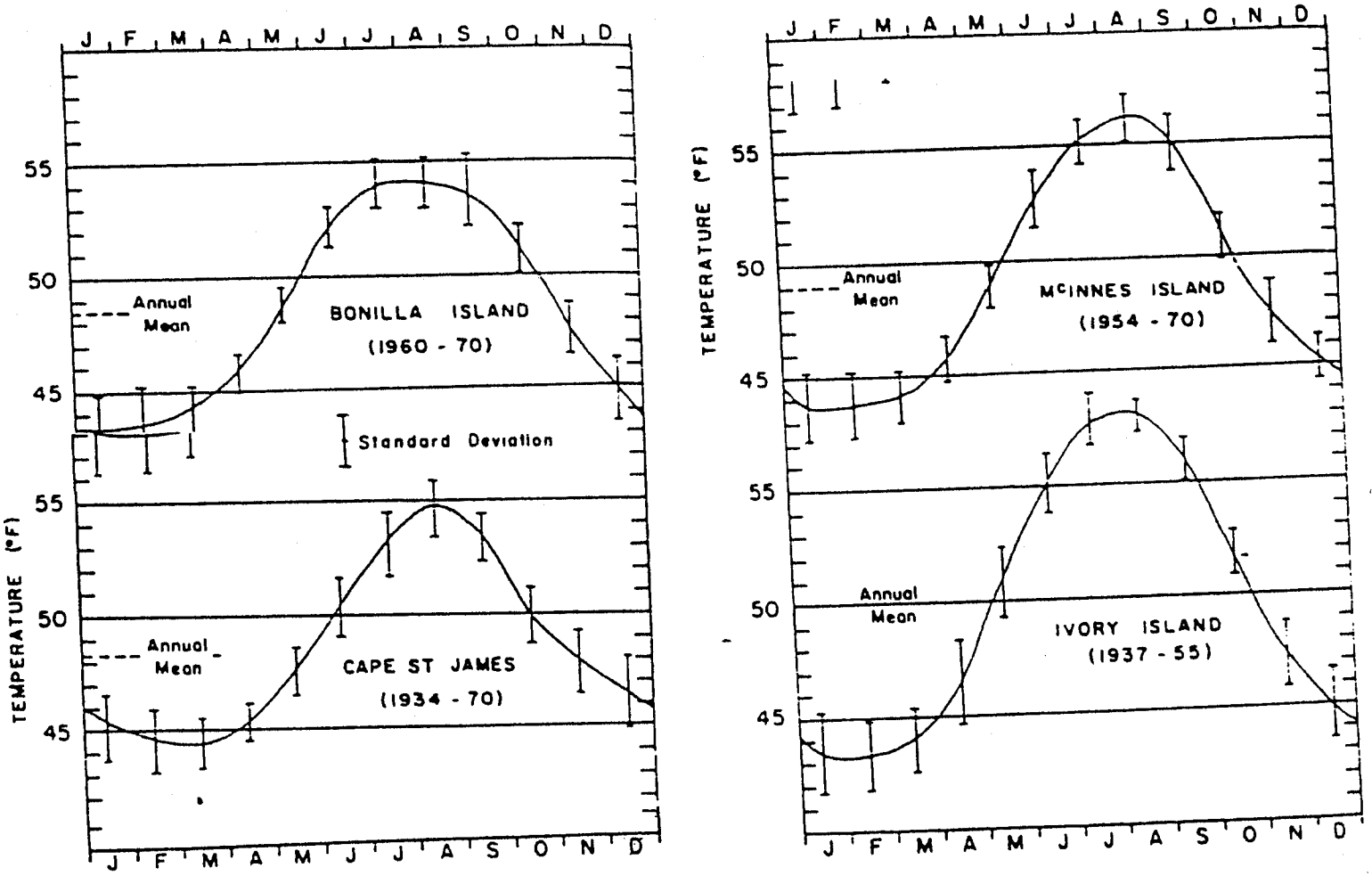

Figure 2 Long-term monthly means and standard deviations of sea surface temperature at 4 lightstations located in the Queen Charlotte Sound-Hecate Strait region (from Dodimead, 1980).

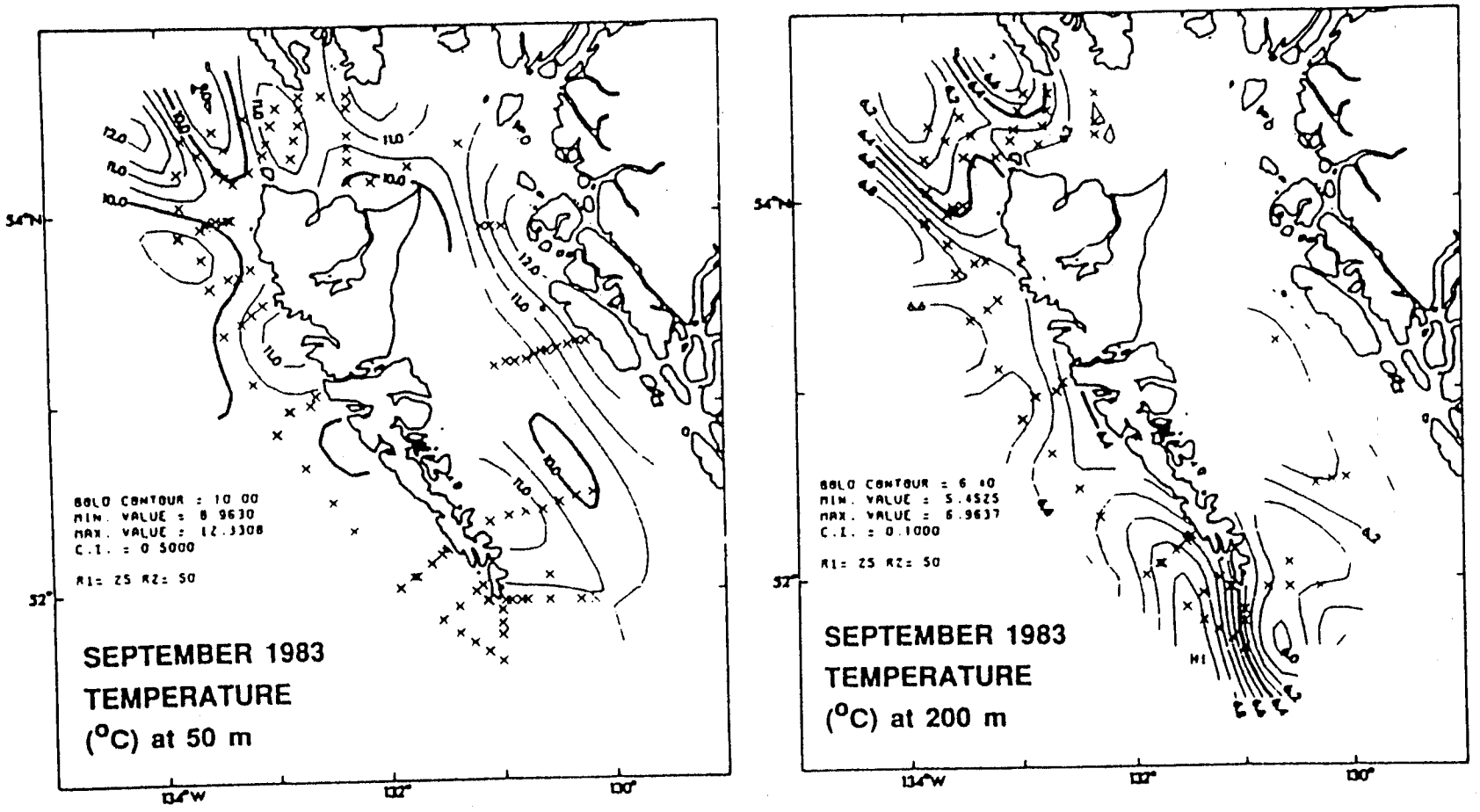

Figure 3 a) Horizontal distribution of temperature at 50m and 200m depths in summer from an oceanographic cruise in the Queen Charlotte Islands region (from Thomson, 1989)

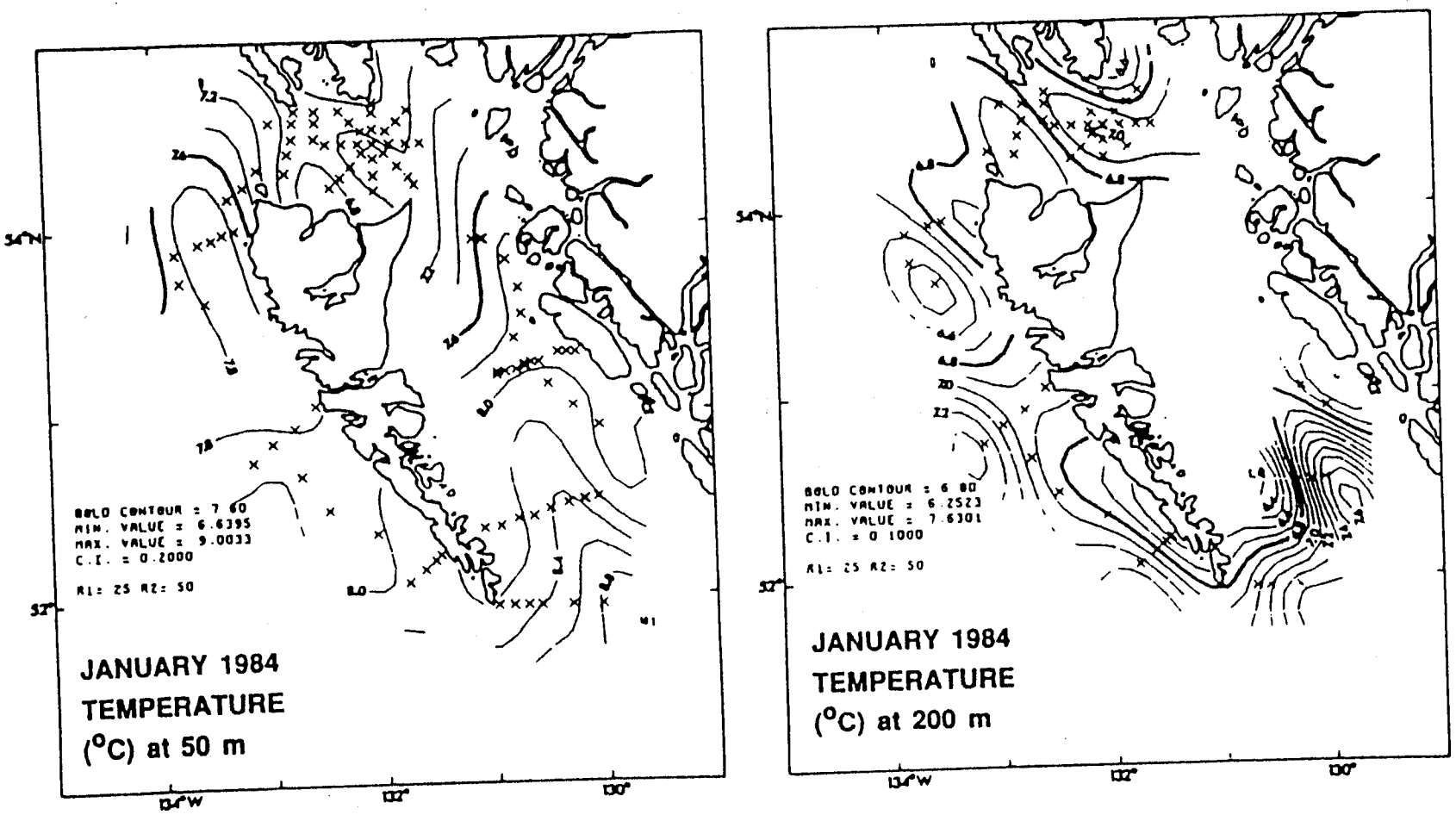

Figure 3 b) Horizontal distribution of temperature at 50m and 200m depths in winter from an oceanographic cruise in the Queen Charlotte Islands region (from Thomson, 1989)

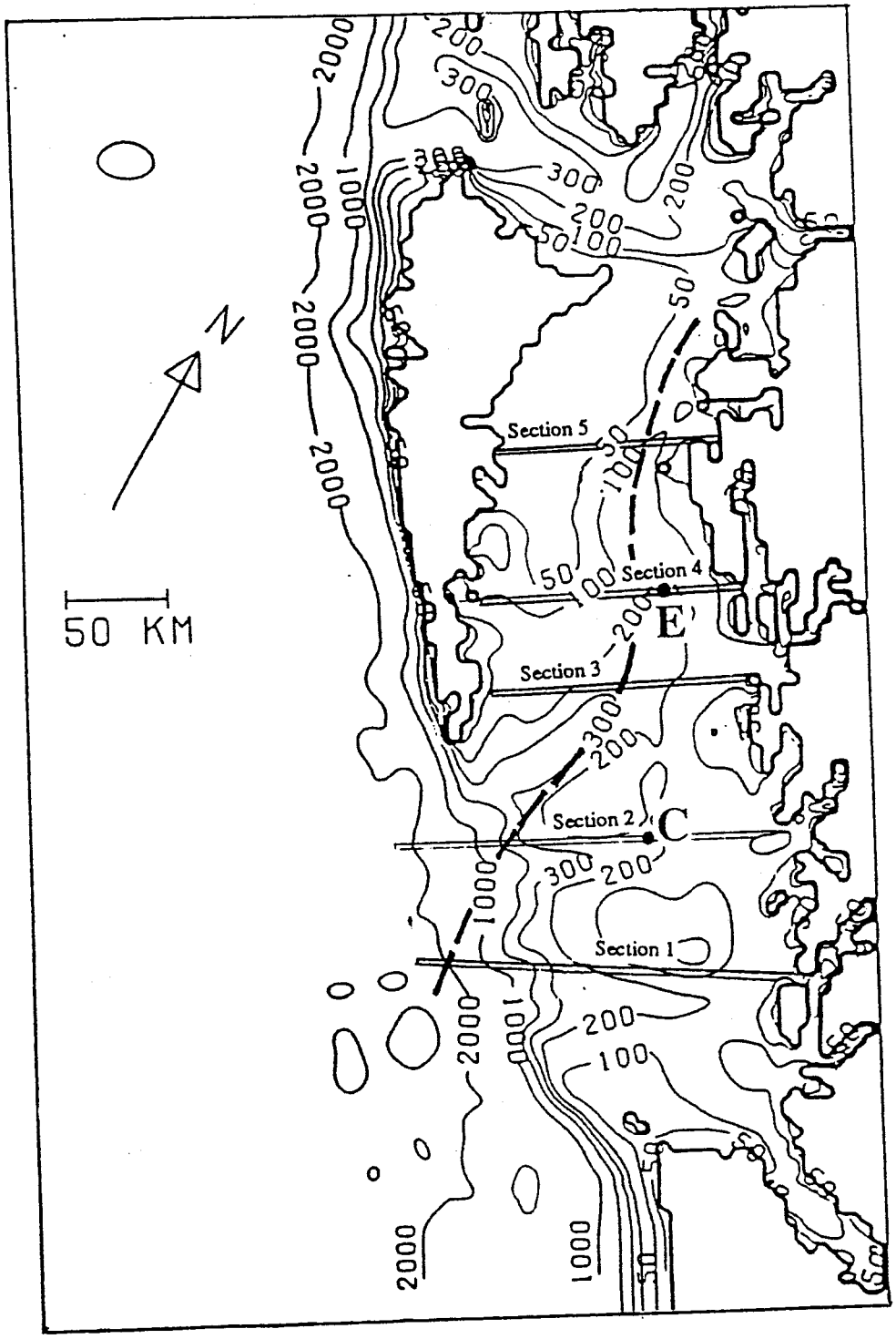

Figure 4 Stations C and E and sections 1-5 in Queen Charlotte Sound—Hecate Strait region (from Dodimead, 1980); thick dashed line shows the axis described in Fig 7.

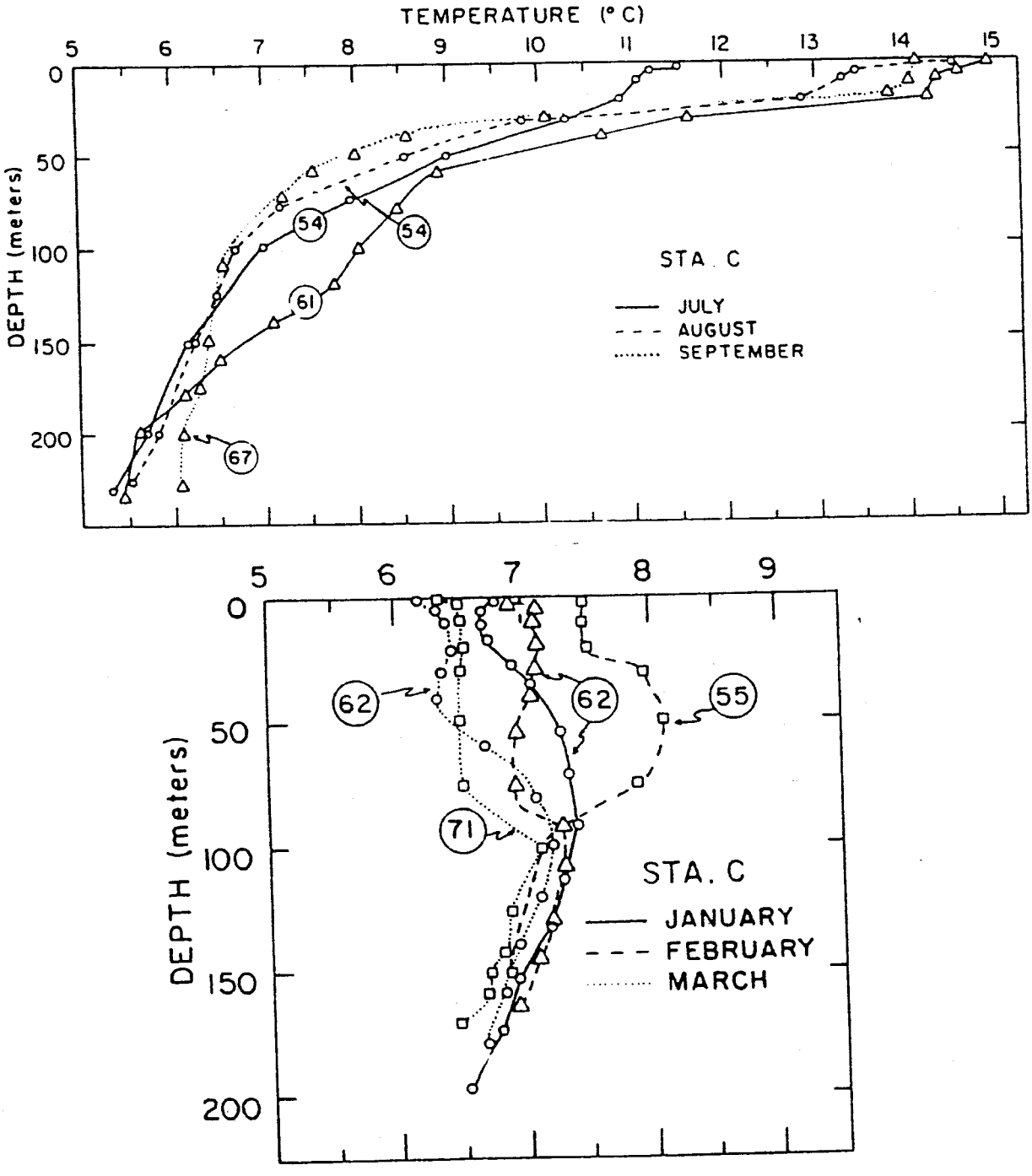

Figure 5 a) Vertical distribution of temperature at station C in summer and winter months.Circled numbers show the year of sampling.

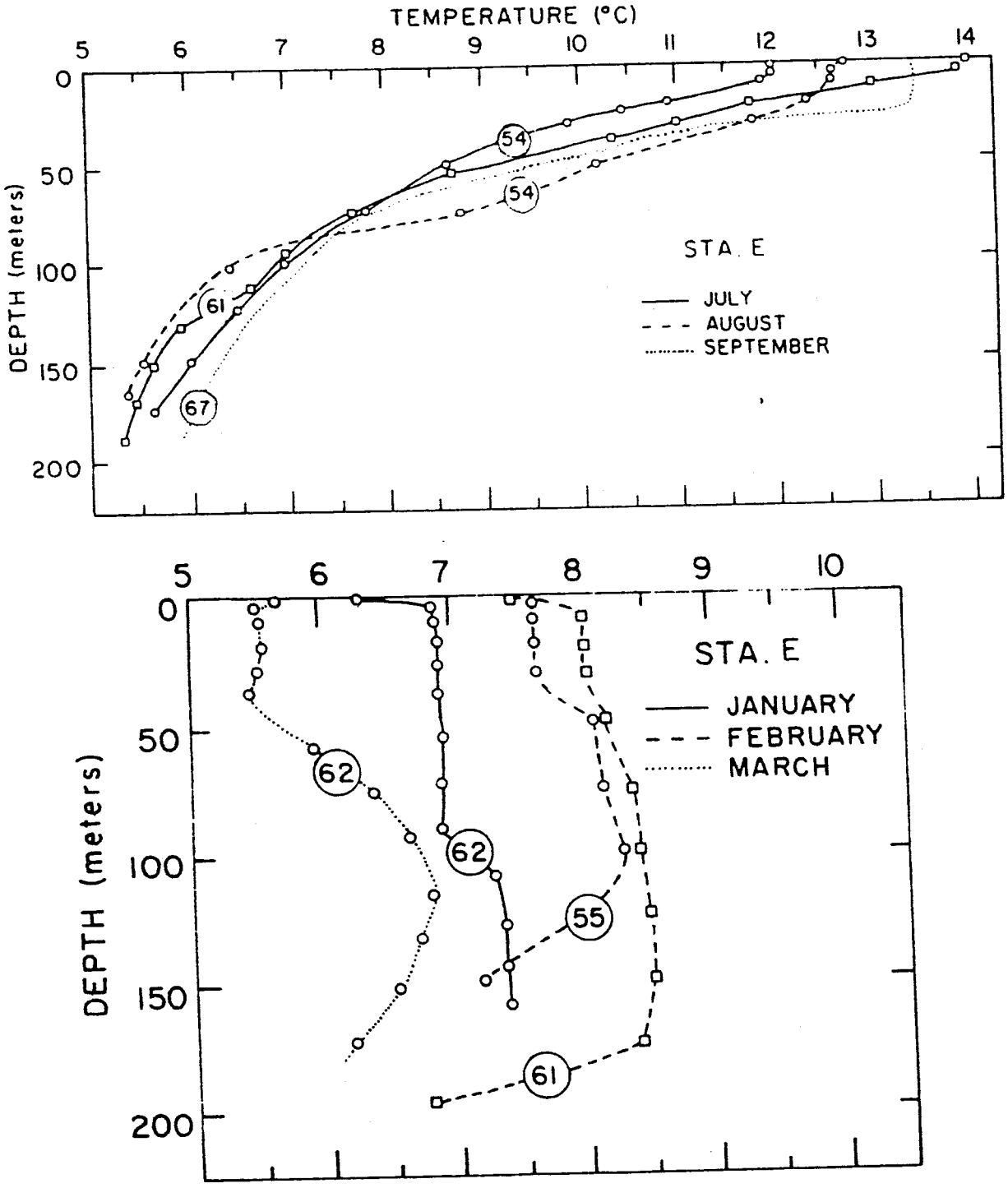

Figure 5 b) Vertical distribution of temperature at station E in summer and winter months.Circled numbers show the year of sampling.

2.3 Bottom cold water intrusion

One of the most interesting features of bottom water in Hecate Strait revealed by the historical data is that the lowest temperature of the year occurs in summer and the highest temperature in winter. This feature is just the opposite to the seasonal variation of surface water. Similar features were also observed off southern Vancouver Island (Freeland and Denman, 1982).

Fig. 6 is a vertical section (section 2, Fig. 4) of water properties in Queen Charlotte Sound on June 22, 1955. It shows strong evidence of upwelling over the continental shelf off the Queen Charlotte Sound in summer. Deep cold water of 5.5 °C (high salinity, ~34 ‰ and low oxygen, ~1.5 ml/l) upwelled from 275 m to about 200 m depth and was believed to intrude into Hecate Strait along the Moresby Trough. In 1961, at station E, the decrease of bottom temperature started in April and reached the lowest valuein August (Fig. 7). During this period, the 6°C isotherm rose about 80 meters, reflecting the progress of the cold water intrusion. This event happened earlier in the southern part of the Strait and later in the northern part, indicating that the event propagated northward from the southern opening of the Strait--Queen Charlotte Sound.

Fig. 8 shows the temperature distribution in time and space at the bottom along the axis of the strait during 1954-1955; the axis runs through 5 cross-strait sections from the south to the north (thick dashed line in Fig. 4). Cold water reached section 3 about ninety days earlier than it reached section 5. Considering the distance between section 3 and section 5 (111 km), this corresponds to a propagating speed of 1.4 cm/s. I argue that advection due to upwelling is responsible for the observed temperature changes. If we assume the speed of 1.4 cm/s is the same as the rate of bottom water intrusion, and the lower portion of section 4 is a triangle of 60 km wide and 100 meters high, an estimated flux through this section based on this speed will be ~ $1.4 \times 0.01 \times 60 \times 1000 \times 100 / 2 = 42,000 m^3 / s$ If we chose an upwelling index

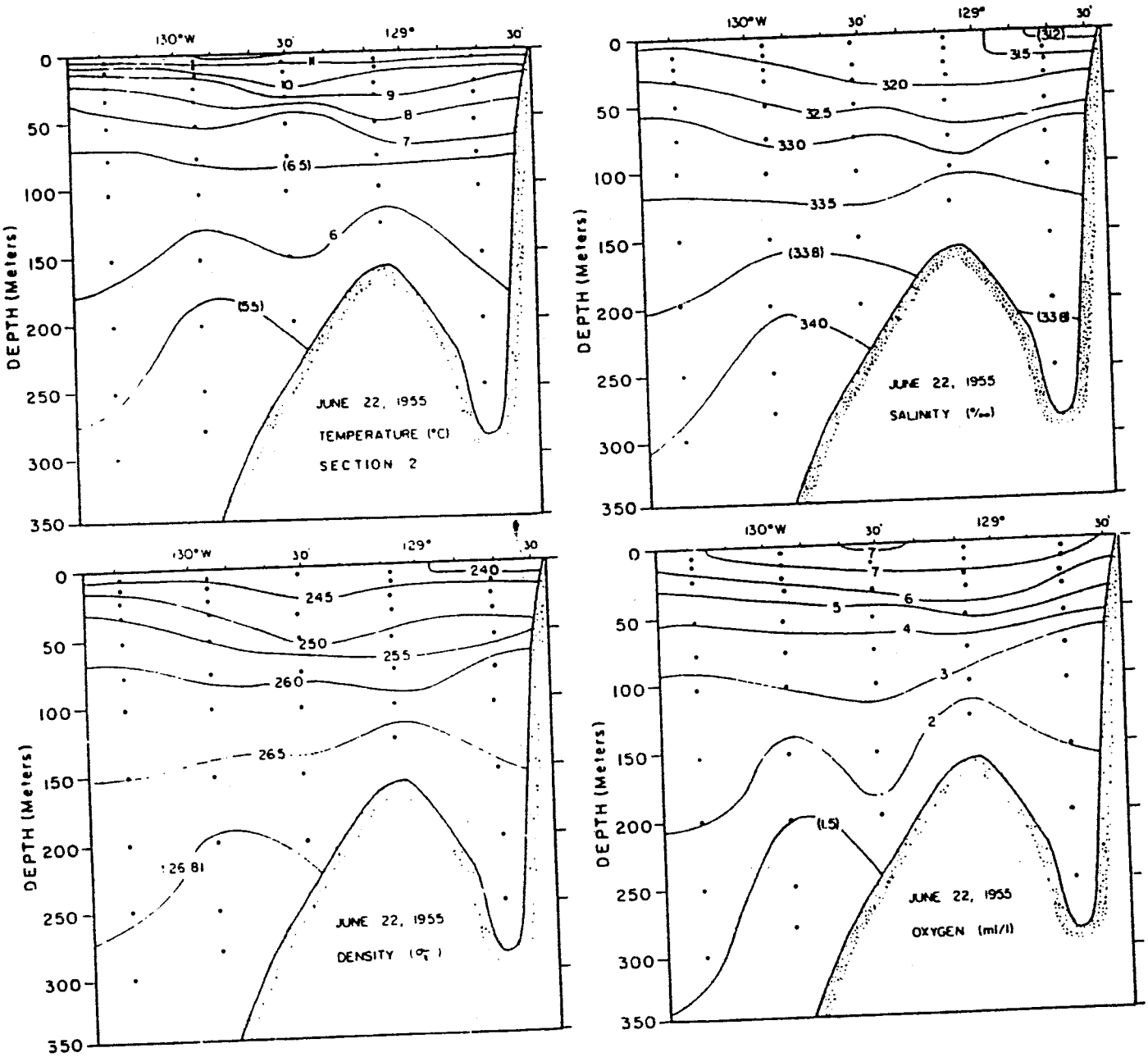

Figure 6 Vertical section of temperature, salinity and dissolved oxygen at section 2 in Queen Charlotte Sound (from Dodimead, 1980)

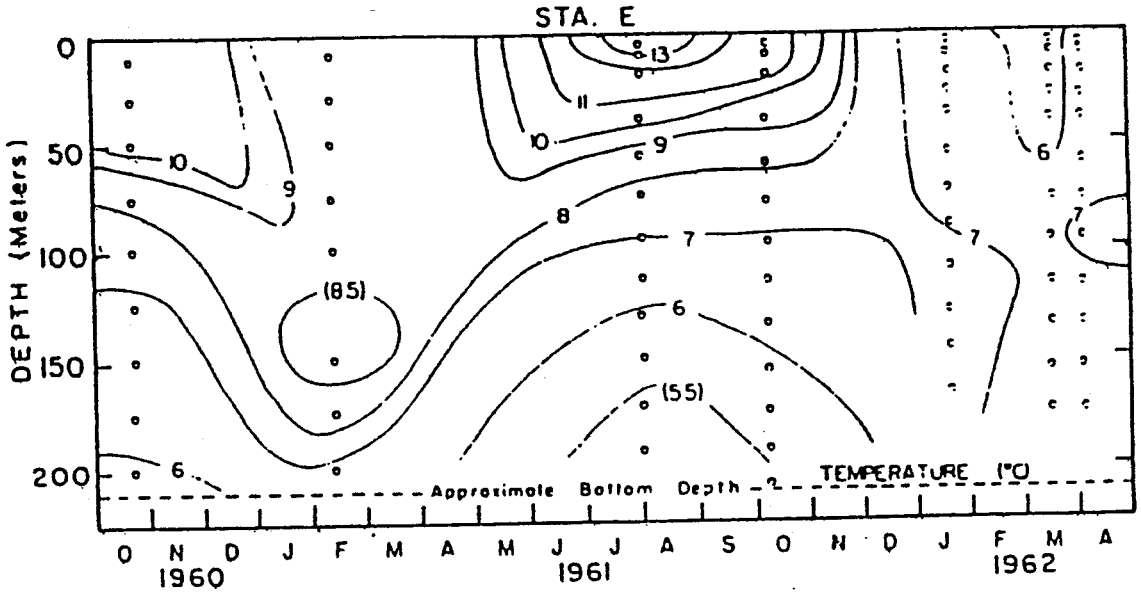

Figure 7 Annual cycle of temperature at station E in Hecate Strait.

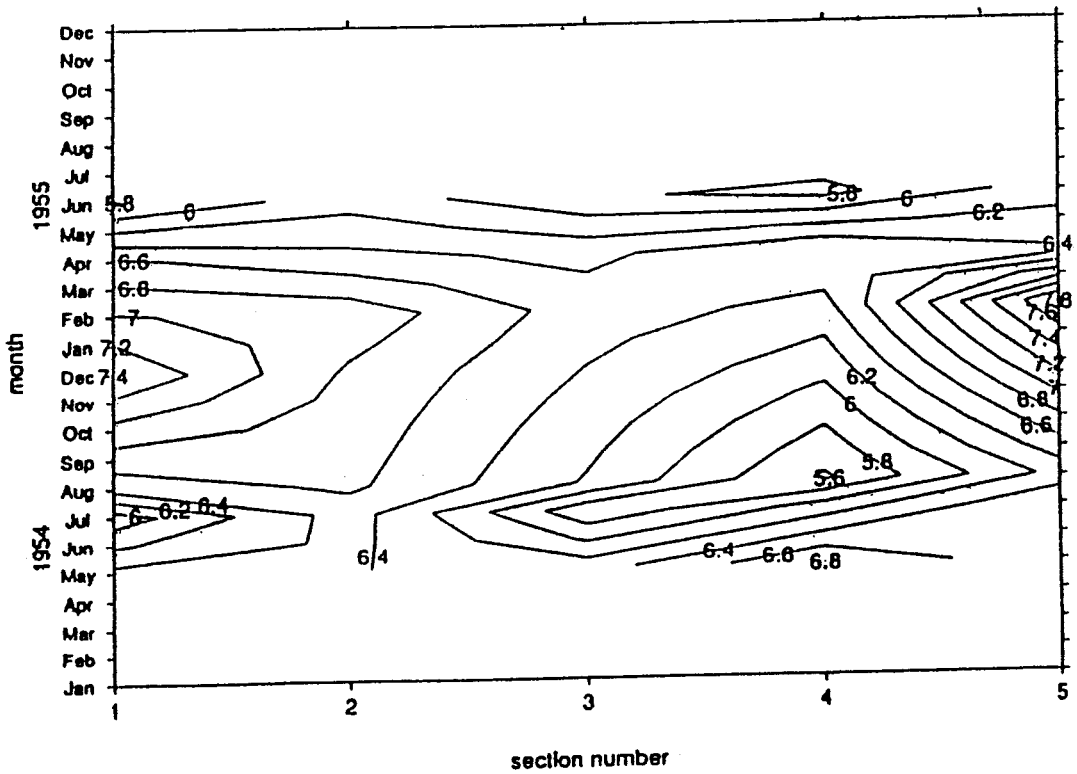

Figure 8 Temperature distribution in time and space at bottom along the axis of Hecate Strait (1954-1955). The axis runs through 5 cross-strait sections from south to north as shown in Fig. 4

of 31 (unit=m^3/sec/100 meters of coastline) as the mean value over 90 days and the width of the southern opening of the strait as 120 km, we calculated an offshore transport of about $31/100 \times 120 \times 1000 = 37,000 m^3/s$, which is in good agreement with the estimated influx.

The above estimation indicate that the bottom cold water intrusion is closely related to wind-induced upwelling at the mouth of the strait. Therefore an upwelling model is considered to be reasonable to represent this event.

The bottom water began to warm up from September in 1954. It is shown that the bottom warming was slower than the cooling and, obviously, due to a different mechanism.

2.4 Wind forcing

The prevailing winds in Queen Charlotte Sound—Hecate Strait region are controlled by the locations and intensity of two semi-permanent atmospheric pressure systems. The Aleutian Low centered in the Gulf of Alaska predominates in winter and produces strong south-to-southeasterly winds along the coast ; the North Pacific High predominates in summer and is responsible for generally north-to-northwesterly wind along the coast (Thomson, 1989).

Westward migrating synoptic-scale atmospheric systems (high and low) are responsible for modification of the prevailing winds over periods of days to weeks. The weather in Queen Charlotte Islands is famous for frequent and intense storms with their attendant fronts and strong southwesterly winds.

Synoptic winds are modified in near-coast areas by the mountainous terrain and within about 50 km offshore tend to blow parallel to the coast. Strongest winds occur in December through February and weakest winds in July and August. Late September to early October usually marks the time of an abrupt increase in mean wind speeds.

Fig. 9 shows the grand mean and standard deviation of monthly total miles of wind resolved along the southeast axis at Prince Rupert, 1954-1962, Sandspit, 1955-1964, McInnes Island, 1955-1963, and Cape St. James, 1955-1963 (Crean, 1967). A marked feature of this figure is that in the northern part of Hecate Strait, say, Prince Rupert, the prevailing wind around the year is southeasterly, while in the southern part of the Strait, such as at Cape St. James, northwesterly winds prevail in summer and southeasterly winds prevail in winter. This divergent distribution of wind may give rise to the specific flow features of the water in Hecate Strait.

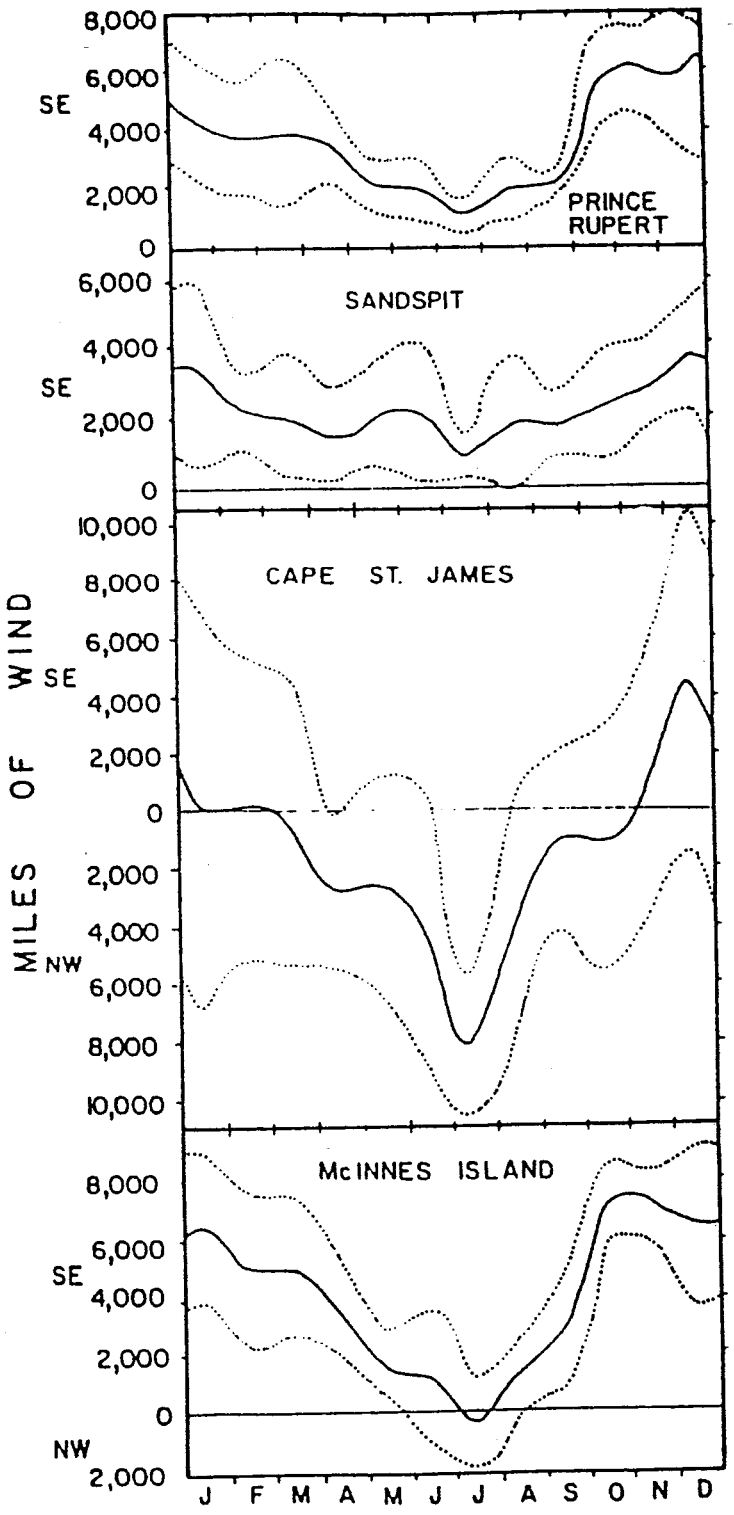

Figure 9 Grand means and standard deviations of monthly total miles of wind resolved along the southeast axis at Prince Rupert, Sandspit, McInnes Island and Cape St. James. (from Crean, 1967)

3. The Models

3.1 The hypotheses

Two hypotheses were made based on the topography of the area and the existing oceanographic conditions.

First, the geography and hydrography of Hecate Strait are modeled in terms of a wedge (Fig. 10), simulating Moresby Trough, containing a two-layer liquid. The northern end is open in the upper layer, allowing flow connection with Dixon Entrance.

Second, the thermal history of the waters is assumed to be controlled by the advection of upwelled waters at depth during summer and vertical mixing during the winter.

The complex geometry and hydrography of Hecate Strait are thus idealized enough to be accessible to simple modeling. We assume that the thermal behavior is controlled by mean seasonal upwelling and vertical mixing, and that all high frequency motions (tides, inertial oscillations, storm response) are filtered out. The model will hold only for slow variations, on time scales of half-a -month and larger; it is the seasonal and interannual behavior that are modeled here. The gyre around the Goose Island Bank is not considered in this model.

Flow in the model wedge is assumed to be forced by the Ekman divergence of surface waters, as characterized by the Bakun Index (Bakun, 1973). Under upwelling conditions, flow is out (seaward through southern opening) at the top. A vertical distribution is assumed and the rest of the flow field follows from continuity. Provision is made for influx through the shallow end of the wedge, representing flow into Hecate Strait from Dixon Entrance.

The model is presented in two sections: the advective part is calculated first, followed by the vertical mixing and /or stratification component. In fact, the two sections describe two different models. One is a two-dimensional upwelling

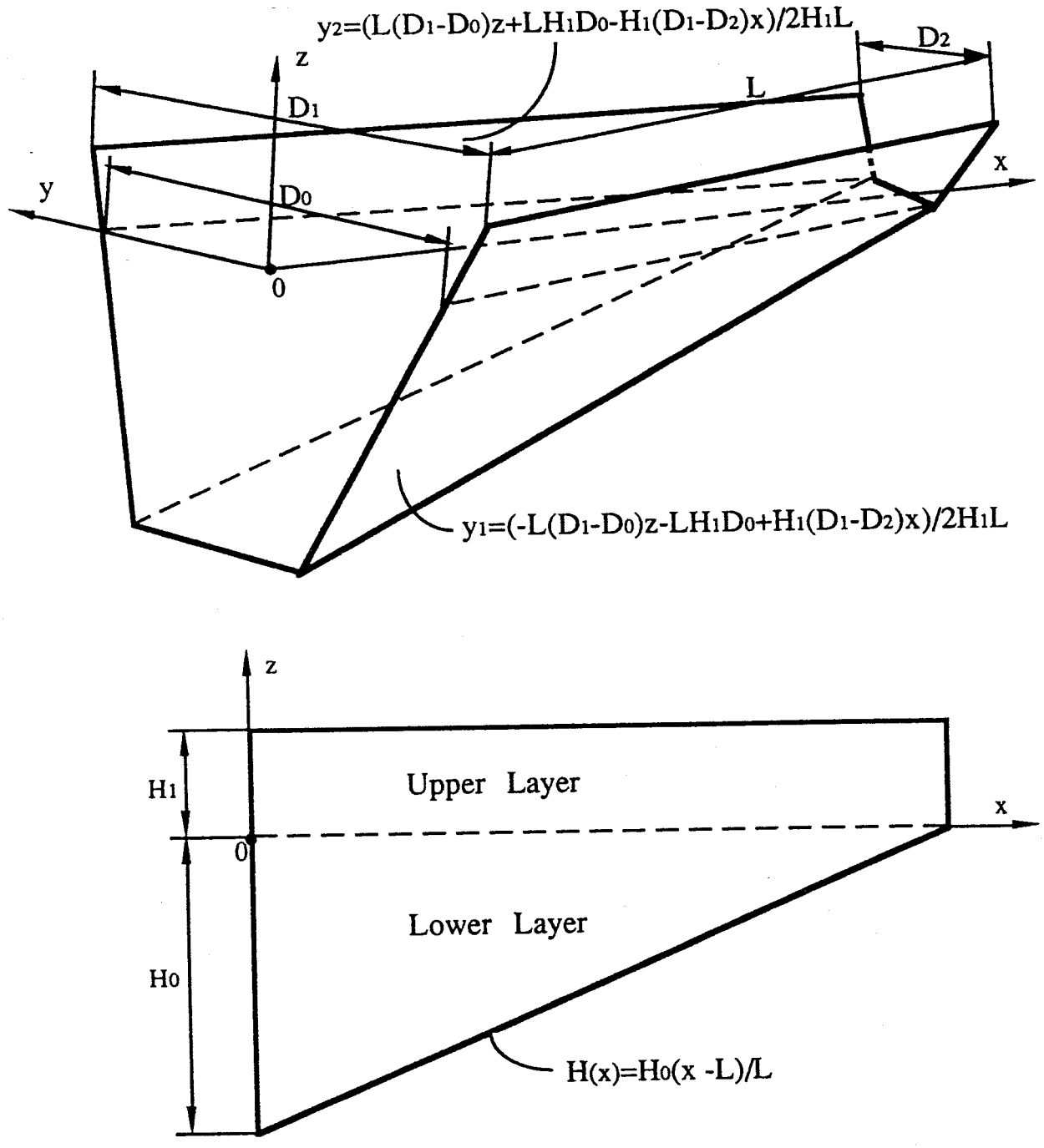

Fig. 10 Model Geometry and Coordinate System

model which takes into account the wind forcing in terms of the Bakun Index and solar radiation; the other is a one-dimensional upper ocean mixed layer model which is controlled by wind stress, turbulent transfer of heat at the air-sea interface and entrainment which occuring at the bottom of mixed layer. The switch between the two models is controlled by Bakun Index. i.e. a positive Bakun Index in a month switches the model to an upwelling regime and a negative Index switches the model to vertical mixing.

3.2 The model geometry

As explained above, the geometry of the region is simplified as a two-layer wedge-shaped water volume with Queen Charlotte Sound at the wide mouth and the northern part of the Hecate Strait being the narrow end of the wedge. The water depth decreases from the mouth to the end. The wedge is 250 km long with a water depth of 320 m at the seaward mouth and 42 m at the northern end. The surface width is about 120 km at the mouth and 30 km at the end (Fig. 10).

3.3 Bakun Index

The Bakun Index is widely used as an upwelling index in the Northeast Pacific. It is in fact the offshore transport of mass in the Ekman layer, which is considered an indication of the amount of water upwelled through the bottom of the Ekman layer to replace that driven offshore. The indices are based on calculations of offshore Ekman surface wind transport from surface atmospheric pressure data. Indices for 1945-1972 were provided by the National Oceanic and Atmospheric Administration (NOAA) on monthly bases. Now NOAA provides both alongshore and offshore transport of 6-hourly, daily, weekly and monthly values for the years from 1973 through present for the locations along the east coast of North Pacific on a three degree grid (Fig. 11, Bakun, 1973)

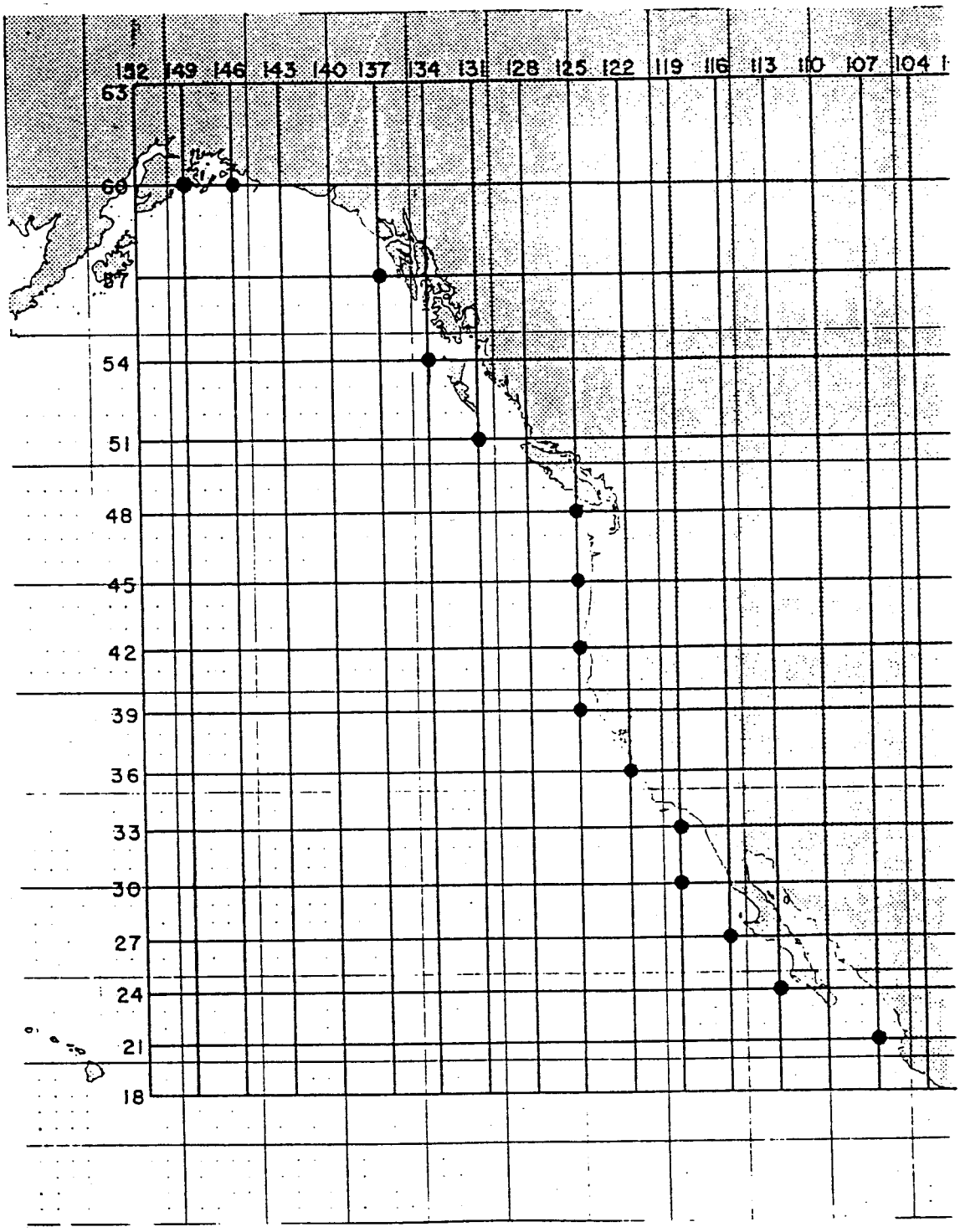

Figure 11 Data grid for Bakun Index. Intersections at which upwelling indices are computed are marked with large dots.

The upwelling index, defined as mass transport in tons per 100 meters of coastline per second is defined as

$$W = \frac{\tau}{f}$$

where: τ is the wind stress;

f is the Coriolis parameter.

The layer in which appreciable transport occurs is referred to as the Ekman layer and extends from the surface to depths not exceeding 50 to 100 meters.

The surface wind stress is calculated from the geostrophic wind

$$\tau = \rho_a C_d \left|\vec{\mathbf{V}}\right| \vec{V}$$

where: ρ_a is the density of the air;

Cd is an empirical drag coefficient;

$\vec{V}$ is the estimated wind vector near the sea surface with magnitude $\left|\vec{\mathbf{V}}\right|$. Its two components are computed from surface pressure maps,

$$u_g = -\frac{1}{f\rho_a R}\frac{\partial P}{\partial \varphi}$$

$$v_g = \frac{1}{f\rho_a R\cos(\varphi)}\frac{\partial P}{\partial \lambda}$$

where: P is the atmospheric pressure;

R is the radius of the earth;

u_g is the northward component of the wind velocity;

v_g is the eastward component of the wind velocity;.

φ is the latitude;

λ is the longitude.

NOAA calculates a coastal upwelling index using wind stress obtained for locations near the west coast of North America. A negative value of the index indicates accumulation of wind-transported surface water at the coast resulting in downwelling. A positive index value is an indicator of how much water is upwelled from below the Ekman layer to replace the water driven off shore (Fig. 12). Both upwelling and downwelling occur as distinct events at various times of the year. In the Queen Charlotte Sound- Hecate Strait region, upwelling predominates during the summer months (May through September) and downwelling dominates during the winter months (October through March).

3.4 Upwelling model

When the Bakun Index in a month is positive, the model switches to an upwelling state, a velocity field is derived from equation of continuity and boundary conditions. The velocity field is driven only by wind forcing in terms of the Bakun Index. It is a two-layer flow and the flow directions in the two layers are opposite. The water in the upper layer of the wedge is driven out of the region by Ekman transport, cold deep sea water comes into the region from below to compensate for the water flow out in the upper layer. Two differently simplified heat equations are used to calculate the temperature changes in the upper and lower layers respectively. In the lower layer, temperature changes due only to the intrusion of cold water at the bottom, while in the upper layer, both solar radiation and advection of cold water from bottom contribute to the temperature changes.

3.4.1 The formulation of velocity field

The wedge-shaped area makes it easier to simplify the equation of continuity from three dimensions to two and reduces the number of boundary conditions. A coordinate system is chosen with the origin at the deep end of the

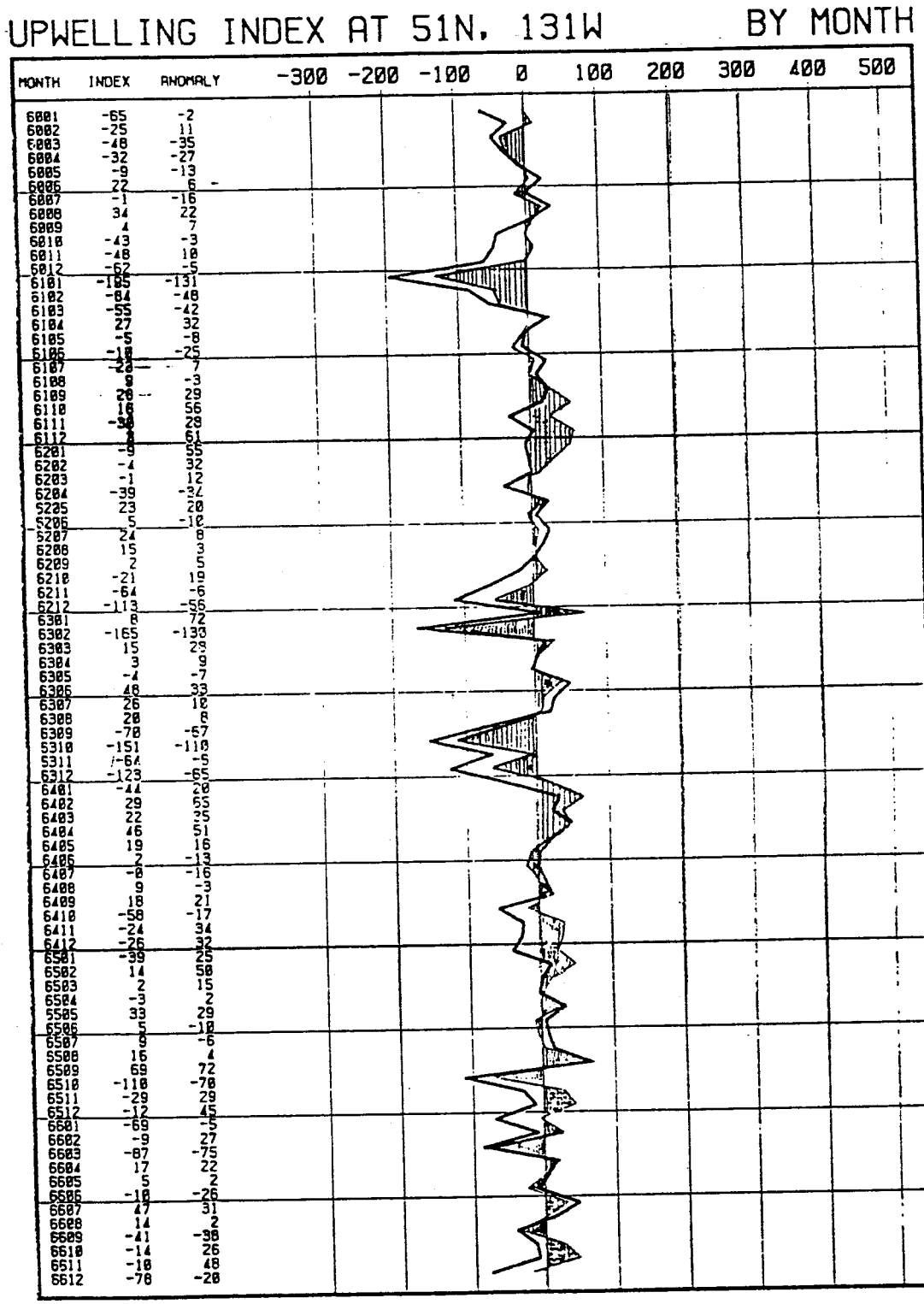

Figure 12 Monthly Bakun index at 51°N, 131°W for the years 1960 through 1966.

wedge on the interface between the two layers. The x-axis is directed horizontally toward the shallow end of the wedge, the y-axis is perpendicular to the axis of the wedge along the interface; the z-axis points upward from the origin (Fig. 10). The simplified equation of continuity is obtained by integrating the equation from one side of the wedge to the other with respect to y.

In the upper layer, the laterally integrated volume continuity is expressed as:

$$\frac{\partial}{\partial x} U_1 D + \frac{\partial}{\partial z} W_1 D = 0 \ , \tag{1}$$

where U_1 and W_1 are the horizontal and vertical velocity components respectively, and

$$D = y_2 - y_1 = \frac{1}{H_1 L}[L(D_1 - D_0)z + D_0 H_1 L - (D_1 - D_2)H_1 x]$$

is the width of the wedge; Subscripts 1 refer to the upper layer, 2 to the lower layer.

At the interface, $z = 0$, the horizontal flow changes sign and the vertical velocity is continuous:

$$\left.\begin{array}{l} U_1 = 0 \\ W_1 = W_2 \end{array}\right\} \quad \text{at the interface,} \quad z = 0 \left\{\begin{array}{l} (2) \\ (3) \end{array}\right.$$

At the sea surface, $z = H_1$, the vertical velocity vanishes,

$$W = 0 \qquad \text{at the sea surface, } z = H_1 \tag{4}$$

At the deep end of the wedge, the horizontal transport out of the upper layer is controlled by the Bakun Index:

$$\int_0^{H_1}\int_{y_1}^{y_2} U_1 dydz = -\frac{D_1 B}{100} \qquad \text{at deep - end,} \quad x=0 \qquad (5)$$

where B is the Bakun Index at 51°N, 131°W.

At the shallow end, the horizontal transport (T) into the upper layer from the Dixon Entrance is expressed as:

$$\int_0^{H_1}\int_{y_1}^{y_2} U_1 dydz = -T \qquad \text{at shallow} - \text{end,} \quad x=L \qquad (6)$$

In the lower layer, the laterally integrated volume continuity is expressed similarly as:

$$\frac{\partial}{\partial x}U_2 D + \frac{\partial}{\partial z}W_2 D = 0 \ , \qquad (7)$$

We have similar boundary conditions at the interface:

$$\left.\begin{aligned} U_2 &= 0 \\ W_2 &= W_1 \end{aligned}\right\} \quad \text{at the interface,} \quad z=0 \qquad \begin{cases} (8) \\ (9) \end{cases}$$

and at the sea bottom the velocity is perpendicular to the bottom, i.e.

$$\frac{H_0}{L}U_2 = W_2 \qquad \text{at sea bottom, } z = H_{(x)} \qquad (10)$$

Assume the vertical dependence of velocity in both layers is exponential and consider (2) and (8), we define:

$$U_1(x,z) = u_1(x)\frac{e^{a_1 z}-1}{e^{a_1 H_1}-1} \qquad (11)$$

$$U_2(x,z) = u_2(x)\frac{e^{a_2 z} - 1}{e^{a_2 H_{(x)}} - 1} \tag{12}$$

where $H_{(x)} = H_0(x - L)/L$.

Assume that the horizontal dependence of transport is also exponential, i.e.

$$\int_0^{H_1}\int_{y_1}^{y_2} U_1(x,z)dydz = \frac{e^{b(L+\delta-x)} - 1}{e^{b(L+\delta)} - 1}\int_0^{H_1}\int_{y_1}^{y_2} U_1(0,z)dydz = -\frac{\mathrm{B}}{100}D_1\frac{e^{b(L+\delta-x)} - 1}{e^{b(L+\delta)} - 1}$$

we also have

$$\int_0^{H_1}\int_{y_1}^{y_2} U_1(x,z)dydz = \int_0^{H_1} U_1(x,z)D(x,z)dz \ ,$$

from which we find:

$$-\frac{\mathrm{B}}{100}D_1\frac{e^{b(L+\delta-x)} - 1}{e^{b(L+\delta)} - 1} = \frac{u_1(x)}{H_1 L(e^{a_1 H_1} - 1)}\int_0^{H_1}[L(D_1 - D_0)z + D_0 H_0 L - (D_1 - D_2)H_1 x](e^{a_1 z} - 1)dz$$

$$= \frac{u_1(x)}{H_1 L(e^{a_1 H_1} - 1)}[LP_0^{H_1} - (D_1 - D_2)H_1 x Q_0^{H_1}]$$

where $\mathrm{P}_c^d = \int_c^d [(D_1 - D_0)z + \mathrm{D}_0 H_1](e^{a_1 z} - 1)dz$

$$Q_c^d = \int_c^d (e^{a_1 z} - 1)dz$$

hence, $$u_1(x) = -\frac{BD_1 H_1 L(e^{b(L+\delta-x)} - 1)(e^{a_1 H_1} - 1)}{100(e^{b(L+\delta)} - 1)[LP_0^{H_1} - (D_1 - D_2)H_1 x Q_0^{H_1}]}$$

$$U_1(x,z) = -\frac{BD_1H_1L(e^{b(L+\delta-x)}-1)(e^{a_1z}-1)}{100(e^{b(L+\delta)}-1)[LP_0^{H_1}-(D_1-D_2)H_1xQ_0^{H_1}]}$$

To obtain the vertical velocity, we first integrate (1) from z to H_1 with respect to z,

$$W_1(x,H_1)D(x,H_1)-W_1(x,z)D(x,z) = -\int_z^{H_1}\frac{\partial}{\partial x}U_1Ddz = -\frac{\partial}{\partial x}\int_z^{H_1}U_1Ddz$$

using (4) we get

$$W_1(x,z) = \frac{1}{D(x,z)}\frac{\partial}{\partial x}\int_z^{H_1}U_1Ddz = \frac{1}{D}\frac{\partial}{\partial x}\frac{u_1(x)[LP_z^{H_1}-(D_1-D_2)H_1xQ_z^{H_1}]D(x,z)}{H_1L(e^{a_1H_1}-1)}$$

$$= -\frac{BD_1[A_{1z}(D_1-D_2)E_1H_1Q_0^{H_1}-A_{1z}A_{10}b(E_1+1)-A_{10}(D_1-D_2)E_1H_1Q_z^{H_1}]}{100D(e^{b(L+\delta)}-1)A_{10}^2}$$

where $A_{10} = LP_0^{H_1}-(D_1-D_2)H_0xQ_0^{H_1}$

$$A_{1z} = LP_z^{H_1}-(D_1-D_2)H_0xQ_z^{H_1}$$

$$E_1(x) = e^{b(L+\delta-x)}-1$$

At the interface, $z=0$, the vertical velocity is reduced to

$$W_1(x,0) = \frac{BbD_1Le^{b(L+\delta)}}{100(e^{b(L+\delta)}-1)[LD_0-(D_1-D_2)x]}$$

Similarly in the lower layer; at any cross wedge section, the transport in the lower layer is the residual of transport in the upper layer from the transport at $x=L$:

$$\int_{H_{(x)}}^{0}\int_{y_1}^{y_2} U_2(x,z)\,dydz = -\frac{e^{b(L+\delta-x)}-1}{e^{b(L+\delta)}-1}\int_{0}^{H_1}\int_{y_1}^{y_2} U_1(0,z)\,dydz + T$$

$$= \frac{B}{100} D_1 \frac{e^{b(L+\delta-x)} - e^{b\delta}}{e^{b(L+\delta)} - 1}$$

Again, since

$$\int_{H_{(x)}}^{0}\int_{y_1}^{y_2} U_2(x,z)\,dydz = \int_{H_{(x)}}^{0} U_2(x,z) D(x,z)\,dz$$

$$= \frac{u_2(x)}{H_1 L(e^{a_2 H_{(x)}} - 1)} \int_{H_{(x)}}^{0} [(D_1 - D_0)Lz + D_0 H_1 L - (D_1 - D_2)H_1 x](e^{a_2 z} - 1)dz$$

$$= \frac{u_2(x)}{H_1 L(e^{a_2 H_{(x)}} - 1)} [LR^0_{H_{(x)}} - (D_1 - D_2)H_1 x S^0_{H_{(x)}}]$$

where $\mathrm{R}_c^d = \int_c^d [(D_1 - D_0)z + D_0 H_1](e^{a_2 z} - 1)dz$

$$S_c^d = \int_c^d (e^{a_2 z} - 1)dz$$

we find then that

$$u_2(x) = \frac{D_1 H_1 LB(e^{a_2 H_{(x)}} - 1)(e^{b(L+\delta-x)} - e^{b\delta})}{100(e^{b(L+\delta)} - 1)[LR^0_{H_{(x)}} - (D_1 - D_2)H_1 x S^0_{H_{(x)}}]}$$

$$U_2(x,z) = \frac{D_1 H_1 LB(e^{a_2 z} - 1)(e^{b(L+\delta-x)} - e^{b\delta})}{100(e^{b(L+\delta)} - 1)[LR^0_{H_{(x)}} - (D_1 - D_2)H_1 x S^0_{H_{(x)}}]}$$

To find the vertical velocity in the lower layer, we integrate (7) from z to 0 with respect to z,

$$W_2(x,0)D(x,0) - W_2(x,z)D(x,z) = -\int_z^0 \frac{\partial}{\partial x} U_2 D dz$$

$$= -\frac{\partial}{\partial x} \frac{u_2(x)[LR_z^0 - (D_1 - D_2)H_1 x S_z^0]}{H_1 L\left(e^{a_2 H_{(x)}} - 1\right)}$$

$$= \frac{BD_1}{100(e^{b(L+\delta)} - 1)} \left\{ \frac{A_{20} A_{2z} b(E_1 + 1) + A_{20}(D_1 - D_2)H_1\left(e^{b(L+\delta-x)} - e^{b\delta}\right)S_z^0}{A_{20}^2} \right.$$

$$- \frac{A_{2z}\left(e^{b(L+\delta-x)} - e^{b\delta}\right)\left\{(D_1 - D_2)H_0 H_1 x - H_0 L\left[(D_1 - D_0)H_{(x)} + H_1 D_0\right]\right\}\left(e^{a_2 H_{(x)}} - 1\right)}{A_{20}^2 L}$$

$$\left. - \frac{A_{2z}(D_1 - D_2)H_1 L S_{H_{(x)}}^0\left(e^{b(L+\delta-x)} - e^{b\delta}\right)}{A_{20}^2} \right\}$$

where $A_{20} = LR_{H_{(x)}}^0 - (D_1 - D_2)H_1 x S_{H_{(x)}}^0$

$$A_{2z} = LR_z^0 - (D_1 - D_2)H_1 x S_z^0$$

Finally we get

$$W_2(x,z) = \frac{D_1 B}{100(e^{b(L+\delta)} - 1)} \left\{ \frac{A_{20}^2 b(E_1 + 1)}{A_{20}^2} \right.$$

$$\left. - \frac{A_{20} A_{2z} b(E_1 + 1) + A_{20}(D_1 - D_2)H_1\left(e^{b(L+\delta-x)} - e^{b\delta}\right)S_z^0}{A_{20}^2} \right.$$

$$-\frac{A_{2z}\left(e^{b(L+\delta-x)}-e^{b\delta}\right)\left\{(D_1-D_2)H_0H_1x-H_0L\left[(D_1-D_0)H_{(x)}+H_1D_0\right]\right\}\left(e^{a_2H_{(x)}}-1\right)}{A_{20}^2L}$$

$$-\frac{A_{2z}(D_1-D_2)H_1LS^0_{H_{(x)}}\left(e^{b(L+\delta-x)}-e^{b\delta}\right)}{A_{20}^2}\Bigg\}$$

3.4.2 Adjustment of velocity field

The velocity field is controlled by parameters a_1 and b in the upper layer and a_2 and b in the lower layer; a_1 and a_2 determine the vertical dependence of the velocity in the upper and lower layers respectively. By choosing a large a_1 we can get strong surface intensification in the upper layer (Fig. 13) while small a_2 results in strong bottom intensification in the lower layer (Fig. 14). By changing b we can adjust the amount of intruding water in the lower layer that will reach the end of the wedge. We note that the horizontal transport from Dixon Entrance, defined as T above (equation (6)), may be expressed as

$$T=\frac{BD_1}{100}\left(\frac{e^{b\delta}-1}{e^{b(L+\delta)}-1}\right)$$

The parameter δ determines the value of T; as seen in (13), $x=L+\delta$ would be the location where the upper layer transport vanishes. Figures 13-15 show velocity profiles in the upper and lower layers for various values of a_1 and a_2, and along the axis of the wedge for various value of b. A two dimensional "vector diagram" of the flow field is shown in Fig 16 for $a_1 = 0.1/H_1$, $a_2 = -1/H_0$, $b = 0.01/L$, and $\delta = 0$, corresponding to no inflow from the north end, and $\delta = 0.2L$, (Fig. 17) which corresponds to $T/(BD_1/100)=0.165$. Therefore we can determine how far the bottom water can intrude before it upwells into the upper layer. If we

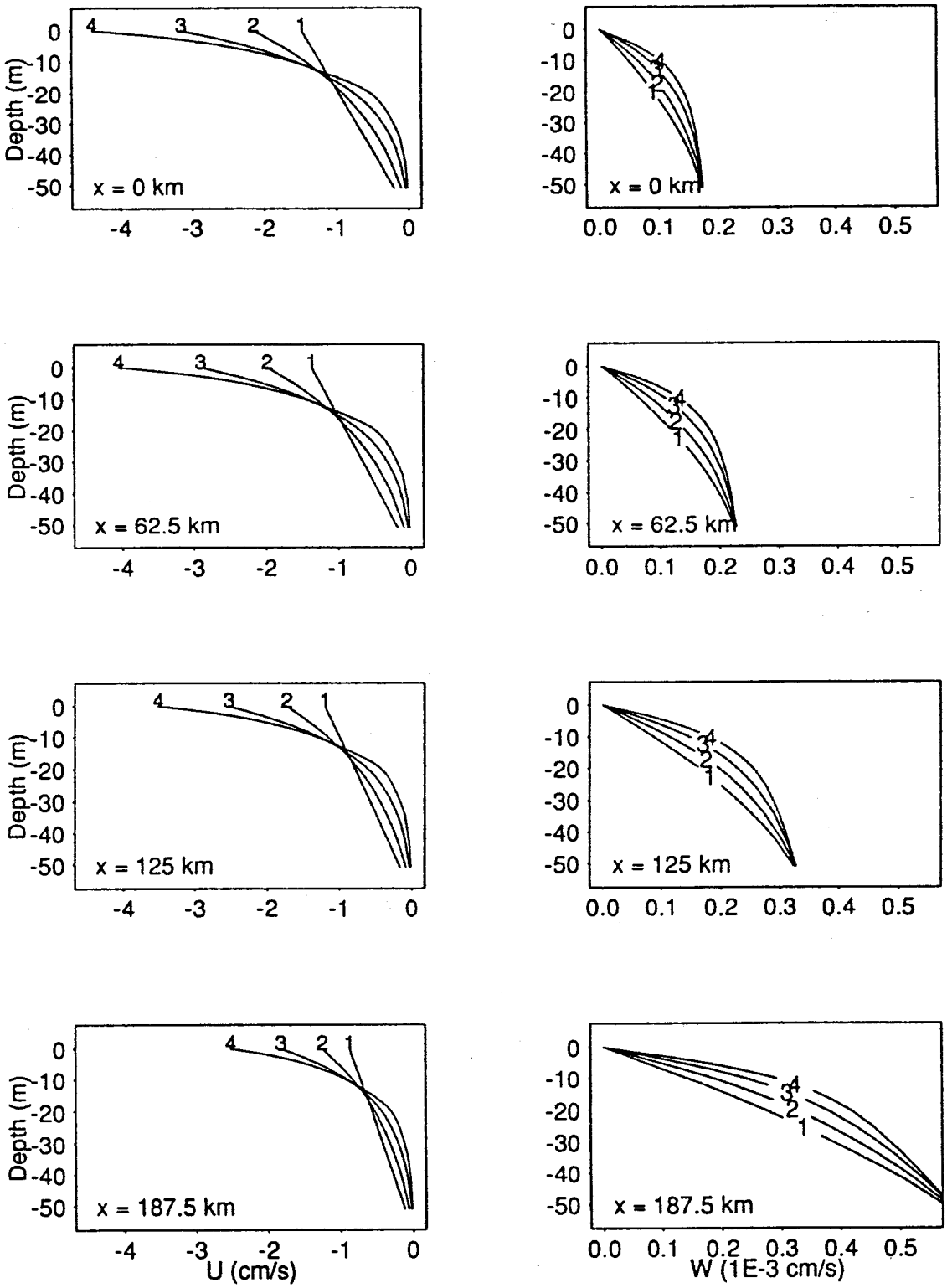

Figure 13 Velocity profiles for different a_1 in upper layer at four selected locations. Curves 1,2,3 and 4 correspond to $a_1 = 0.1, 1.1, 2.1$ and 3.1

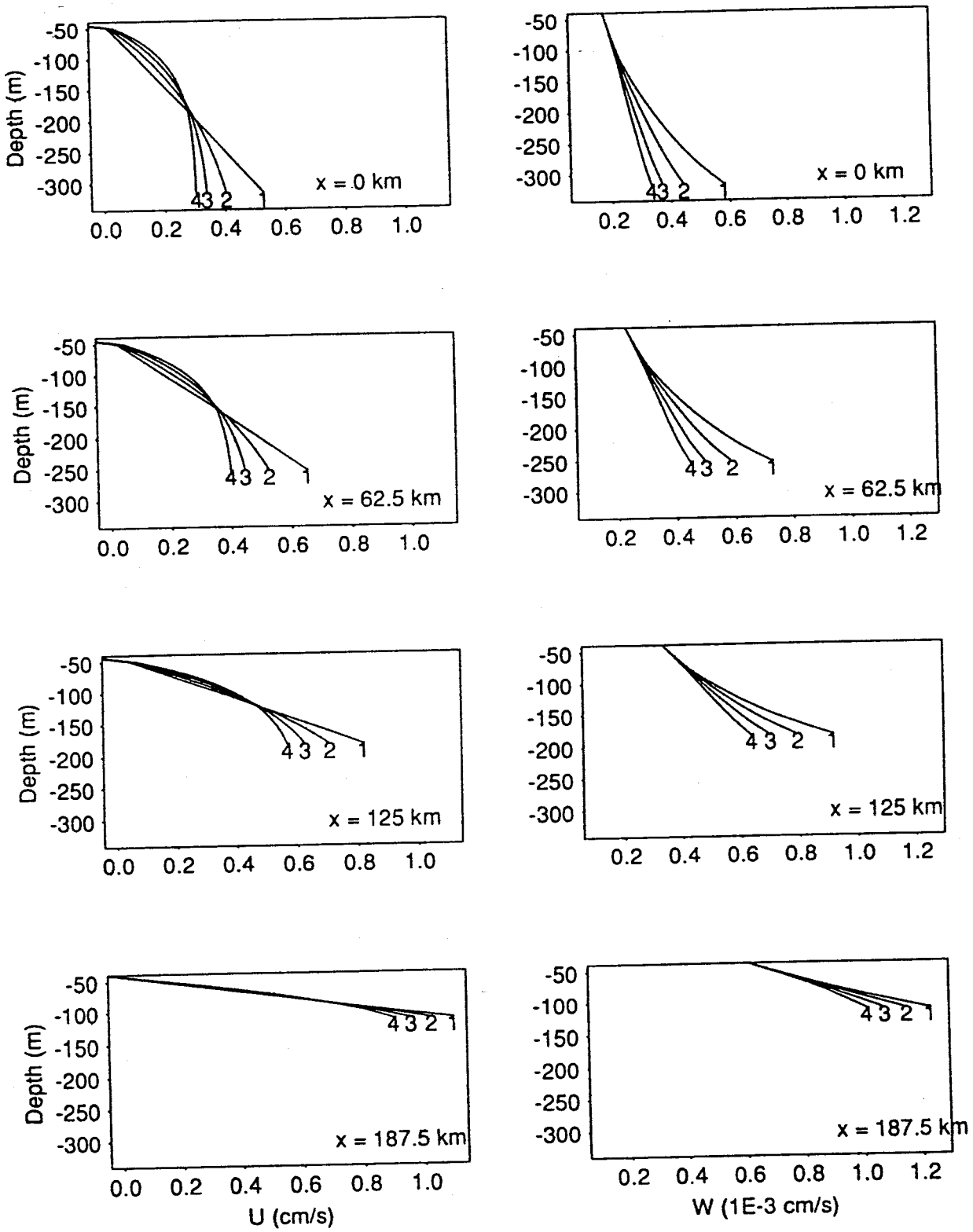

Figure 14 Velocity profiles for different a_2 in lower layer at four selected locations. Curves 1, 2, 3 and 4 correspond to a_2 =0.05, 1.05, 2.05and 3.05.

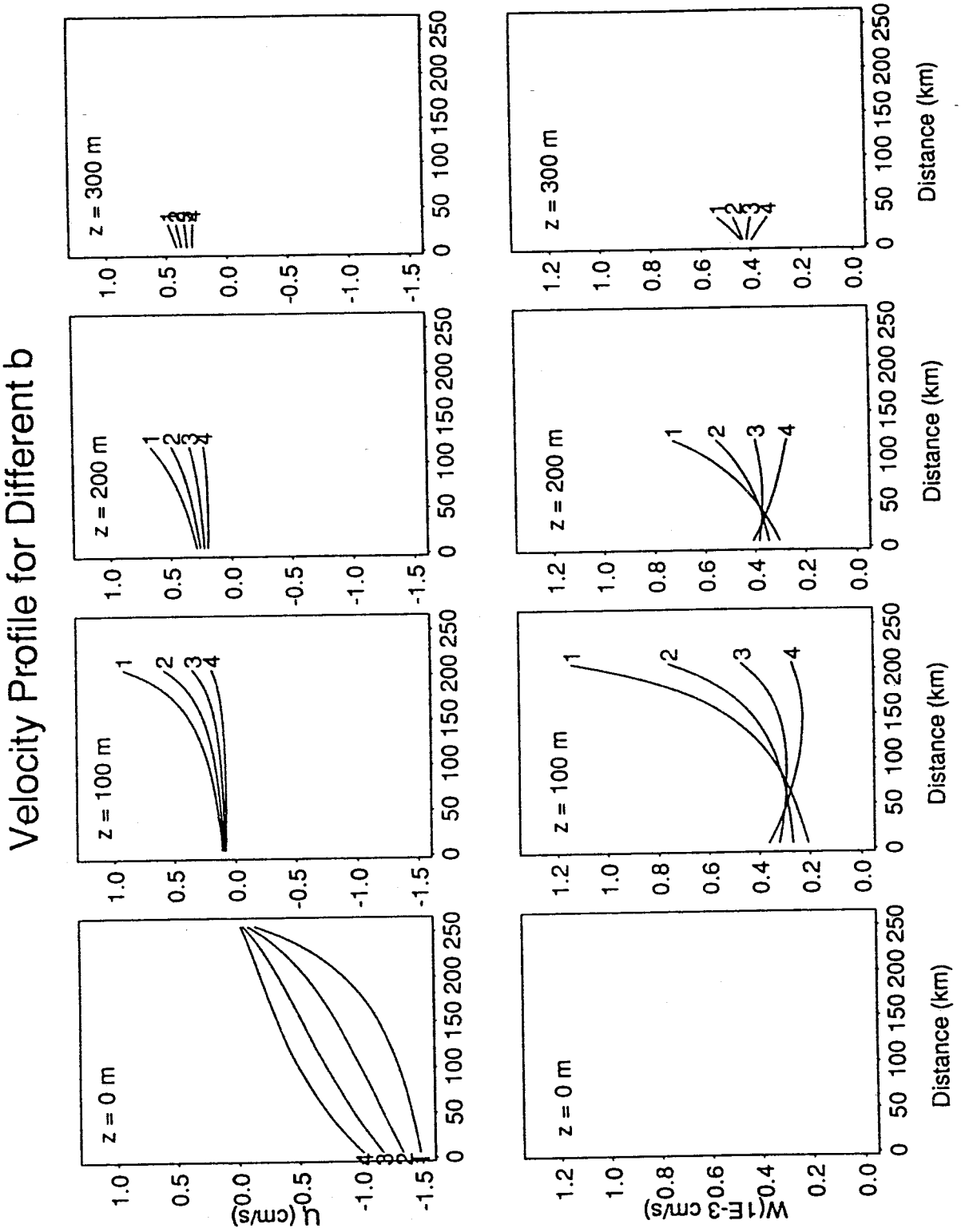

Figure 15 Velocity profiles for different b.at fout selected depths. Curves 1, 2, 3 and 4 correspond to b=0.01, 1.01, 2.01 and 3.01

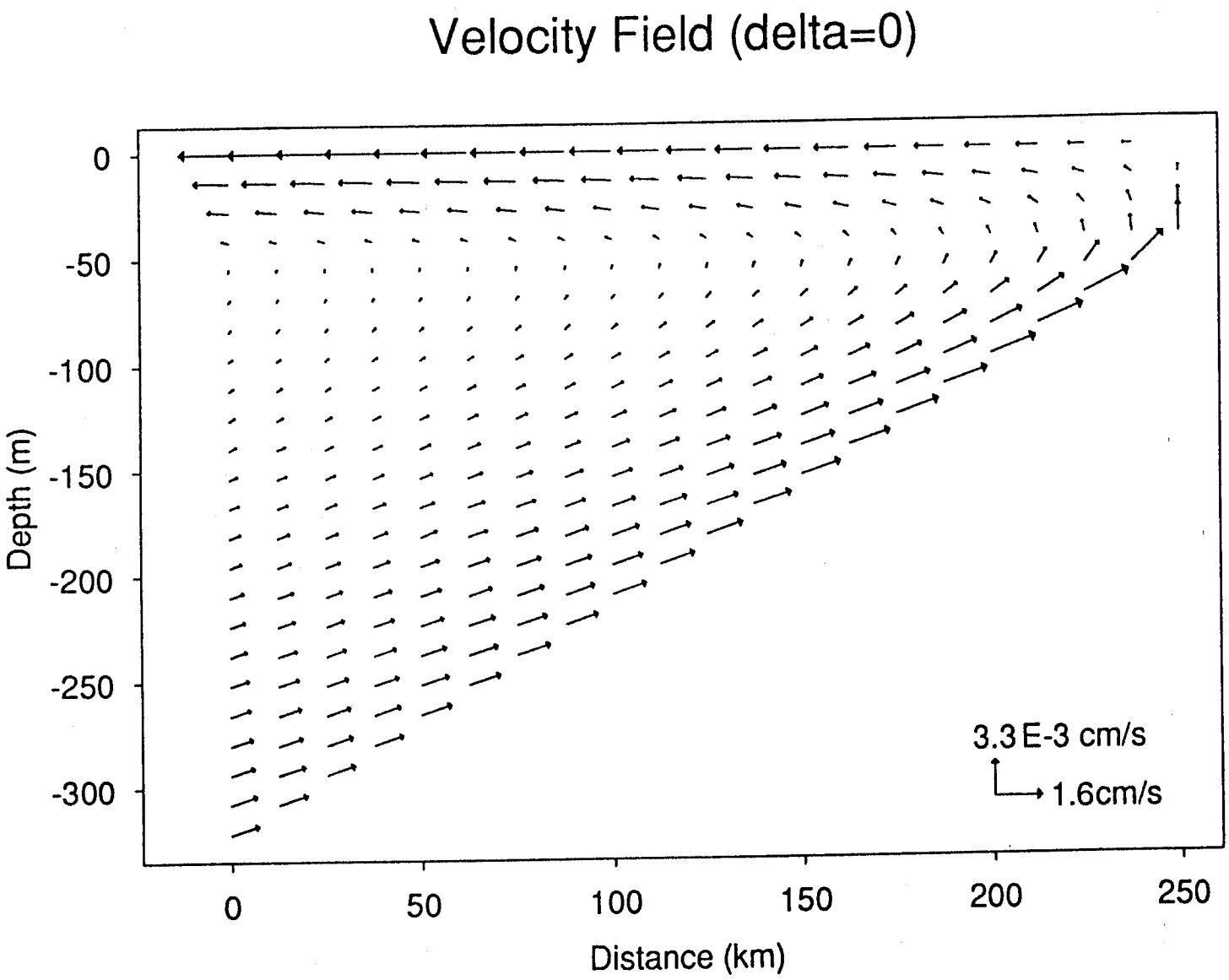

Figure 16 Modeled velocity field for δ=0.

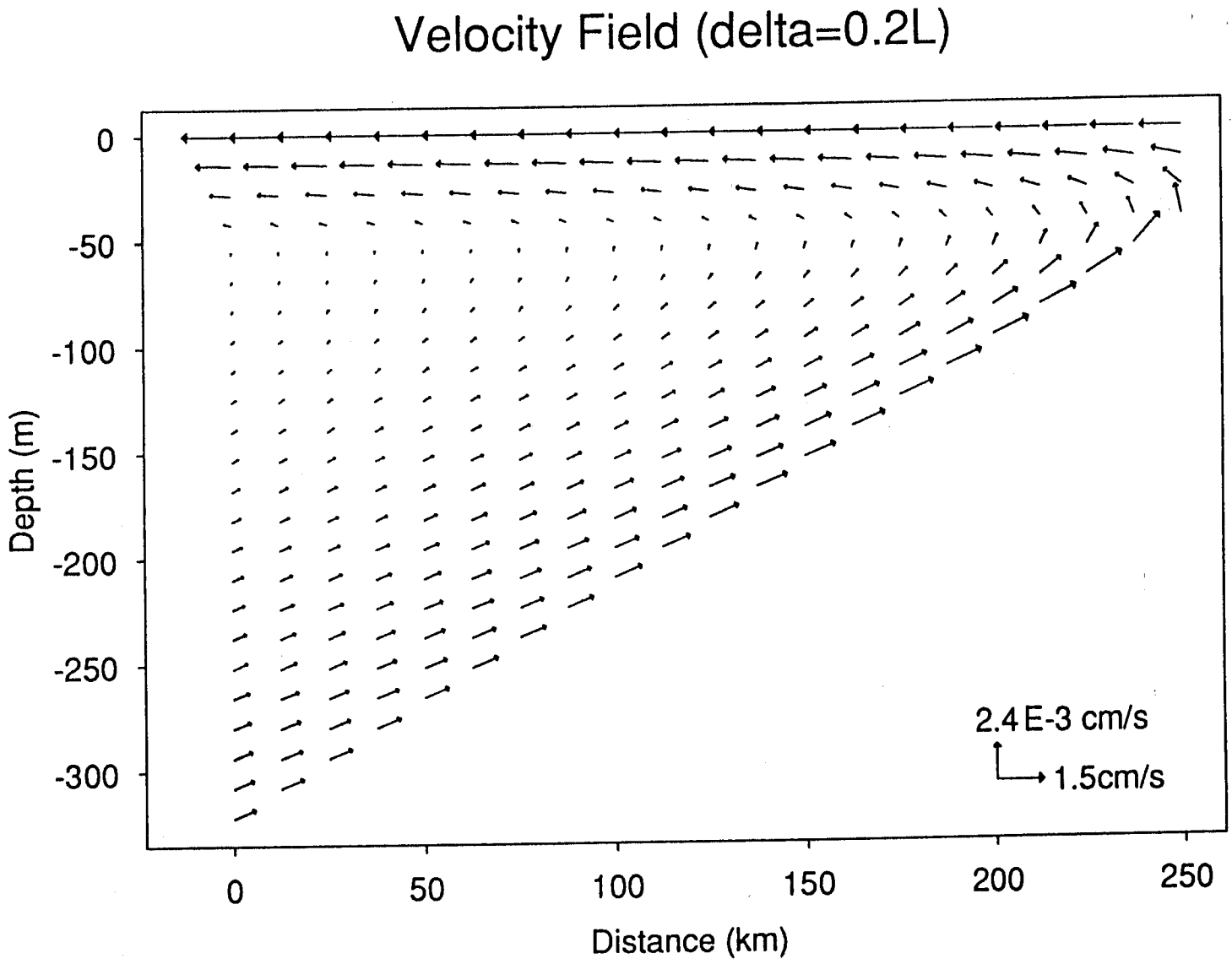

Figure 17 Modeled velocity field for δ=0.2L.

choose a smaller b, we can get stronger current near the northern end of the wedge. (Fig. 15)

3.4.3 Determination of Solar Radiation in the Upper layer

The amount of solar energy which reaches the sea surface is affected by many factors, such as the elevation of the Sun, the cloudiness of the sky, the molecular scattering and absorption and scattering by aerosols, etc., in addition, the amount of solar energy absorbed by the ocean depends upon the optical property of the sea water, the penetration angle and the sea surface roughness and so on.(Ivanoff, 1977)

In this thesis, a simple formula of the penetrating component of solar radiation is used as follows

$$I(z,t) = I_0(t)e^{\gamma z} \tag{13}$$

where $I_0(t)$ is a time series of monthly mean solar irradiation at ground level at Cape St. James (51°20'N, 130°30') for clear weather (Table 1); γ is the attenuation coefficient which varies with depth (Table 2).

Table 1 Monthly mean solar irradiance at ground level during clear weather at Cape St. James (Cal cm^{-2} day^{-1}) obtained from Atmospheric Environment Service(AES)

month	Jan.	Feb.	Mar.	Apr.	May	Jun.	Jul.	Aug.	Sep.	Oct.	Nov.	Dec.
$I_0(t)$	159	270	438	608	729	780	742	628	474	318	190	131

Table 2 Attenuation coefficients for total downward irradiance at depths 0-80 m (from Ivanoff, 1977)

depth(m)	0 - 5	5 - 10	10 - 20	20 - 40	40 - 60	60 - 80
γ (m^{-1})	0.26	0.04	0.04	0.04	0.04	0.04

As most of the solar energy reaching sea surface is absorbed in the upper layer, the radiation term is only considered in the upper layer of the model.

3.4.4 Formulation of Temperature Field

Different simplifications of the heat equation are used in the upper layer and lower layers during the upwelling period.

In the upper layer, both the advection term and radiation term are included in the heat equation:

$$\frac{\partial T_1}{\partial t} + U_1 \frac{\partial T_1}{\partial x} + W_1 \frac{\partial T_1}{\partial z} = -\frac{1}{c_p \rho_w} \frac{\partial I}{\partial z} \tag{16}$$

In the lower layer, no radiation is considered. The change of temperature is due only to the advection of cold water:

$$\frac{\partial T_2}{\partial t} + U_2 \frac{\partial T_2}{\partial x} + W_2 \frac{\partial T_2}{\partial z} = 0 \tag{17}$$

where: T_1 is the temperature in the upper layer;

T_2 is the temperature in the lower layer;

c_p is the specific heat of water;

ρ_w is the density of the water.

U_1 is the horizontal velocity component in the upper layer;

U_2 is the horizontal velocity component in the lower layer;

W_1 is the vertical velocity component in the upper layer;

W_2 is the vertical velocity component in the lower layer;

These equations are discretized by using the finite difference method. A centered differencing scheme is applied for the spatial derivatives and the leap-frog method is used to advance the solution in time. The grid for the scheme is

6.25 km in the horizontal by 70 cm in the vertical. The time step is chosen as 600 seconds. U_i and W_i (i=1,2) are calculated once a month at each grid point according to the previously derived formulae during upwelling months.

3.4.5 Boundary conditions

Boundary conditions for the velocity field have been given in the formulation of velocity field. For the temperature field, a non-diffusive condition is applied at the bottom of the wedge and air temperature is used as the surface boundary condition. At the seaward opening of the wedge, a time dependent boundary condition is applied to reflect the seasonal variation of the water coming into the region. Information is obtained from the thermal conditions at the ocean stations on line P (Tabata and Peart, 1985).

3.4.6 Modeled results

The upwelling model is run separately for several months with a_1=0.1,a_2=1,b=0.05. The model starts from a presumed stratified ocean (Fig. 18). The velocity field is turned on at t=0. Cold water starts to come into the strait from the seaward opening at the bottom. Water in the surface layer moves out of the strait due to Ekman transport. At the same time, solar radiation works on the sea surface and cause surface temperature to rise. The calculated result shows clearly cold water upwelling and surface warming (Fig. 19)

It can be seen from Fig 19 that after 4 months of upwelling the 7°C isotherm rose from 200m to about 130 m and the surface temperature increased from 7.8 °C to 11.0 °C. Upwelling was more significant in lowering the temperature along the sloping bottom, but was not strong enough to upwell cold water to the surface. Therefore on most of the study region the surface water temperature increased during an upwelling period with a reducing rate from the seaward opening to the narrow end. This is consistent with the historical data.

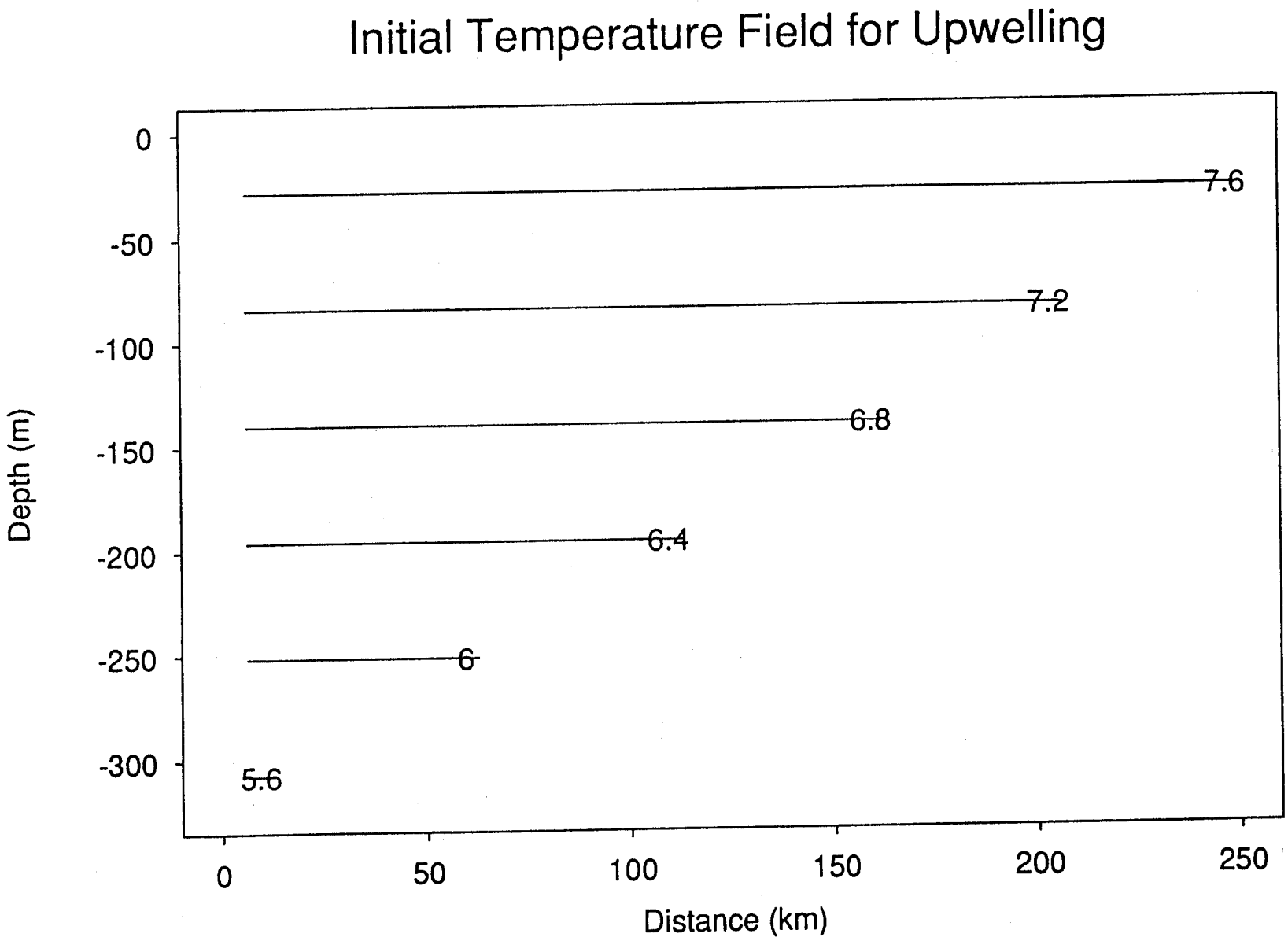

Figure 18 Initial temperature field.

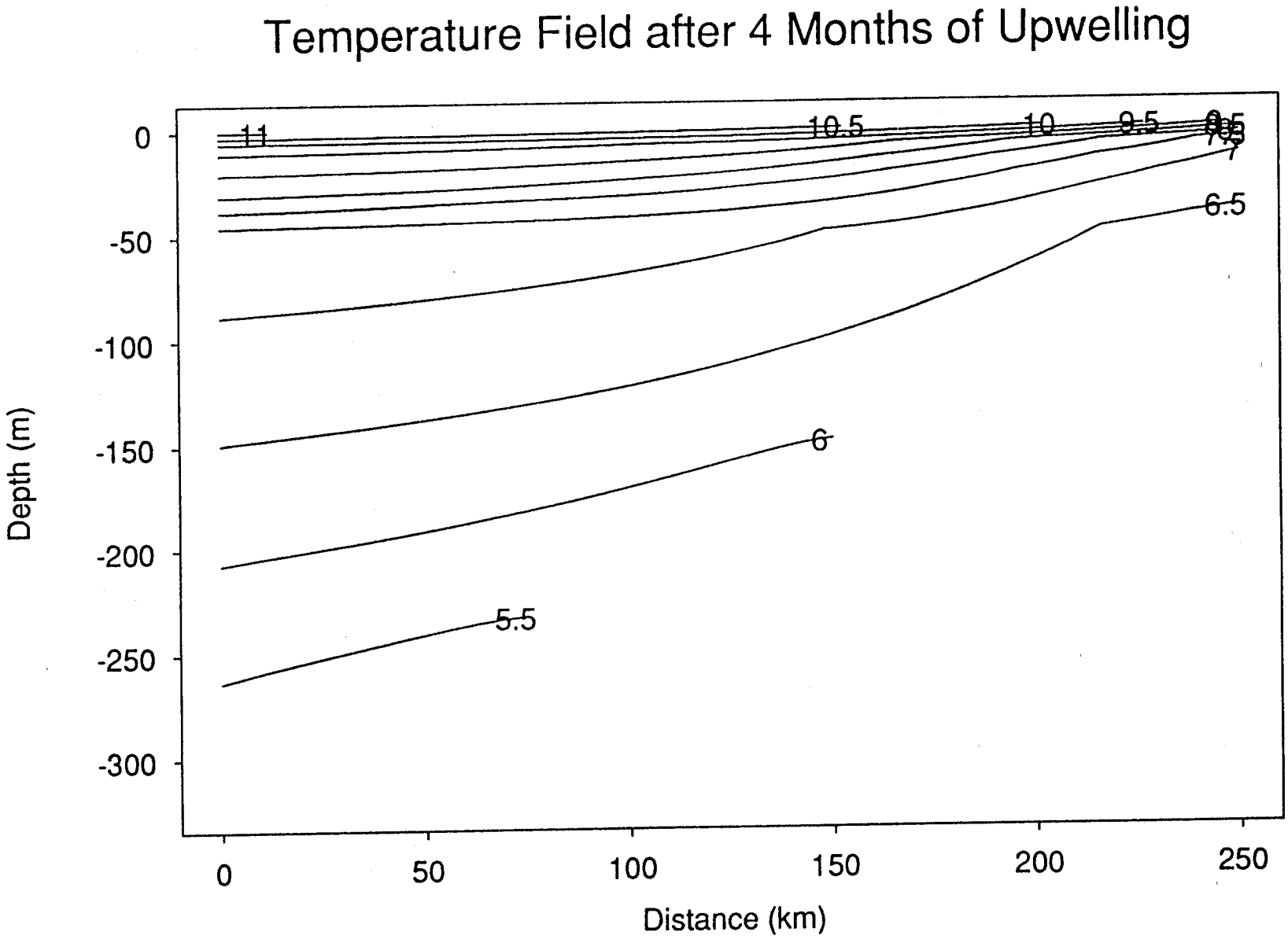

Figure 19 Temperature field after 4 months of upwelling.

3.5 Mixing/Cooling model

3.5.1 Introduction

The mixing model is applied in the months when the Bakun Index is negative.

During mixing/cooling period, a simplified Niller-Kraus one-dimensional upper mixed layer model is applied (Niller and Kraus, 1977). In this model, turbulent heat transfer at the air-sea interface generated by wind stirring and entrainment of cold water from the bottom of the mixed layer are considered. Wind stress plays a most important role in the process. No advection/convection is taken into account and the effect of topography is ignored. Therefore a uniform thickness mixed layer is formed over the whole region. Only the deepening of the mixed layer depth and the mixed layer temperature are simulated. The opposite process of creation of a mixed layer due to turbulent tidal mixing at the bottom is not included in this model, over most of which depths are too large for this effect to be important.

3.5.2 Wind forcing

Daily wind speed at Cape St. James is used in the calculation of entrainment speed, sensible and latent heat transport. In considering the elevation of the station, a factor of 0.85 was used to convert the wind speed at 89 meters high to 10 meters above sea level after a simple comparison of the mean wind speed at Cape St. James and at 7 meters above the sea surface from a buoy near Cape St. James.

3.5.3 Radiation and effective back radiation.

In calculating the heat flux at the air-sea interface, daily solar radiation is obtained from the monthly mean radiation normal at Cape St. James by linear

interpolation.

The effective back radiation is calculated at each time step as (Rosemary and Walker, 1990):

$$H_b = -E\sigma T_1^4 (0.39 - 0.05 e_a^{1/2})(1 - 0.83C) \quad (18)$$

where E is the emmisivity;

σ is the Stefan-Boltzman constant;

T_1 is water temperature in the upper mixed layer;

e_a is the vapor pressure at the sea surface;

C is the cloud coverage in tenths for the region.

3.5.4 Sensible heat flux

Similarly, the turbulent flux of sensible heat is calculated at each time step from (Pickard and Emery, 1990):

$$H_s = -1.88V(T_1 - T_a) \quad (19)$$

where V is the daily mean wind speed;

T_a is the daily mean air temperature interpolated from climate normal.

3.5.5 Latent heat flux

The latent heat flux is calculated at the same time as sensible heat from (Pickard and Emery, 1990):

$$H_e = 1.4(e_s - e_a)V(2494 - 2.2T_1)10^{-3} \quad (20)$$

where e_s is the saturated vapor pressure;

The latent heat flux is calculated at each time step.

3.5.6 Entrainment speed

From Stigebrandt (1981) the entrainment speed is obtained from:

$$We = \frac{2}{gHa(T_1 - T_2)}\left[\frac{\rho_a}{\rho_w} mC_{10}V^3 - \frac{gHa}{2\rho c_p}(I_0 - H_b - H_s - H_e) + \frac{gI_0 a}{\rho c_p \gamma}\right] \qquad (21)$$

where T_2 is the water temperature below the mixed layer;

ρ_a is the air density;

ρ_w is the water density;

g is the acceleration due to gravity;

m is a constant;

C_{10} is the drag coefficient;

c_p is the heat capacity of sea water;

γ is the attenuation coefficient of radiation;

H is the mixed layer depth;

a is the coefficient of expansion;

I_0 is the incident solar radiation at the sea surface.

The above equation suggests that the entrainment speed is determined from the contribution of wind stress; the turbulent heat flux at the air-sea interface which is the combined effect of incident solar radiation, effective back radiation, latent heat flux and sensible heat flux, and penetrating solar radiation which decreases with the increase of the attenuation coefficient. The buoyancy flux due to salinity changes is neglected. The first term in the bracket is proportional to the cube of wind speed and is always positive. It shows that the stronger the wind, the larger the entrainment speed. The second term in the bracket represents the balance between the four heat fluxes at the air-sea surface. All the fluxes into the upper layer are positive and those out of the layer are negative. In summer, when the incident radiation is strong, the inward flux is larger than the outward flux,

and the thermocline is strengthened. The increased stratification prevents entrainment from developing. In winter, when the influx is less than the outflux, the entrainment speed is increased, therefore the mixing becomes stronger. The third term in the bracket is the contribution from the penetrating part of solar radiation. It is inversely propotional to the attenuation coefficient which represents the optical properties of the sea water. Therefore the clearer the water (the smaller γ), the stronger the entrainment speed. Apart from the second term in the bracket, the contribution of the other two terms is inversely proportional to the mixed layer depth. i.e. the deeper the mixed layer depth, the weaker the entrainment speed. This results in a reduced deepening rate of the mixed layer as it gets thicker.

3.5.7 Mixed layer depth

The deepening of the mixed layer depth is determined by the entrainment speed as:

$$\frac{\partial H}{\partial t} = \Lambda W_e \tag{22}$$

where $$\Lambda = \begin{cases} 1 & W_e > 0 \\ 0 & W_e \le 0 \end{cases}$$

3.5.8 Mixed layer temperature

The mixed layer temperature is determined by the following equation:

$$\frac{\partial T}{\partial t} = -\frac{1}{H}\left[\frac{1}{\rho c_p}\left(H_b + H_s + H_e\right) + (T_1 - T_2)W_e + \frac{I_0}{\rho c_p}\left(1 - e^{-\gamma H}\right)\right] \tag{23}$$

The change of the mixed layer temperature is controlled by the balance of

turbulent heat flux at the sea surface, the entrainment of cold water from below, and absorption of penetrating solar radiation. It also shows that the deeper the mixed layer depth, the slower the bulk temperature changes.

3.5.9 Model results

The above equations are discretized and integrated with time. As a test the model was run separately for the winter months. It started from $t=t_0$ with an initial mixed layer depth of H_0 , which is assumed to be the same as the diurnal thermocline depth, and with an initial mixed layer temperature T_0 , which is obtained by mixing the stratified upper layer of depth H_0 to uniform. The integration is performed at each horizontal grid point and leads to a uniform upper mixed layer on the surface of the region. It should be pointed out that since this model does not take into account tidal mixing on the bottom,which may be important in shallow areas, the result of the model deviates more in the shallow waters.

The mixing/cooling model was run for four months using data from October 1954 to January 1955. Calculation shows that, after 120 days of mixing, the mixed layer deepens from 5 meters to about 300 meters. The mixed layer temperature decreased from 8.2°C to 6.6 °C. (Fig. 20).

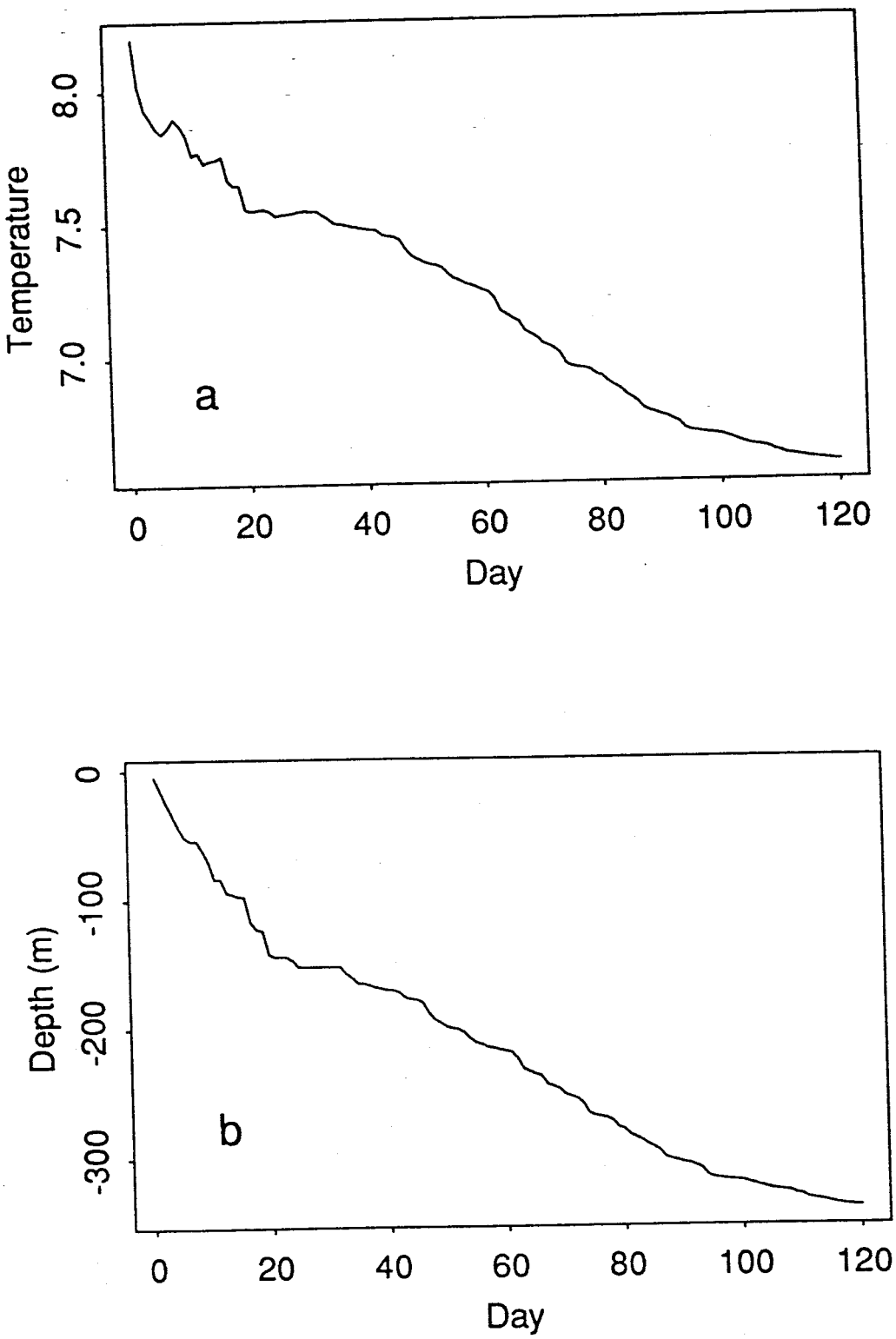

Figure 20 Results from the mixing model
a) change of the mixed layer temperature
b) change of the mixed layer depth

4 Coupled upwelling-mixing model

It is assumed that upwelling and mixing are two distinct processes. When the Bakun Index is positive, upwelling is the dominant process in the area. No turbulent mixing is considered during the upwelling period. When the Bakun Index is negative, the current in the area is assumed weak, turbulent mixing becomes the dominant process in the change of temperature and the mixing model is used. These two processes do not exist simultaneously.

4.1 Forcing conditions

In the upwelling period wind stress, as parameterized by the Bakun Index, and solar radiation are the only forcing terms to the model. Air temperature is used as a boundary condition at the sea surface. The wind drives the velocity field and the water in the wedge moves following the conservation of mass. Figure 21 shows the time series of monthly mean Bakun Index for the period 1953-1989. Only the positive values which imply upwelling are used to derive the velocity field.

During the cooling period, wind forcing at the sea surface, solar radiation and the turbulent heat flux at the air-sea interface are considered. Figure 22 shows the daily wind speed at Cape St. James. Since the station on Cape St. James is 89 meters high above the sea level, an attempt has been made to convert these values to wind speed at 10 meters above the sea surface. A simple factor of 0.8 was chosen after a comparison between the mean wind speed at Cape St. James (6.95 m/sec) and mean over-the-ocean winds (5.63 m/sec) measured by WOTAN anemometers on a surface buoy near Cape St. James. The average was applied to the period from June 4, 1982 to September 15, 1982. This is the only sea surface wind data we obtained in the area near Cape St. James. Figure 23 shows the comparison between the two time series. The mean speed is shown by a dashed

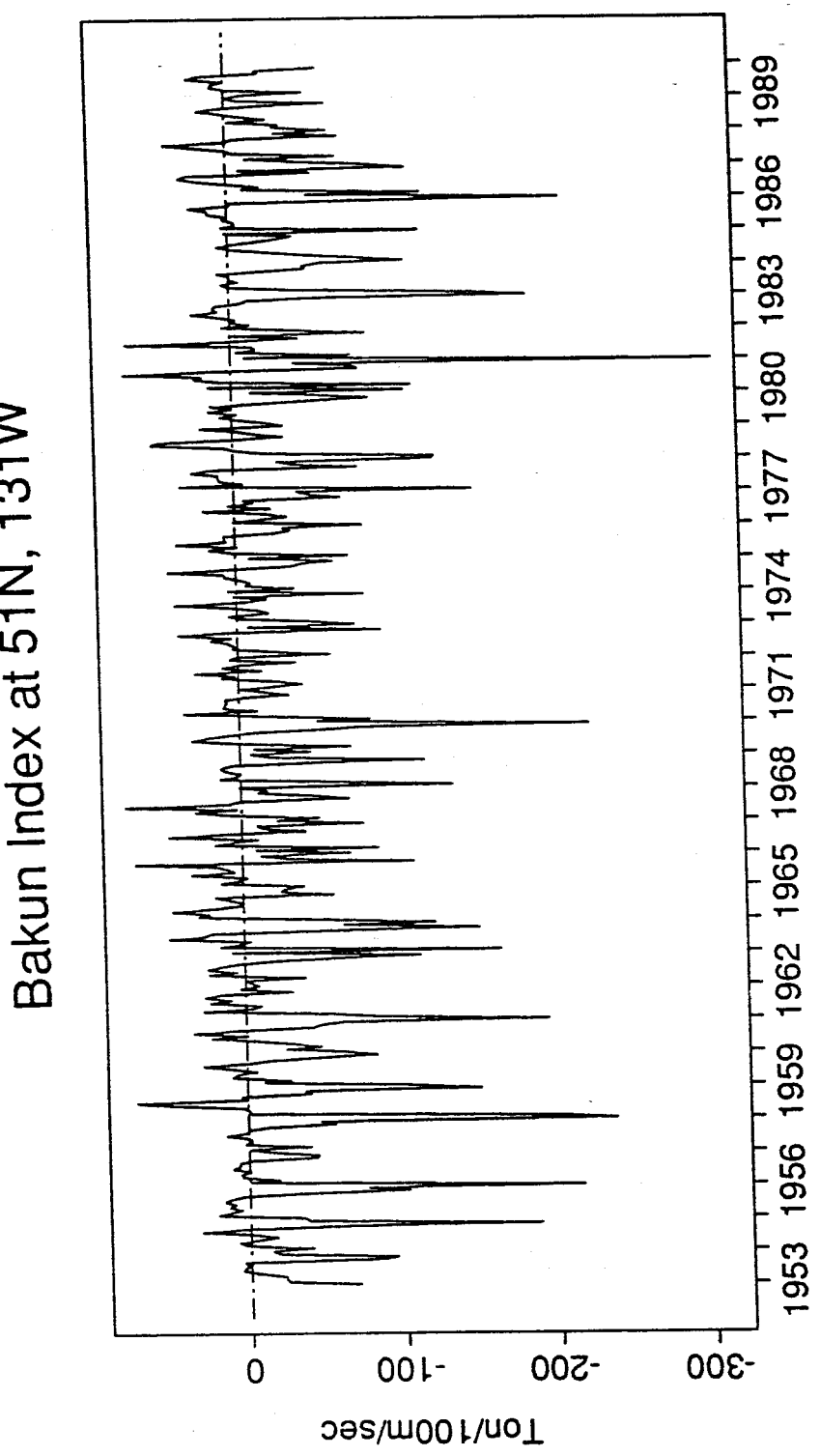

Figure 21 Monthly Bakun Index during 1953-1989

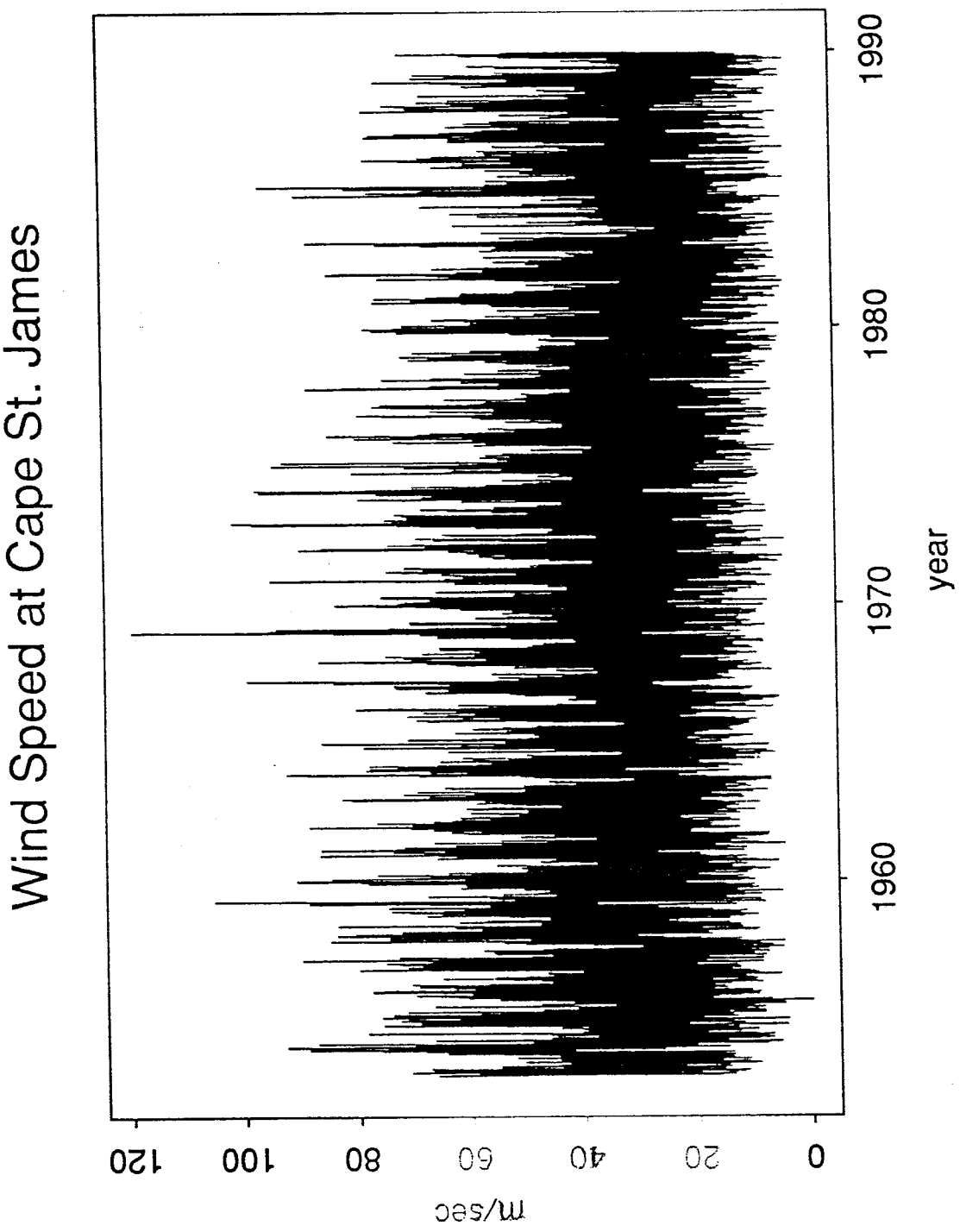

Figure 22 Daily wind speed at Cape St. James during 1953-1989

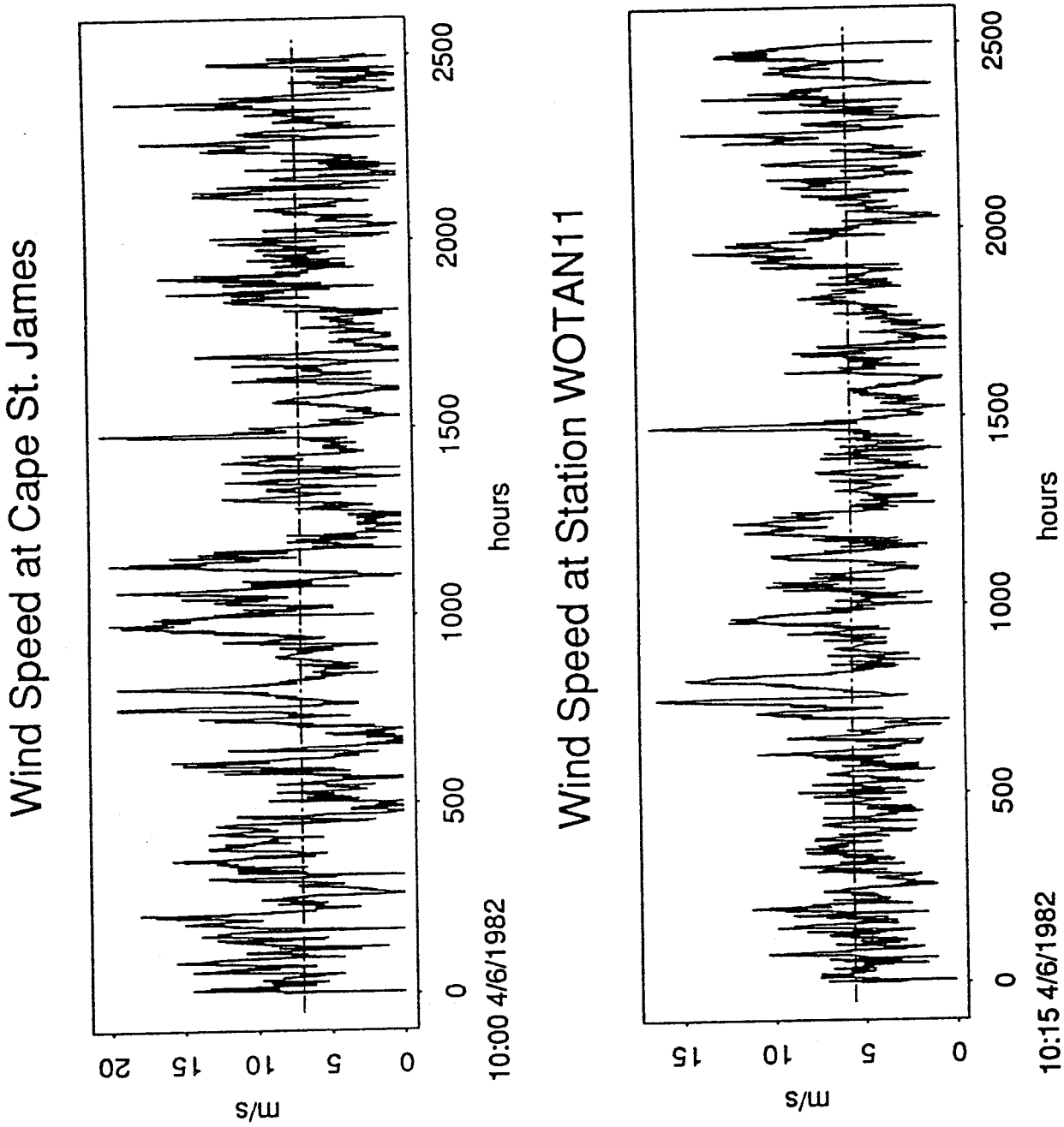

Figure 23 Comparison of wind speed at Cape St. James and WOTAN11

line on each panel.

Figure 24 shows the daily air temperature at Cape St. James obtained from the Canadian Climate Center. It was used to calculate the sensible heat flux during the mixing period and as a boundary condition for the upwelling period.

Monthly mean values of solar radiation and vapor pressure were obtained from the Canadian Climate Normals compiled by the Atmospheric Environment Service (AES). They are shown in Figure 25 and Figure 26 respectively. This means that the same values were used for each year of modeling. To obtain a smooth shift from one month to the next, these monthly mean values were interpolated linearly into daily values and are updated daily during the integration.

Cloud coverage is always a uncertain parameter to handle. A simple constant coverage of 0.15 is used in the model.

Because the longest time series of the above forcing parameters that meet the requirement of the model were obtained from Cape St. James, they were used as representative for the whole modeled area. Except for the wind data, the deviations from the sea level value due to the station elevation are ignored.

4.2 Modeled results and discussion

Running the upwelling and mixing model consecutively, temperature goes through a cooling-warming-cooling cycle. At the end of the cooling period, the model switches to upwelling. The end state of cooling period becomes the initial state of the upwelling model. A new thermocline starts from the surface on the start of the upwelling model. At the end of upwelling period, the model switches back to the cooling regime again. The end state of upwelling period becomes the initial state for the next cooling period. A new mixed layer starts from the surface. The consecutive execution of the two models generate a complete annual cycle of temperature in the study region.

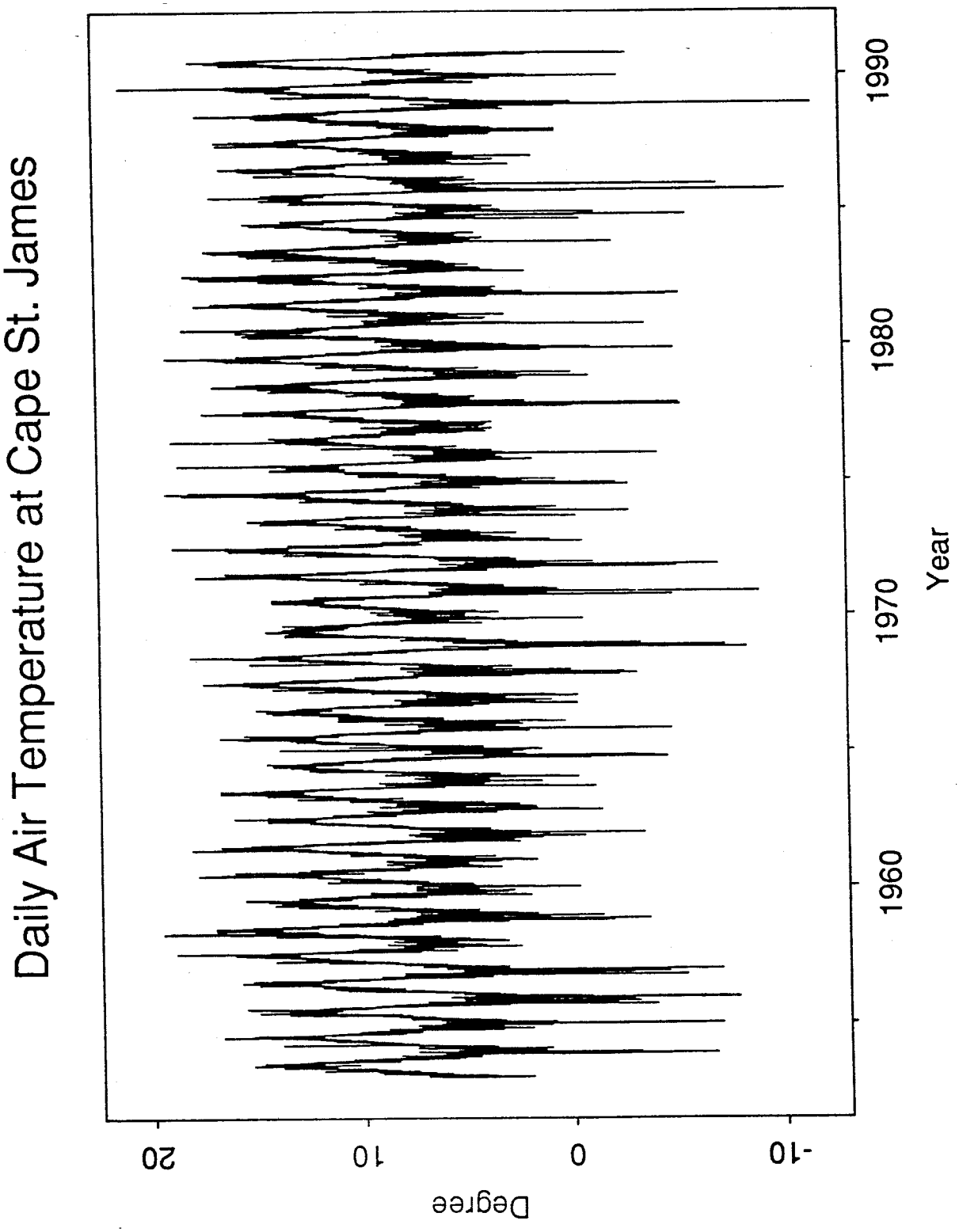

Figure 24 Daily air temperature at Cape St. James 1953-1989

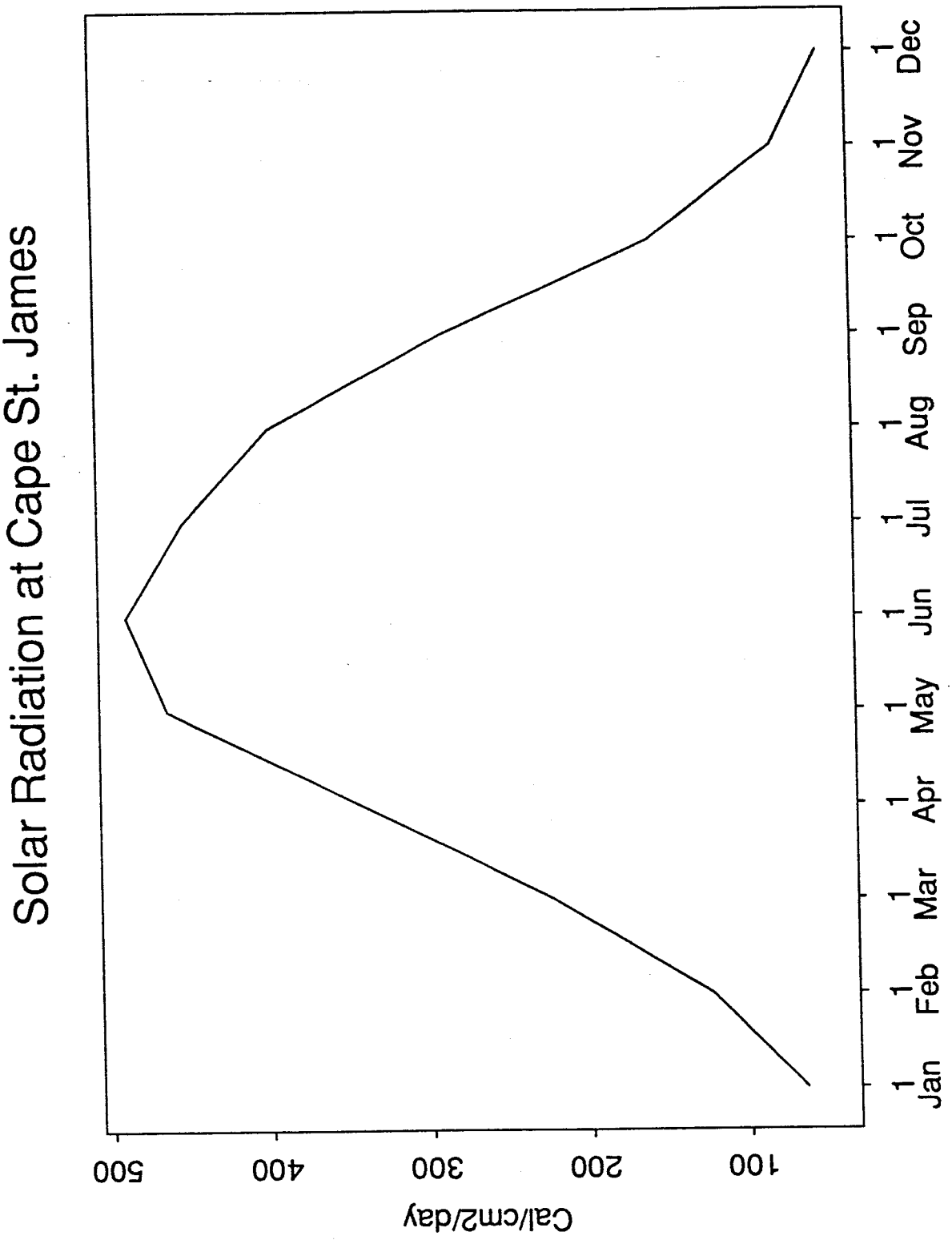

Figure 25 Solar radiation normal at Cape St. James

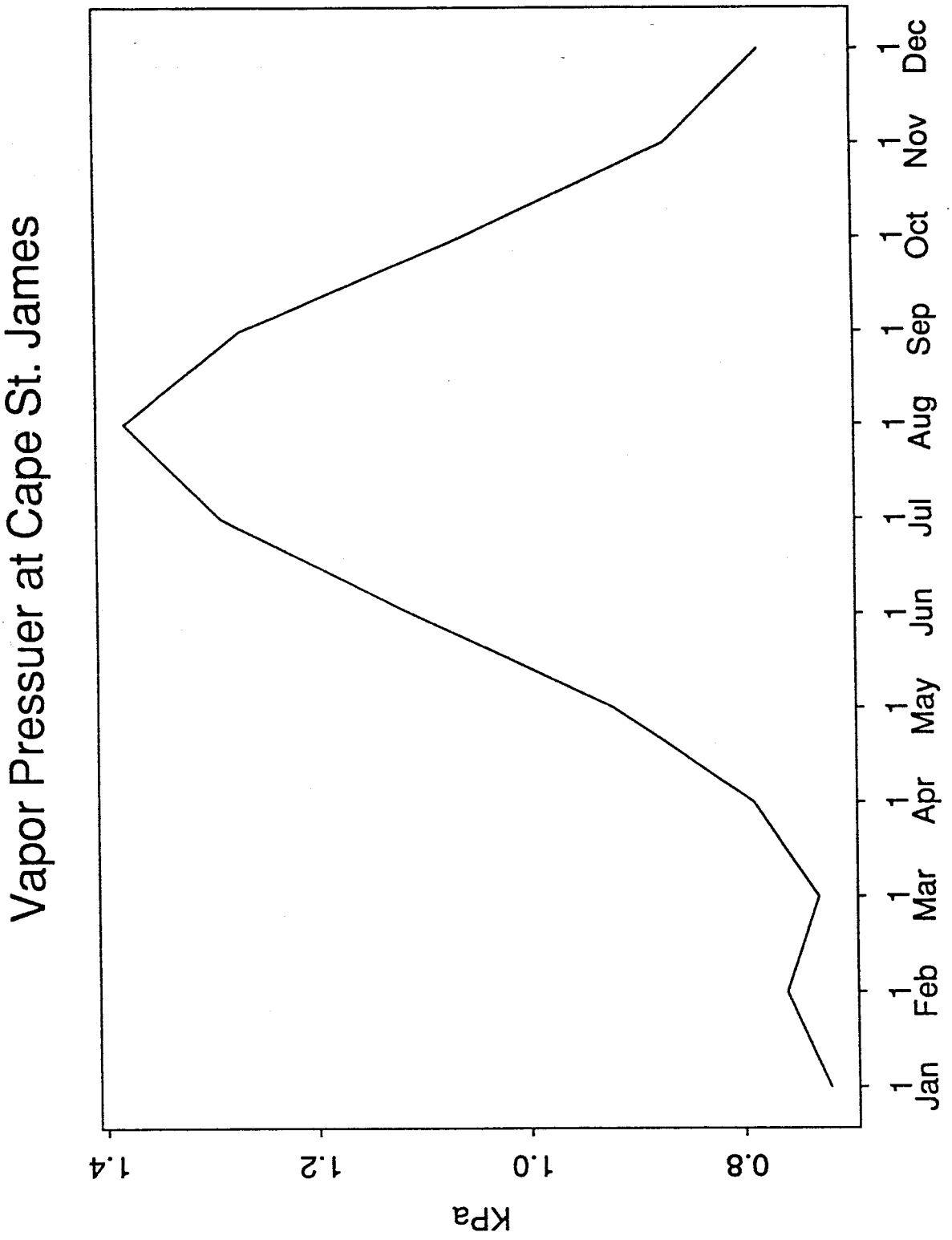

Figure 26 Vapor pressure normal at Cape St. James

The model was run from January 1951 to December 1989. To eliminate the effect of assumed initial conditions, output from the first two years of integration were dropped. Plotted results start on January 1, 1953.

Results from the coupled model of upwelling and cooling at the two locations of the wedge (Fig. 27) at four selected levels are shown in Figure 28 (a-d) and Fig. 29 (a-d) respectively. The first location is at the seaward opening of the wedge (x=0) through where the cold deep sea water is expected to come. The second location is 100 km northward from the first one (x=100 km). The four selected levels are 7m, 105m, 203m and 301m.

The same features observed by Dodimead (1980) of opposite variations in the top and bottom waters are shown in the model results. A typical year is indicated by a vertical dashed line in Fig. 28a.

The modeled temperature fields show a clear annual cycle in the upper layer, i.e. high temperature occurs in summer and lower temperature in winter, as we would expect from the boundary conditions. In the bottom layer an annual cycle shows up when both summer upwelling and winter mixing are strong. A strong upwelling brings enough cold water into the lower layer of the wedge therefore the bottom water becomes cold. A strong fall/winter mixing brings warm surface water down to the lower layer, causing the temperature there to increase.

If the winter mixing is not strong enough, then the water column is not completely mixed, the bottom water will stay cold for years until a strong mixing event happens. For instance, following the summer of 1962, cold water of 5.5 °C stayed at 300m depth at x=0 for four years until a strong mixing occurred in the winter of 1965/1966 (Fig. 28b). Similar events also happened during 1966-1968,1975-1978, etc. If the upwelling is not strong enough, the cold water can only reach a lower level, and water in a higher level will keep warm. For example during 1983 - 1985 the water temperature at x=0 at 203m depth stayed above 7.5

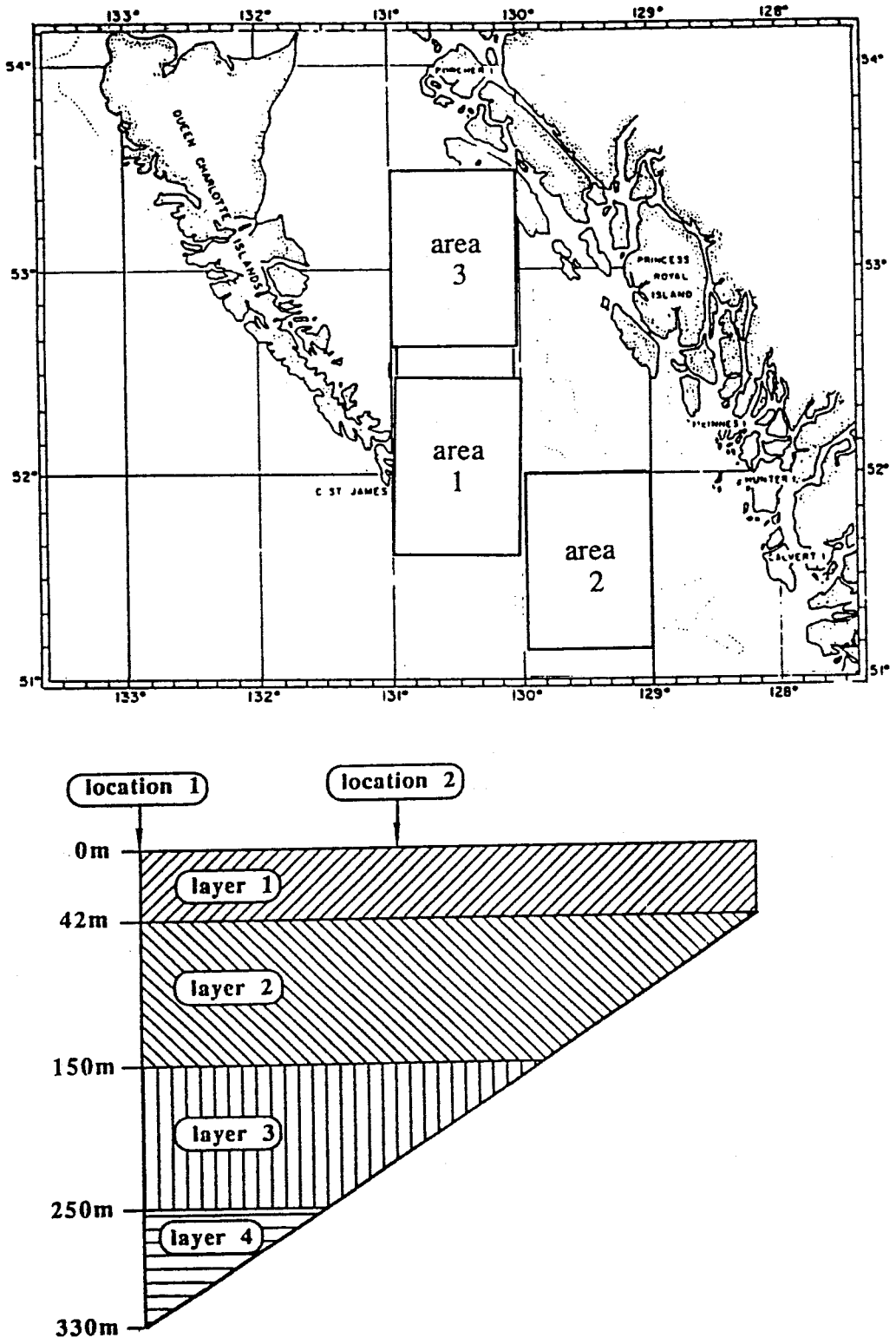

Figure 27 Locations of comparison and the layer thickness corresponding to each modeled level

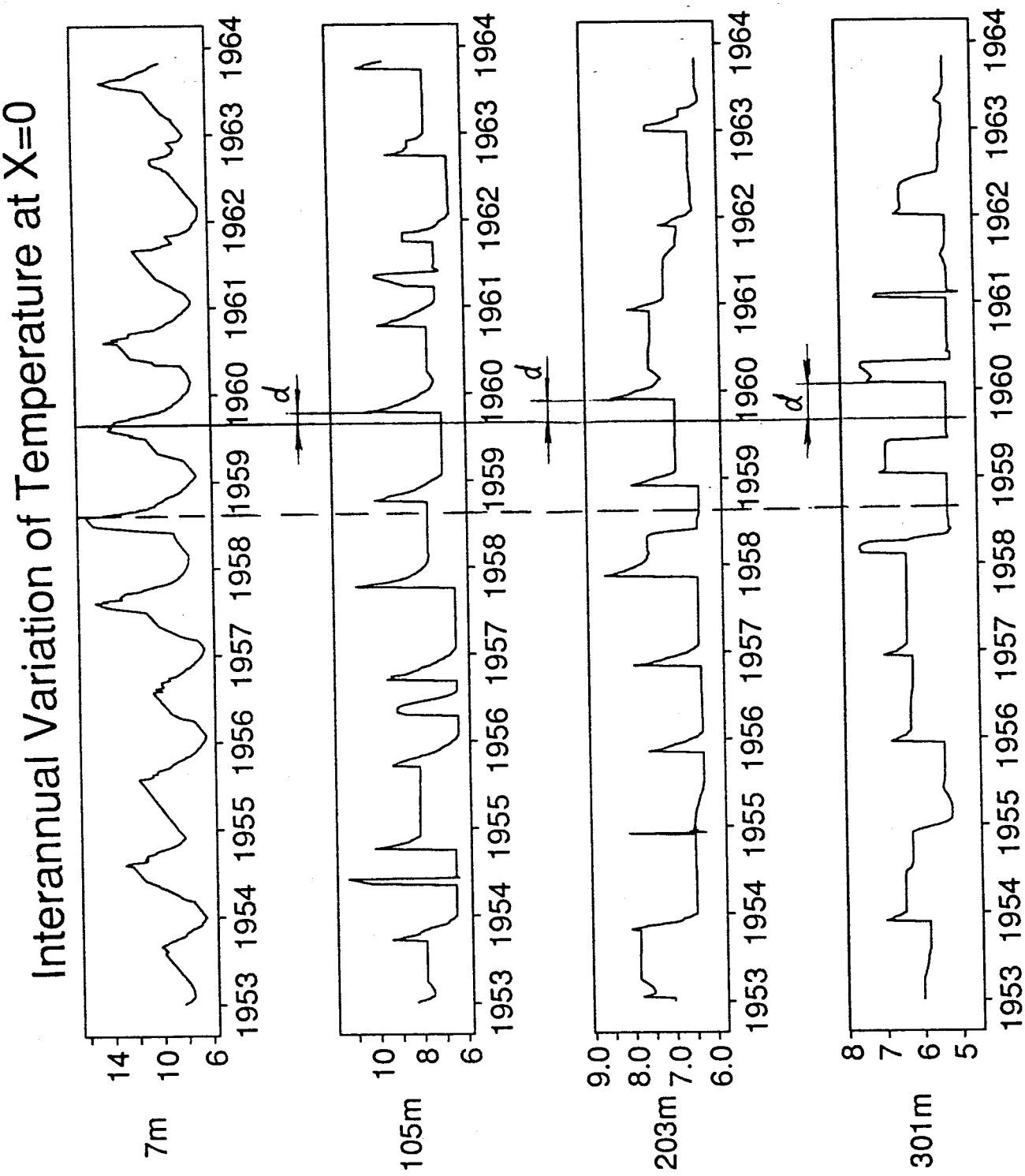

Figure 28 a) Interannual variation of Temperature at X=0 during 1953-1963. The vertical solid line shows the start of cooling; d indicates the delay at lower levels; The dashed line shows a typical example of opposite variations in the surface and the bottom layers

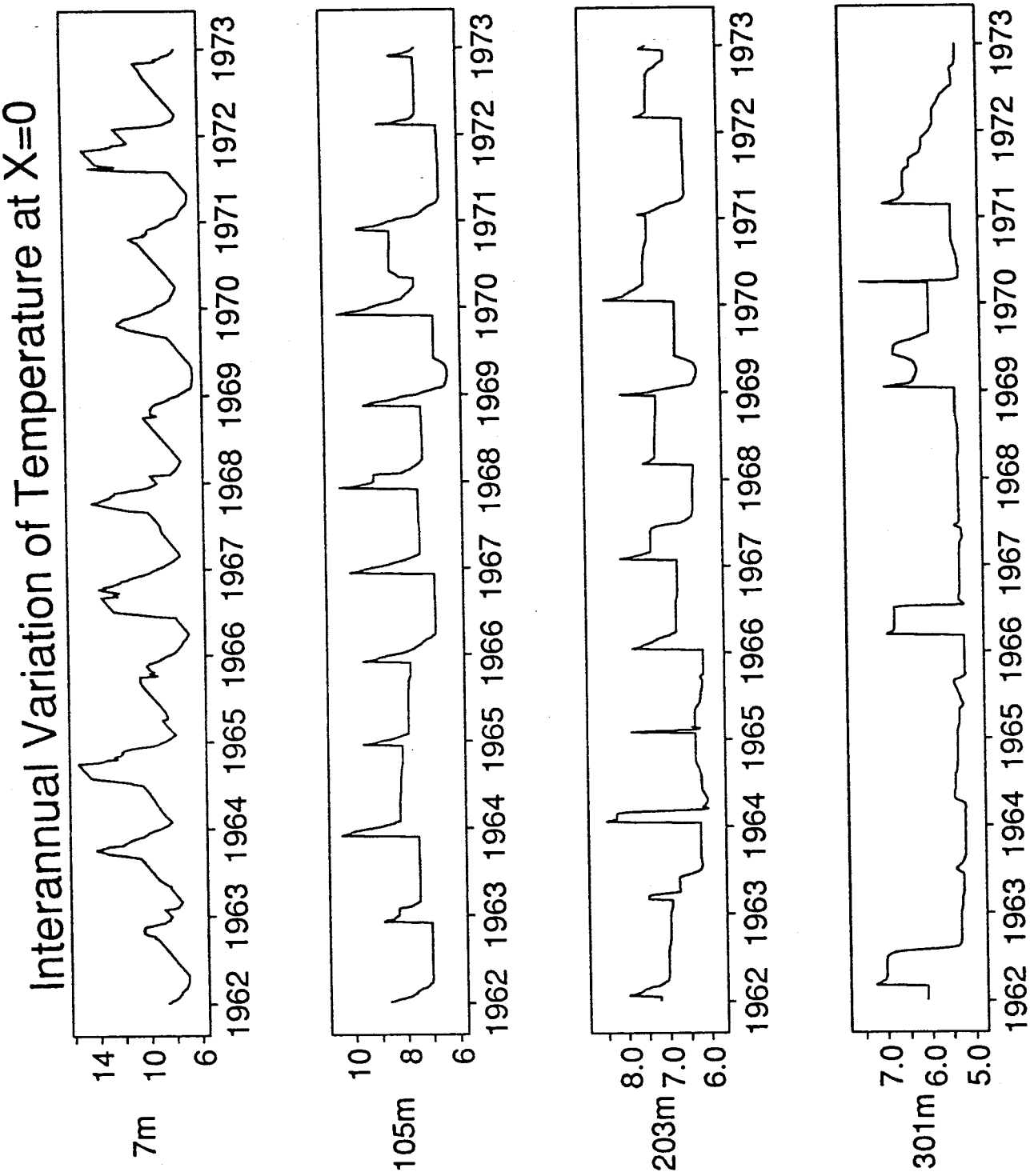

Figure 28 b) Interannual variation of Temperature at X=0 during 1962-1972

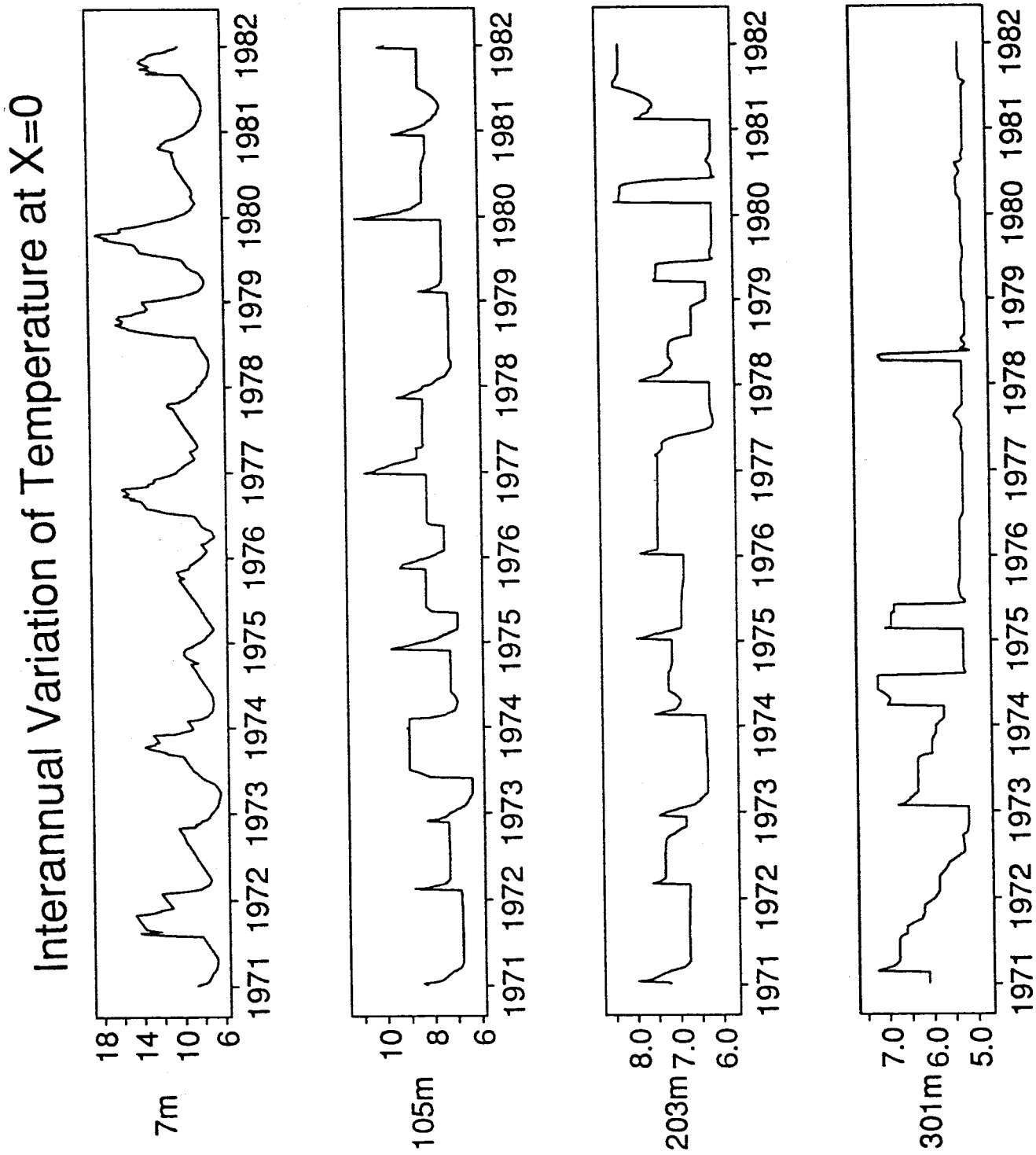

Figure 28 c) Interannual variation of Temperature at X=0 during 1971-1981

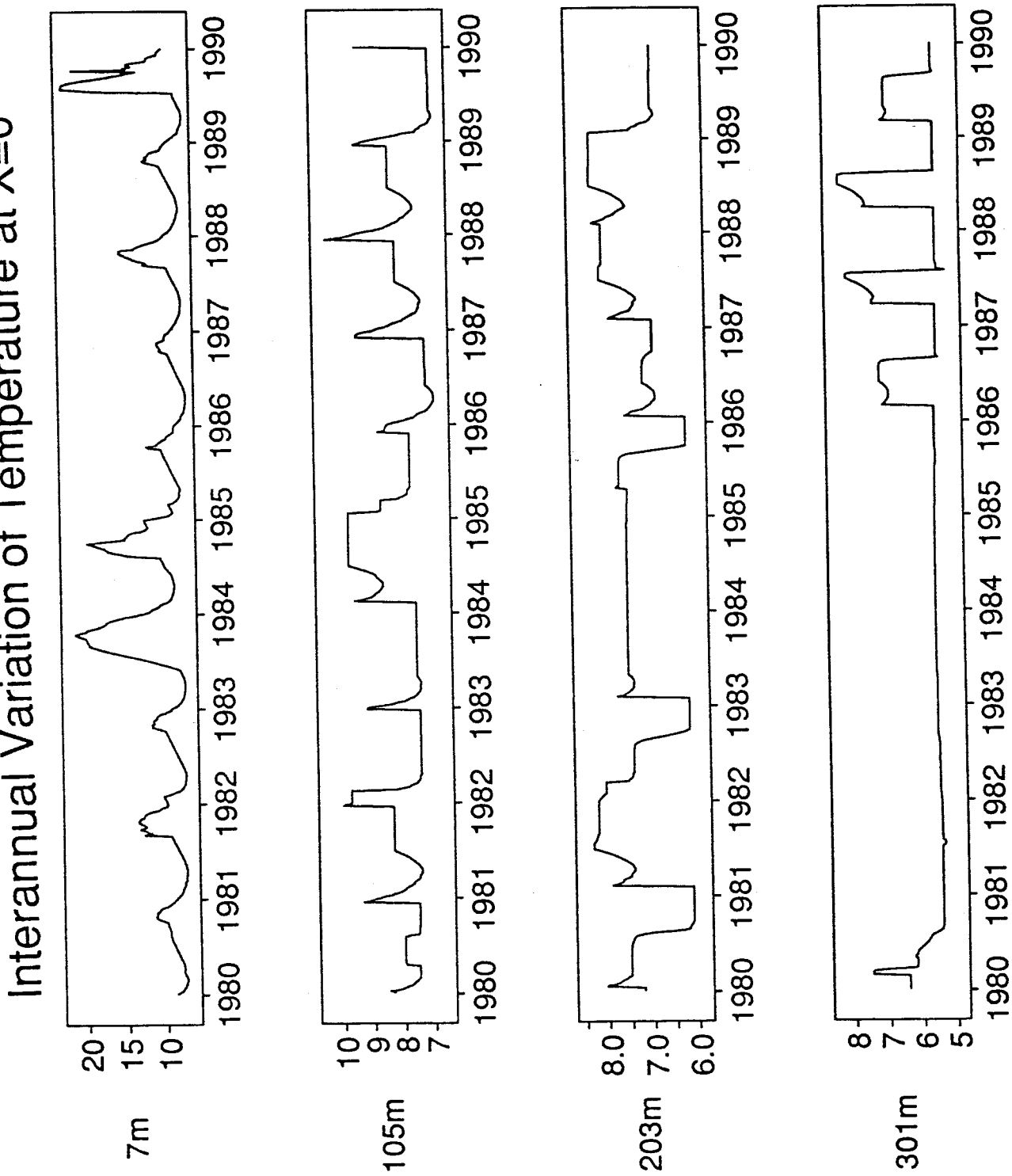

Figure 28 d) Interannual variation of Temperature at X=0 during 1980-1989

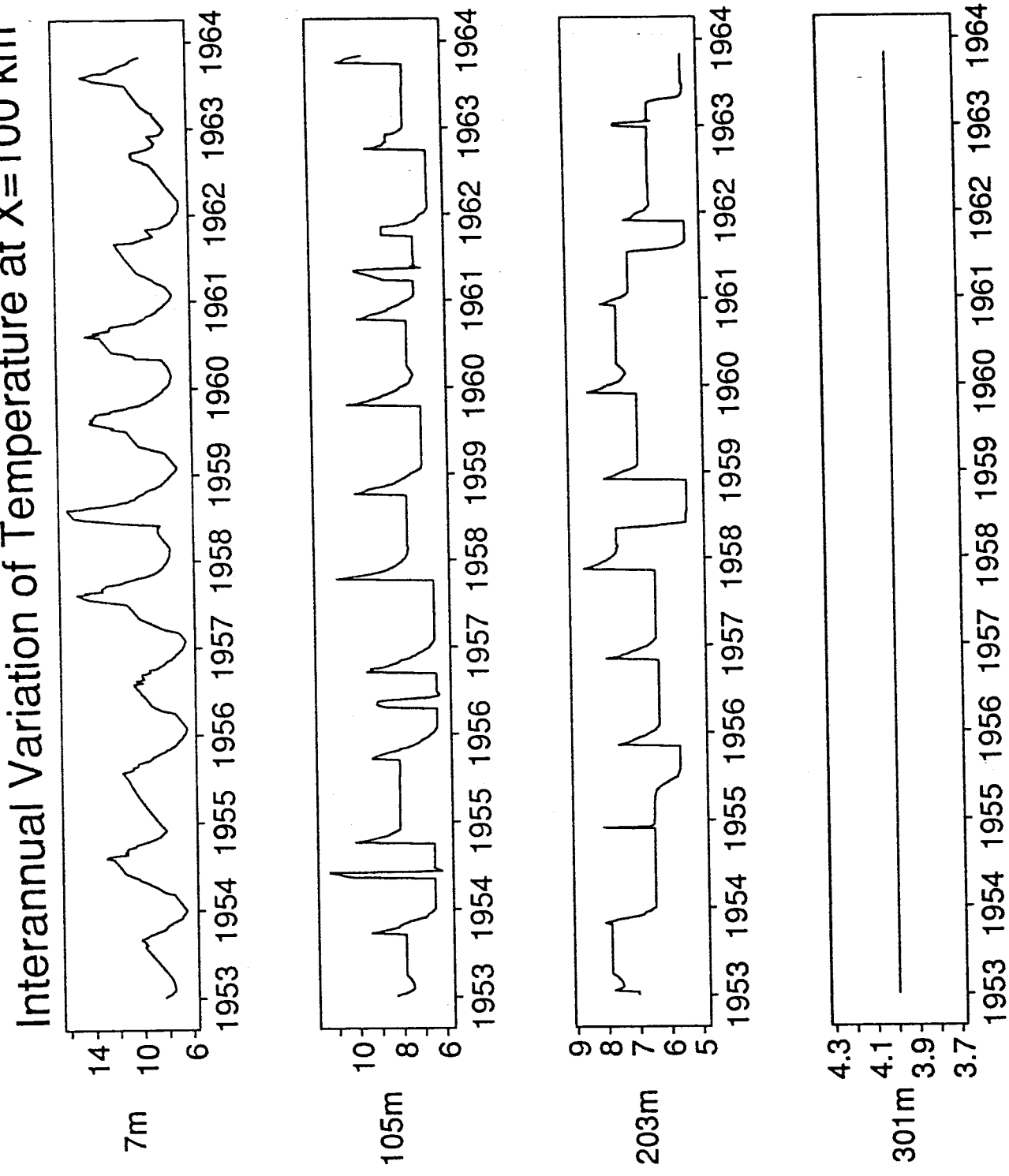

Figure 29 a) Interannual variation of Temperature at X=100 km during 1953-1963

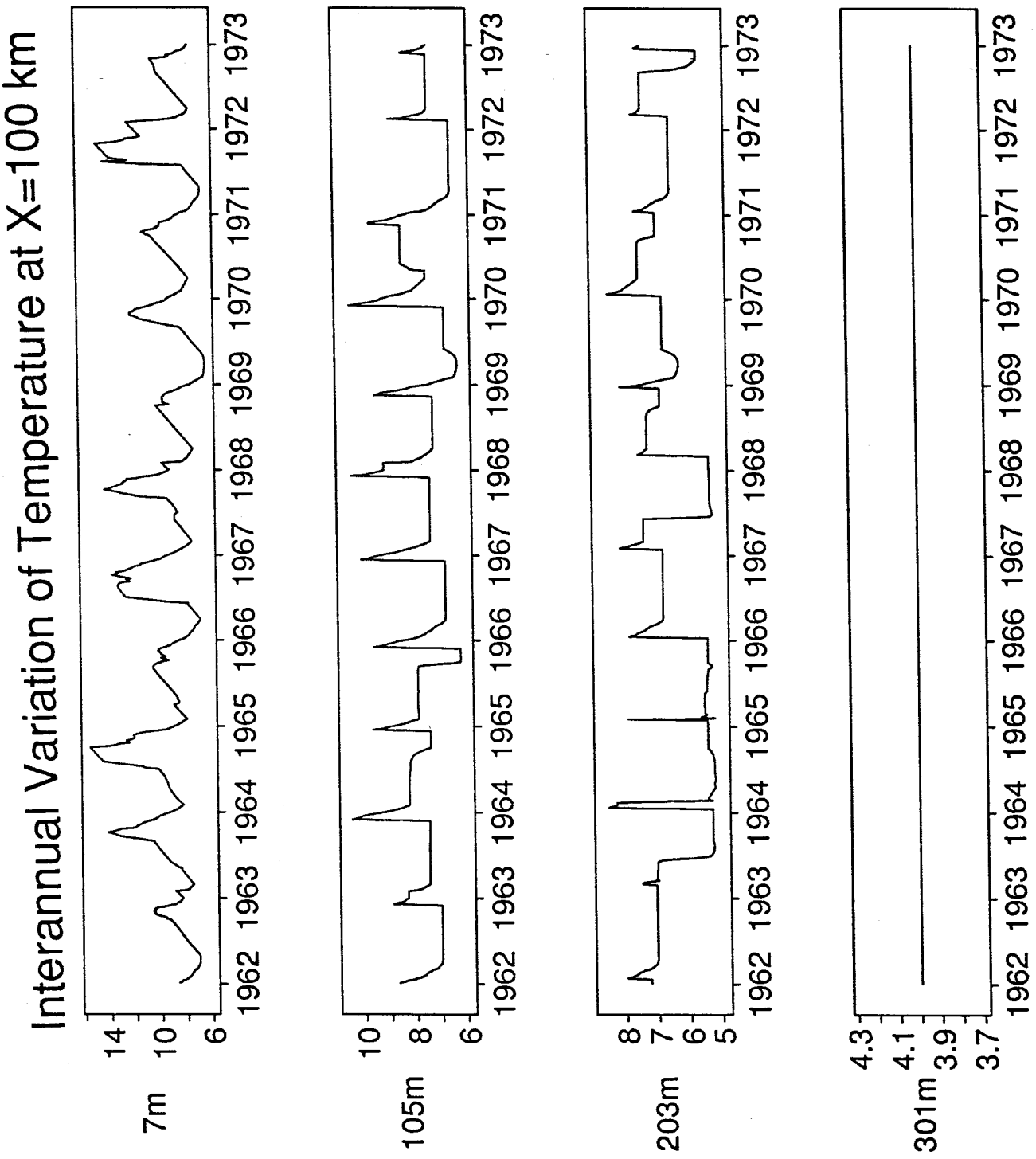

Figure 29 b) Interannual variation of Temperature at X=100 km during 1962-1972

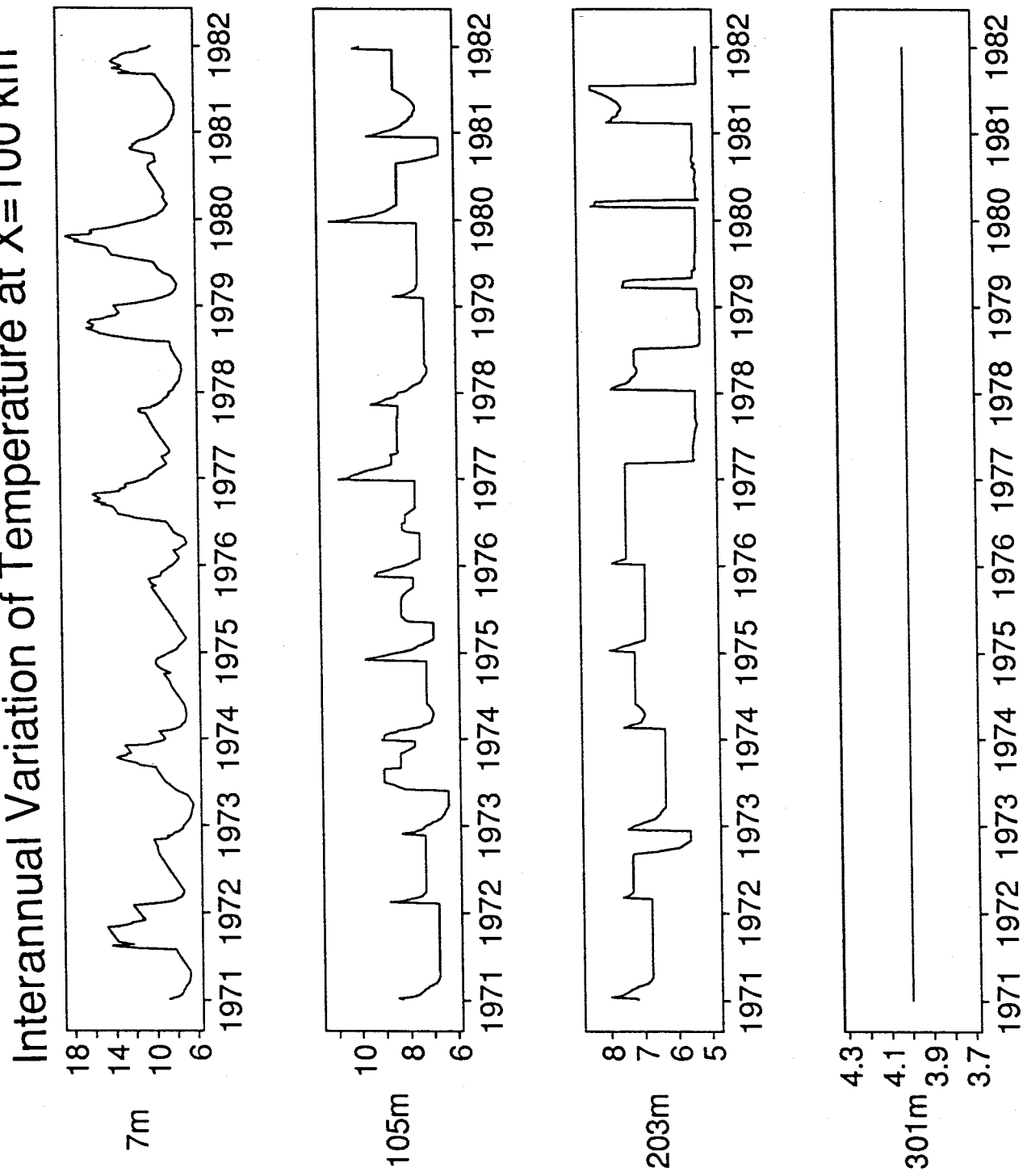

Figure 29 c) Interannual variation of Temperature at X=100 km during 1971-1981

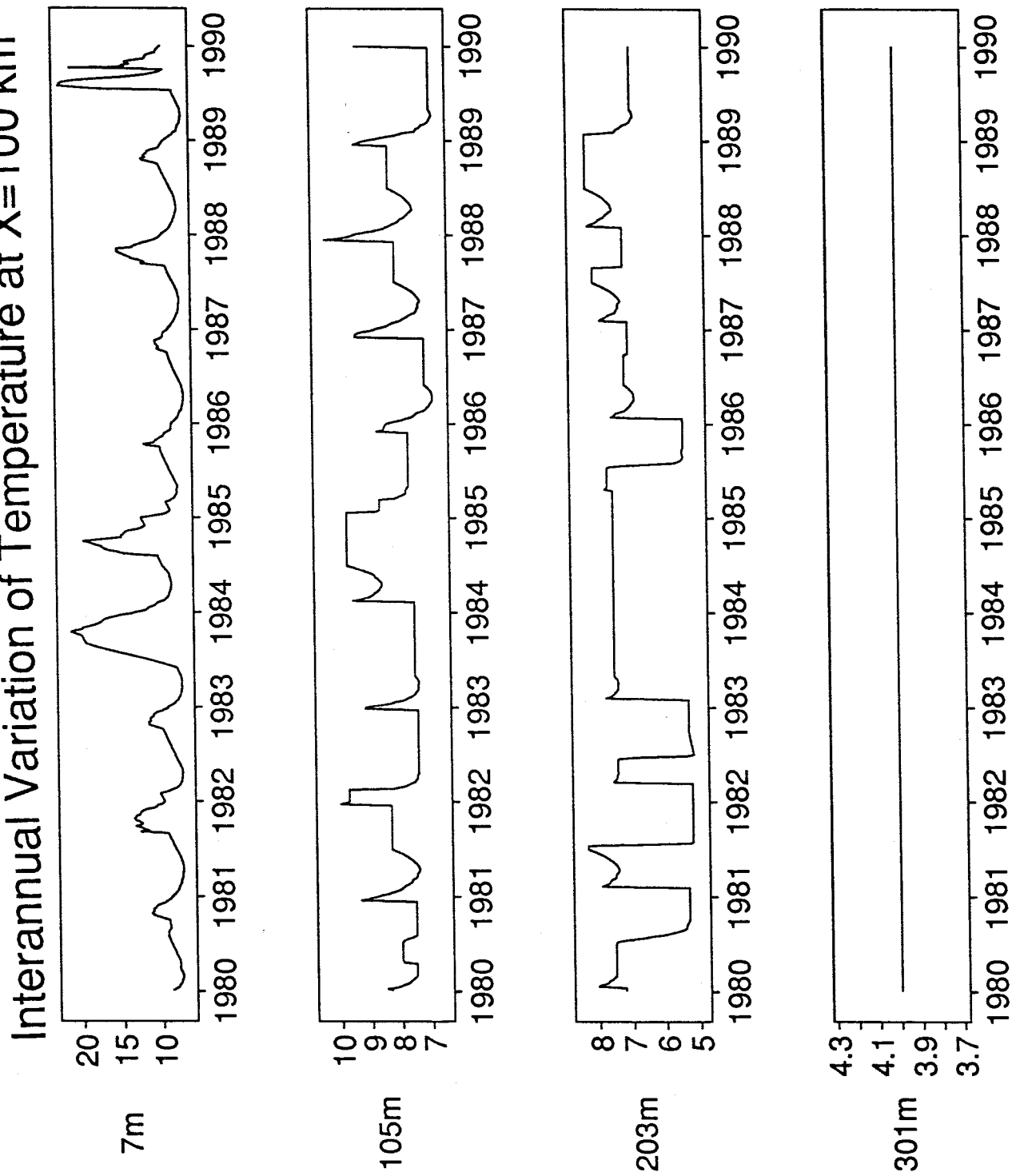

Figure 29 d) Interannual variation of Temperature at X=100 km during 1980-1989

°C (Fig. 28d). The difference between the annual cycle at the surface and that in the lower layer is that the former depends on the alternation of heating from solar radiation in summer and wind cooling and mixing in winter, whereas the latter owes its existence to cold water upwelling in the summer and mixing and warming in the winter.

There is a delay for the lower layer to warm up because of surface mixing and for the cold water to reach higher layers due to upwelling. An interesting phenomenon shown in Fig. 28 and Fig. 29 is that when surface layer temperature begins to decrease, the temperature in the layer just below it often shows a sharp increase, indicating warm surface water has been mixed down to that level. After this sharp increase, the temperature in the lower layer begins to decrease in the same manner as surface water. Similar features are shown in even lower layers, too, though the time of sharp increase occurs even later than in the upper layer. Such is the case in the fall of 1959, where delays of 40 days, 85 days and 140 days are shown at level 2, 3 and 4 in Fig. 28a after cooling in level 1.

During strong upwelling years, the decrease of temperature in the lower layer shows a two-step process (Fig 30). The first decrease in temperature is due to the winter surface cooling, while the second drop of temperature reflects the cold water intrusion from below.

Cold water of 5.5 °C rose to a higher level at the location 2 than at location 1, reflecting that it climbs along the slope of the Moresby Trough from south to north, the same feature as shown in Fig. 8.

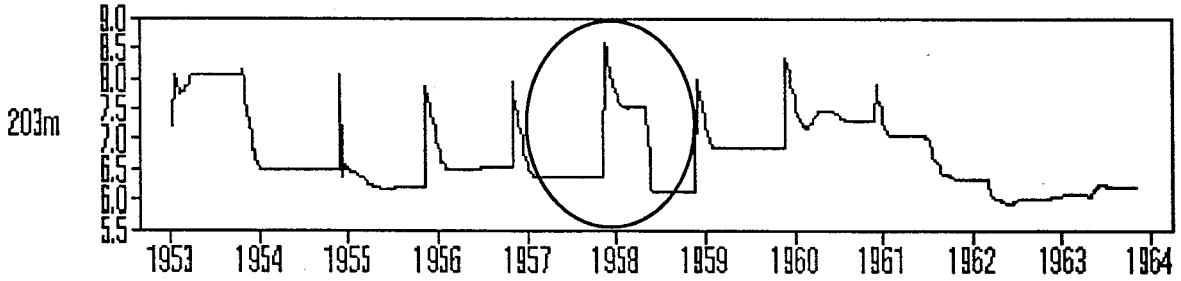

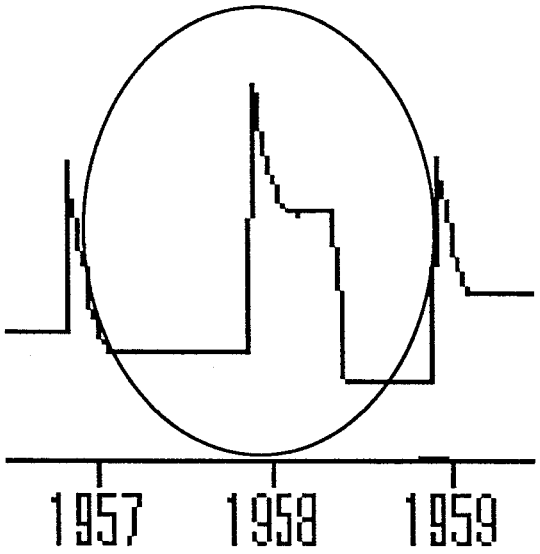

Figure 30 Two-step decrease of temperature due to different mechanisms.

5. Comparison of model results and observed data

Corresponding to the above two locations, observed data from the nearby areas were obtained for comparison with the modeled results. In order to have more data points for comparison, observed data from three areas were extracted from the MEDS (Marine Environmental Data Services Branch of the Department of Fisheries and Ocean) data for the years 1953-1971 and from IOS CTD data for the period 1971-1989 (Figure 27). Observed data from area 1, which is on the main axis of Moresby Trough, are used to compare with the modeled results at x=0. Data from area 3 are compared with the modeled results at x=100 km. Area 2 is not on the main axis of Moresby Trough, but there were numerous observations during 1953-1968 (this area covers station A and C of Dodimead, 1980); data from this area were also used to compare with modeled results at x=0.

In comparing the modeled results with the MEDS data, the wedge is divided into four layers ranging from 0-42m, 43-150m, 151-250m and 251-330m respectively (Fig. 27). All the observed data falling into these four layers were used to compare with the modeled results at the four corresponding levels (7m, 105m, 203m and 301m).

For CTD data, because of the denser sampling interval, only data from within 10 meters above and below the four corresponding levels were extracted for comparison.

All the extracted data were plotted on the corresponding panels as symbols (Fig. 31 a-d, Fig. 32 a-d).

To evaluate quantitatively the modeled results, part of the extracted data were used to calculate the closeness of modeled results and observed data. Only the points within 10 meters from the selected levels were used in the statistics for x=0 and x=100 km. A deviation of ± 0.8 °C is defined as good and ± 1.5 °C is regarded as fair. The percentage of good and fair points at four selected levels are

shown in Table 3 and Table 4 for location 1 and 2 respectively. Those points are also plotted on the corresponding panels as big dots (Fig 31 a-d, Fig. 32 a-d).

Table 3 comparison of model results with observed data at x=0

	layer 1	layer 2	layer 3	layer 4
No. dots	919	398	208	78
% good	33.6	71.1	61.5	75.6
% fair	24.3	19.1	27.4	23.1

Table 4 comparison of model results with observed data at x=100 km

	layer 1	layer 2	layer 3
No. dots	432	230	64
% good	47.5	89.5	29.7
% fair	22.5	5.2	62.5

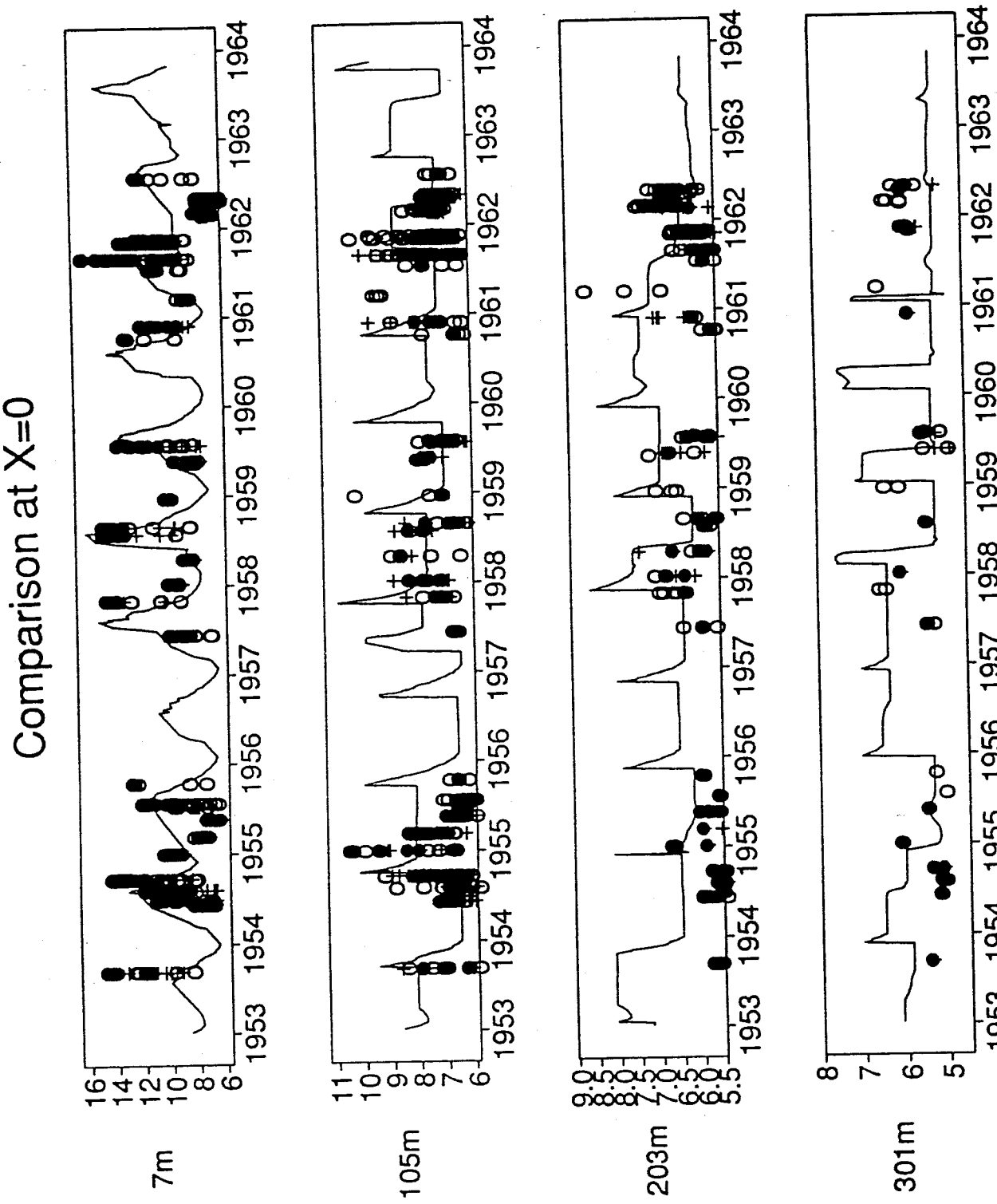

Figure 31 a) Comparison of modeled results and the observed data at x=0 during years 1953-1963. Data from area 1 are plotted as crosses; Data from area 2 are plotted as circles; Those used for statistics (within 10 m of model depth in area 1 and 2) are plotted as solid dots

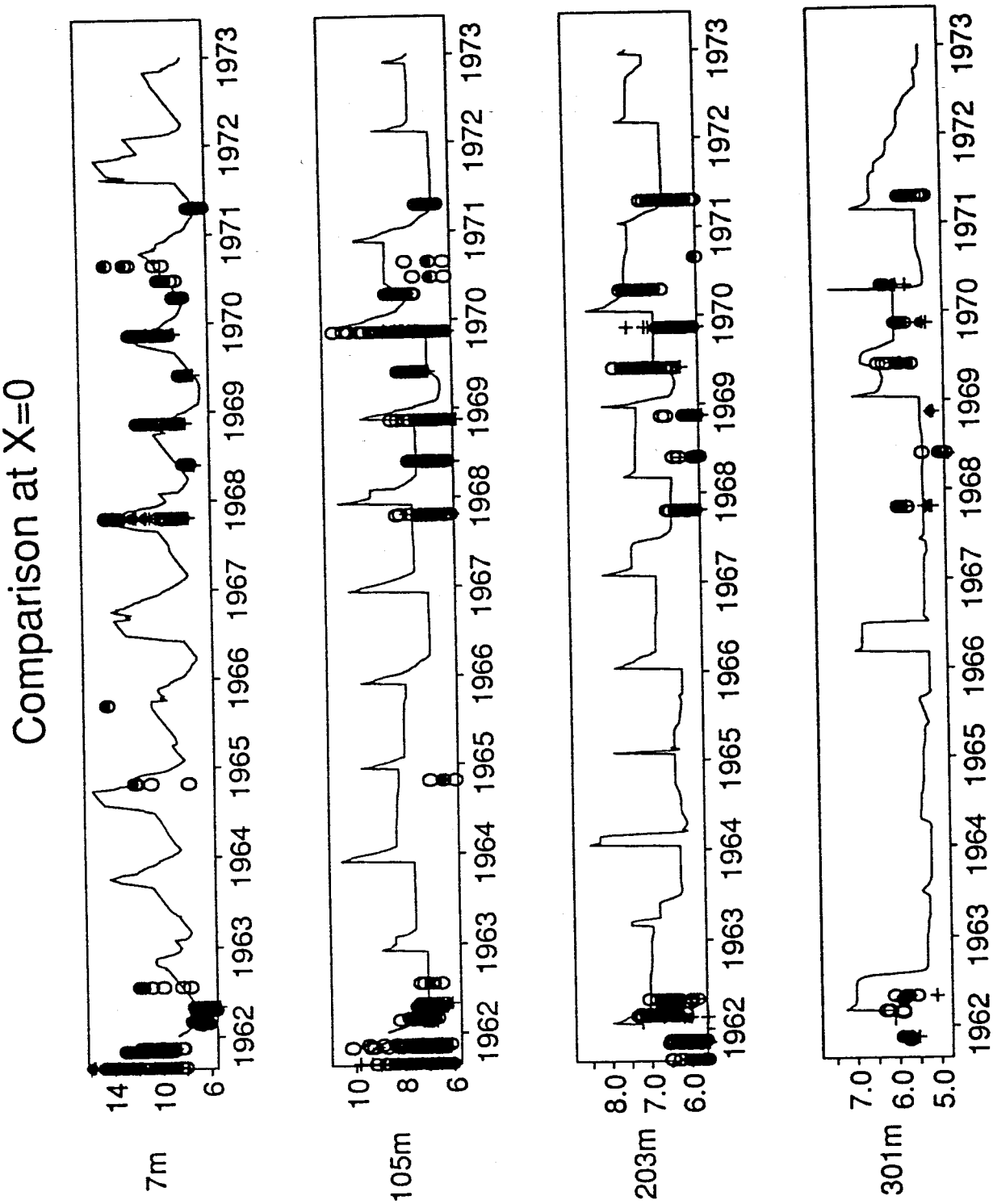

Figure 31 b) Comparison of modeled results and the observed data at x=0 during years 1962-1972

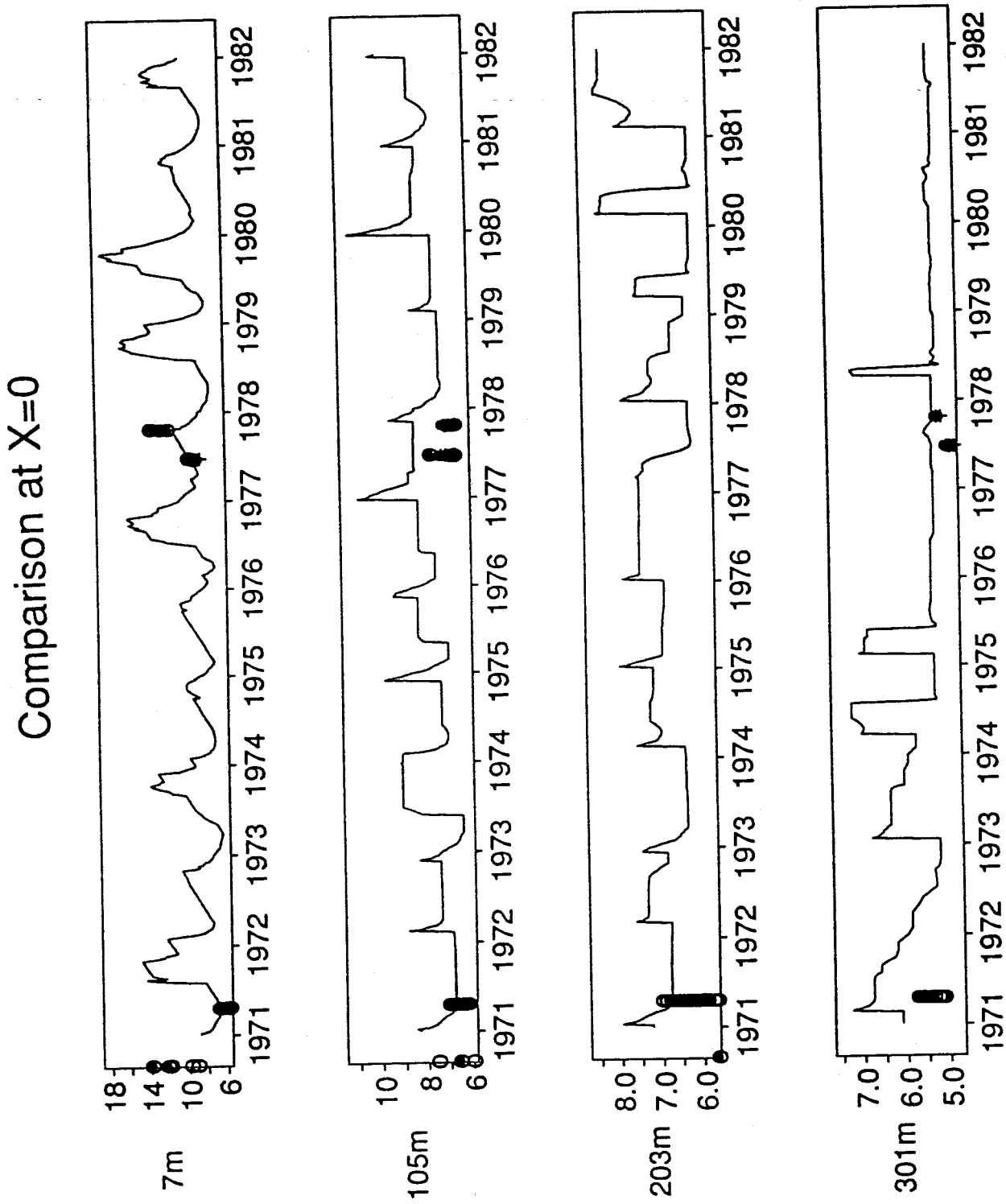

Figure 31 c) Comparison of modeled results and the observed data at x=0 during years 1971-1981

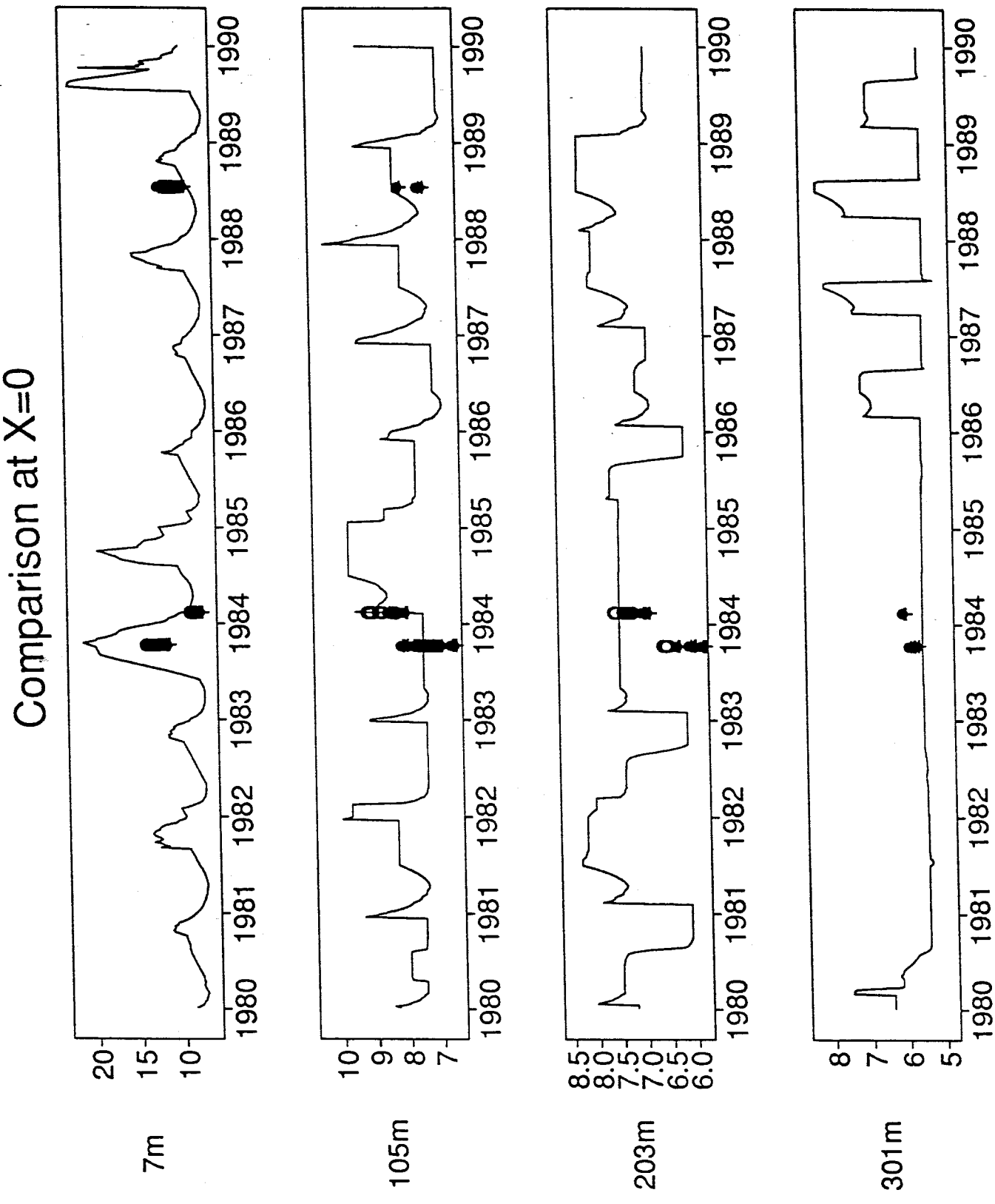

Figure 31 d) Comparison of modeled results and the observed data at x=0 during years 1980-1989

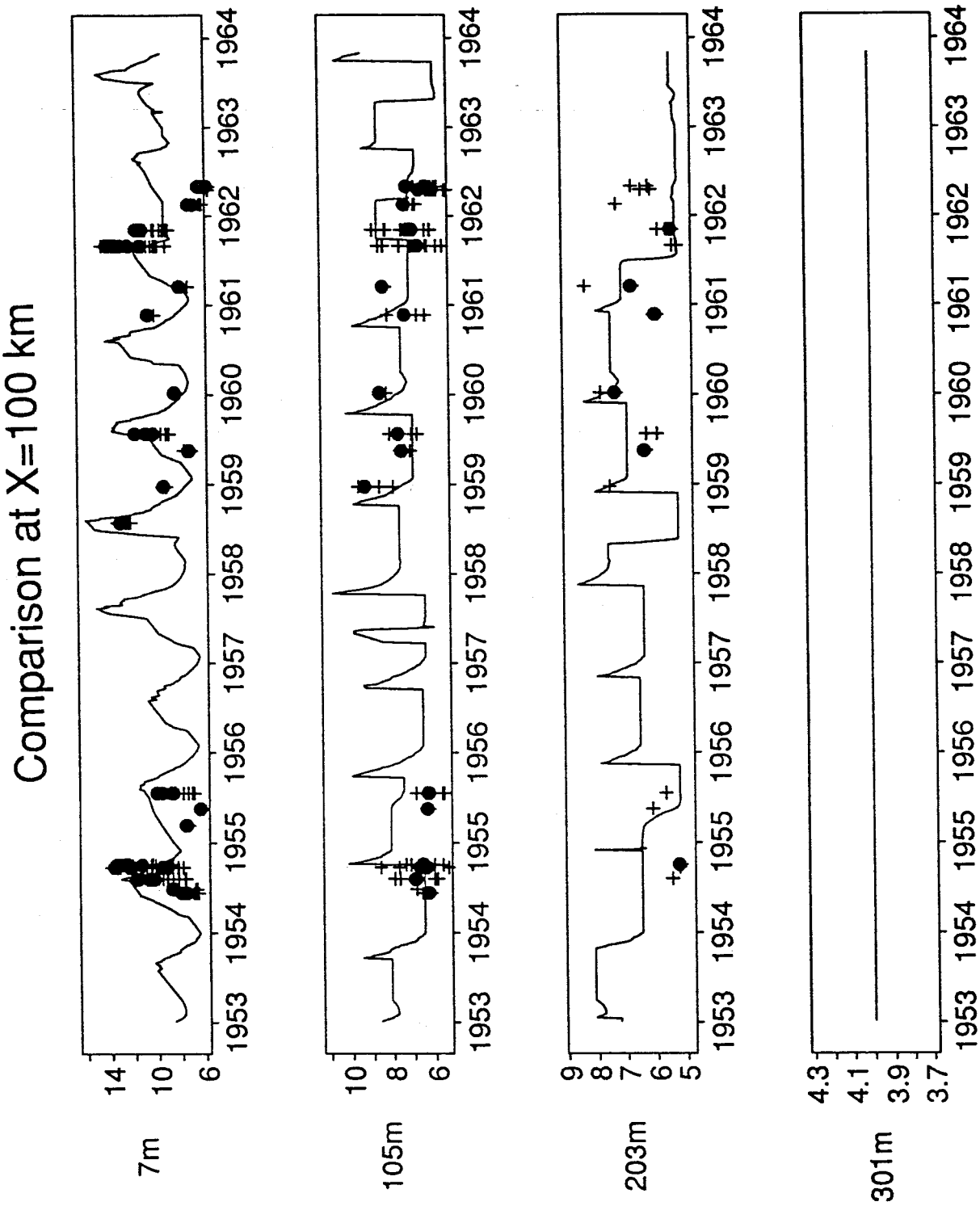

Figure 32 a) Comparison of modeled results and the observed data at x=100 km during years 1953-1963. Data from area 3 are plotted as crosses; those used for statistics (data from area 3 within 10 m of the model depth) are plotted as solid dots.

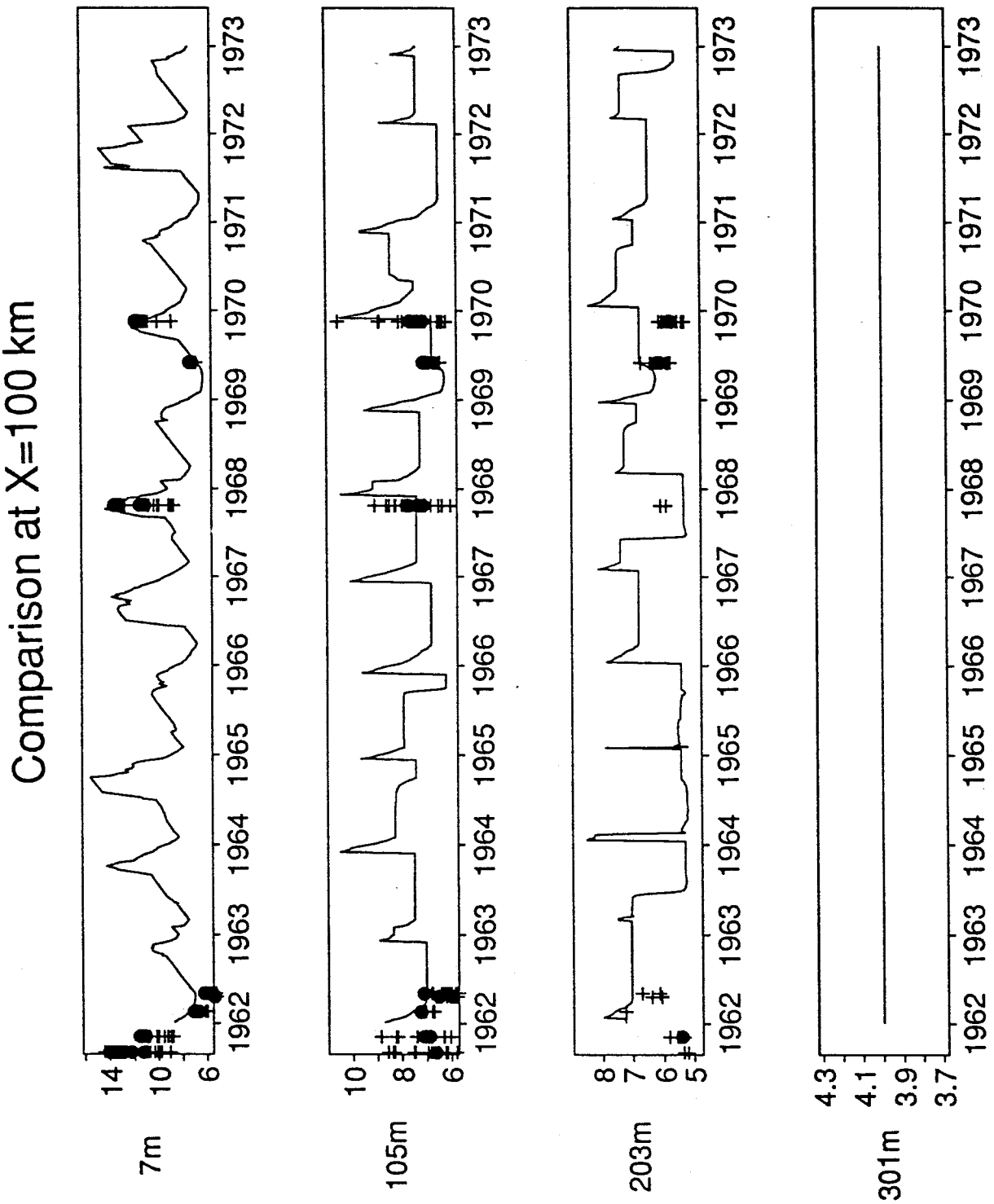

Figure 32 b) Comparison of modeled results and the observed data at x=100 km during years 1962-1972

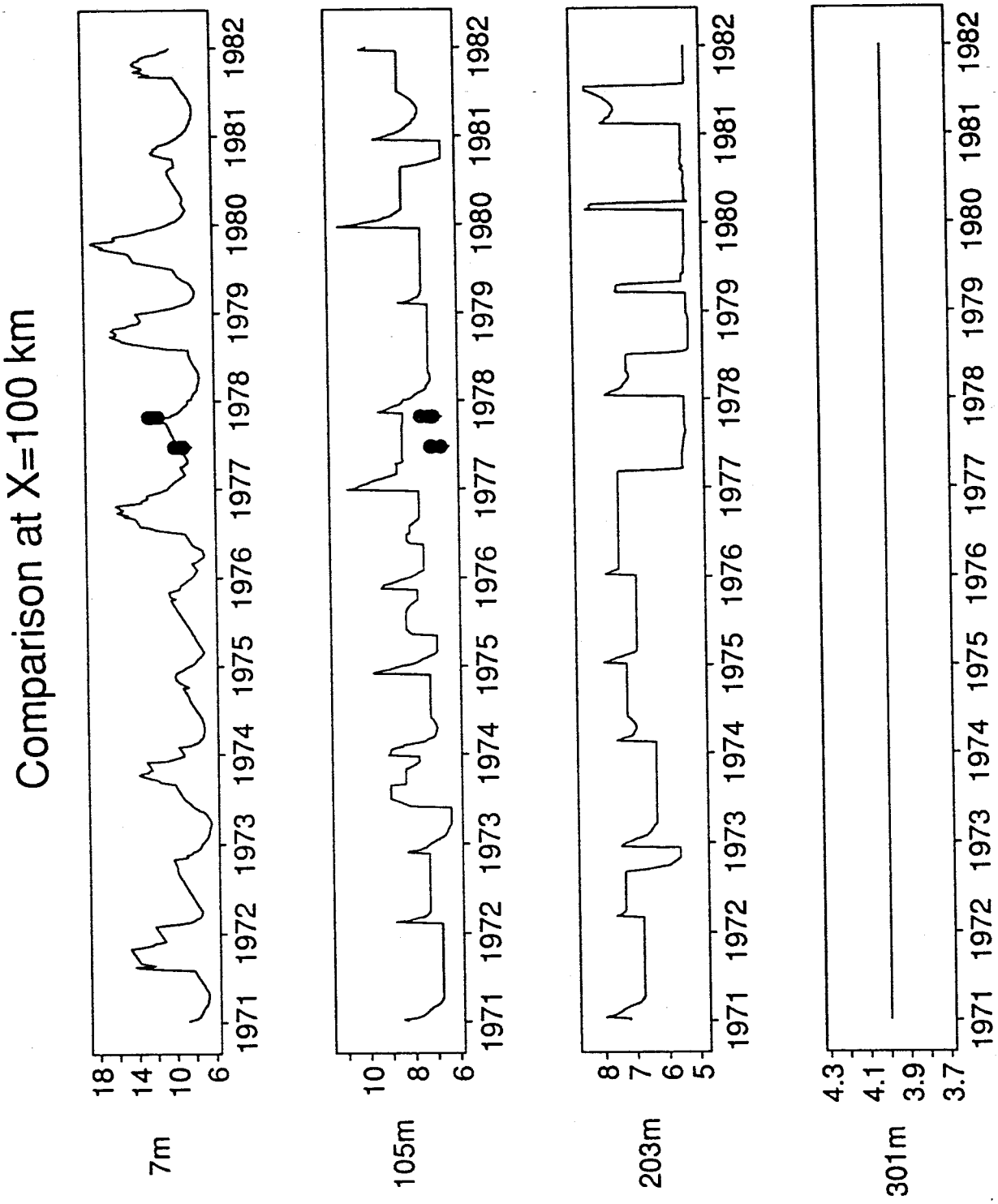

Figure 32 c) Comparison of modeled results and the observed data at x=100 km during years 1971-1981

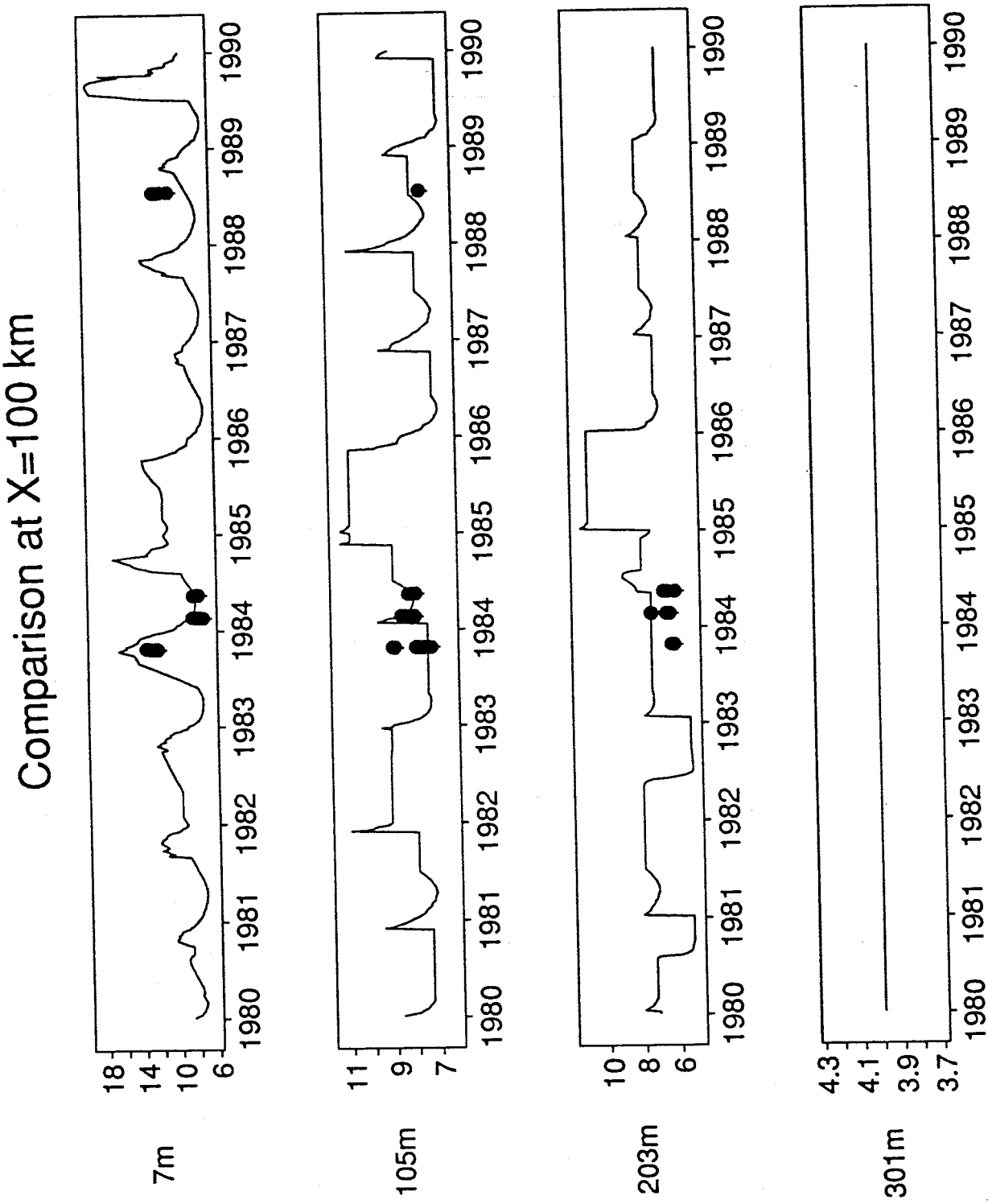

Figure 32 d) Comparison of modeled results and the observed data at x=100 km during years 1980-1989

6. Conclusions

Interannual variations of temperature in Hecate Strait-Queen Charlotte Sound region have been studied using a composite upwelling/mixing model. The dominant processes of summer upwelling and winter mixing have been investigated by different models separately, which were then coupled to model the annual cycle of temperature field. The switch between the two models depends on the sign of monthly Bakun Indices. The studied area is simplified as a wedge-shaped water volume. In the two-dimensional upwelling model, a velocity field was derived analytically from the off-shore transport in terms of the Bakun Index and the equation of continuity. This velocity drives cold water into the bottom of the wedge and moves warm water out of the wedge in the surface layer. In the mixing model, a one-dimensional upper mixed layer model was developed. The coupled model starts from a uniformly stratified ocean, either an upwelling or a mixing regime is chosen by examining the sign of the Bakun Index in the starting month. The end state of the former regime becomes the initial state of the latter regime. The model was run for 37 years and reproduced profiles of interannual variations of temperature in the region for the period 1953-1989.

The model reproduced a clearer annual cycle in the surface layer than that in the lower layers, but a comparison of modeled result with observed data show that in the lower layers, modeled results are closer to the observations. The modeled results also show the relative importance of mixing and upwelling in the variation of temperature in the lower layers. Weak winter mixing results in longer cold water residence on the bottom (1962-1966 at 300 m depth); strong upwelling sends cold water to higher levels (1957, 1962, 1972, etc.).

A comparison was made between modeled results and observed data. Two measures, good and fair, were used to evaluate the deviation of modeled results from the observed data. It is shown that, in the lower layers, 69.4% and 59.6% of the compared points are in good agreement with the modeled results at x=0 and

x=100 km respectively, while in the surface layer, 33.6% and 47.5% are good at x=0 and x=100 km respectively.

The model assumes upwelling and mixing are two distinct processes and never happen simultaneously. This may cause some deviation from the real nature, because mixing effects also exist during upwelling months, although it is not as important as upwelling.

The forcing parameters, such as, wind speed, solar radiation and air temperature, etc. are all from Cape St. James, a station with elevation of 89 meters, not as required at the sea surface or at 10 meter above sea level. Except for wind speed, all parameters were used without converting to the required height. This is another source of error.

Although the model has the above limitations, it explains well the two important processes happening in the region. The main features of temperature variations of the surface and bottom temperature in the region have been represented clearly. The model hindcasted the last 37 years of temperature profiles with reasonable accuracy. This result may improve our understanding of the dynamics of Hecate Strait- Queen Charlotte Sound region and contribute to the implementation of "reconstruction of the oceanographic conditions" within the region. It may also provide background physical oceanographic knowledge to the fisheries researchers involved in the OPEN project and may lead to a better understanding of variations in the habitat of ground fish.

Bibliography

Allen, J.S. 1980: Models of Wind-driven Currents on the Continental Shelf. Ann. Rev. Fluid Mech. 12: 389-433.

Bakun, A., 1973: Coastal Upwelling Indices, West Coast of North America, 1946-1971. NOAA Tech. Rep. NMFS SSRF 671.

Crawford, W.R. , W.S. Huggett, M.J. Woodward and P.E. Daniel, 1985: Summer Circulation of the Waters in Queen Charlotte Sound. Atmosphere-Ocean, 23:393-413.

Crawford, W.R. , W.S. Huggett and M.J. Woodward, 1988: Water Transport through Hecate Strait, British Columbia, Atmosphere-Ocean, 26: 301-320.

Crean, P.B., 1967: Physical Oceanography of Dixon Entrance, British Columbia. Fish. Res. Board Can. Ottawa . Bulletin 156. 66pp.

Dodimead, A.J., 1980: A General Review of the Oceanography of the Queen Charlotte Sound-Hecate Strait-Dixon Entrance Region. Canadian Manuscript Report of Fisheries and Aquatic Sciences. No. 1574.

Freeland, H.J. and K.L. Denman, 1982: A topographically Controlled Upwelling Center off Southern Vancouver Island. J. Marine Res. 40: 1069-1093.

Ivanoff, A., 1977: Oceanic Absorption of Solar Energy. Modeling and Prediction of the Upper Layers of the Ocean. Pergamon Press, 325pp.

Niiler, P.P. and E.B. Kraus, 1977: One-Dimensional Models of the Upper Ocean. Modelling and Prediction of the Upper Layers of the Ocean. Pergamon Press, 325pp.

Pickard, G.L. and W.J. Emery, 1990: Descriptive Physical Oceanography. Pergamon Press. 320pp.

Rosemary, D. Mey and Nan D. Walker, 1990: Surface Heat Fluxes and Marine Boundary Layer Modification in the Agulhao Retroflection Region. J. Geophys. Res. 95:C9 15,997-16,015.

Stigebrandt, A., 1981: Cross Thermocline Flow on Continental Shelves and the Locations of Shelf Fronts. Ecohydrodynamics, Elsevier Scientific Publishing Company.

Tabata, S. and J.L. Peart, 1985: Statistics of Oceanographic Data Based on Hydrographic/STD Casts Made at Station 1 through 6 along Line P During January 1959 through June 1981. Canadian Data Report of Hydrography and Ocean Sciences. No. 38.

Thomson, R.E., 1989: The Queen Charlotte Islands Physical Oceanography. The Outer Shores. Queen Charlotte City, B. C.